NOTE TO USERS

Université d'Ottawa · University of Ottawa

Université d'Ottawa · University of Ottawa

FACULTÉ DES ÉTUDES SUPÉRIEURES ET POSTDOCTORALES

FACULTY OF GRADUATE AND POSTDOCTORAL STUDIES

Joanna RENWICK

AUTEUR DE LA THÈSE - AUTHOR OF THESIS

M. Sc.(Cellular and Molecular Medicine)

GRADE - DEGREE

Department of Cellular and Molecular Medicine

FACULTÉ, ÉCOLE, DÉPARTEMENT - FACULTY, SCHOOL, DEPARTMENT

TITRE DE LA THÈSE - TITLE OF THE THESIS

XIAP-Mediated Rescue of Ischemic Neural Tar Retina from Death

C. Tsilfidis

DIRECTEUR DE LA THÈSE - THESIS SUPERVISOR

CO-DIRECTEUR DE LA THÈSE - THESIS CO-SUPERVISOR

EXAMINATEURS DE LA THÈSE - THESIS EXAMINERS

P. Liston

B. Tsang

J.-M. De Koninck, Ph.D.

LE DOYEN DE LA FACULTÉ DES ÉTUDES SUPÉRIEURES ET POSTDOCTORALES

DEAN OF THE FACULTY OF GRADUATE AND POSTDOCTORAL STUDIES

XIAP-mediated rescue of ischemic neural rat retina from death

By Joanna Renwick

This thesis is submitted as a partial fulfillment of the M.Sc. program in Cellular and Molecular Medicine

Submitted May 5, 2004

University of Ottawa, Faculty of Medicine, Department of Cellular and Molecular Medicine

Your file Votre référence
ISBN: 0-494-01591-8
Our file Notre référence
ISBN: 0-494-01591-8

Table of Contents

Abstract

XIAP-mediated gene therapy has been shown to protect brain neurons from ischemic cell death. However, it has not been shown whether XIAP can protect retinal neurons as well. To determine this, an acute retinal ischemia rat model was utilized. Eyes were injected with AAV-XIAP or AAV-GFP and, six weeks later, rendered ischemic by raising intraocular pressure to 110 mmHg and maintaining the pressure for one hour. Retinas were analyzed both functionally and structurally at various time points following ischemia. Functional analysis shows that XIAP, when overexpressed, rescues retinal neurons up to 4 weeks post-ischemia (wpi). Structural rescue is also evident from cell counts of H+E stained retinas. There are also significantly less TUNEL positive cells in the inner nuclear layer of the XIAP-treated retinas at 24 hpi. Therefore, XIAP-mediated gene therapy appears to functionally and structurally rescue retinal neurons from death following a transient ischemic episode.

List of Figures and Tables

List of abbreviations

AAV	Adeno-associated virus
ANOVA	Analysis of Variance
BIR	Baculoviral IAP Repeat
CARD	Caspase Recruitment Domain
dUTP	deoxyuracil triphosphate
ERG	Electroretinography or Electroretinogram
GCL	Ganglion Cell Layer
GFP	Green Fluorescent Protein
H+E	Haematoxylin and Eosin
HPI	Hours post-ischemia
IAP	Inhibitor of Apoptosis Protein
INL	Inner Nuclear Layer
IPL	Inner Plexiform Layer
ONL	Outer Nuclear Layer
OPL	Outer Plexiform layer
PBS	Phosphate buffered saline
PFA	Paraformaldehyde
PMSF	Phenylmethyl sulfonyl fluoride
PVDF	Polyvinylidene difluoride
RGCL	Retinal Ganglion Cell Layer (same as GCL)
RING	Really Interesting New Gene
STDEV	Standard Deviation

SE	Standard Error
TdT	Terminal deoxynucleotidyl transferase
TUNEL	TdT-dUTP Terminal Nick End Labelling
WPI	Weeks post-ischemia
XIAP	X-chromosome-linked Inhibitor of Apoptosis Protein

Acknowledgements

"...Blessed be the name of God forever and ever! For wisdom and might are His! He changes the times and the seasons; He removes kings and sets up kings. He gives wisdom to the wise and knowledge to those who have understanding! He reveals the deep and secret things; He knows what is in the darkness, and the light dwells with Him!" Daniel 2:20-22, Amplified Bible.

My profuse thanks go to Dr. Catherine Tsilfidis (Cathy) for her guidance and for having confidence in me to carry out this project. Special thanks to Dr. Stuart Coupland for lending his expertise and guidance with respect to the electrophysiology tests and interpreting the electrophysiological data. As well, thanks to Dr. Peter Liston for his expertise and guidance on apoptosis as it relates to this thesis. I also thank Dr. William Hauswirth for the adeno-associated viral constructs. Many thanks go to Adam Baker, Dino Petrin, Jian-Ying Xuan, and Jennifer Brousseau for their assistance, advice and expertise.

I would like to especially thank my family (Mom, Dad, Charm, Paul and Jon) for their continuous support. Thank you all for believing in me! Your words of encouragement and your friendship have meant so much to me. Thank you also for keeping me humble and reminding me of what truly matters.

"A scoffer seeks Wisdom in vain [for his very attitude blinds and deafens him to it], but knowledge is easy to him who [being teachable] understands." Proverbs 14:6, Amplified Bible

Chapter 1. INTRODUCTION

1.1 Structure of the Retina

The retina is divided into several distinct histological layers (see Figure 1-adapted from Ross, MH et al., 1995). The outermost layer of the retina is the retinal pigment epithelium (RPE). This epithelium rests on the choroid, which provides nutritive support for the outer retina. Next to the RPE is the outer nuclear layer (ONL), which contains the photoreceptors (rods and cones). It is from the ONL that the response to light and the generation of an electrical signal, which will ultimately reach the brain, is initiated. Rods make up 97% of the outer nuclear layer of the human retina and mediate vision in dim light (Van Soest, S et al., 1999). Cones are responsible for detailed visual acuity and colour vision and are most concentrated in the macula. Cells in the ONL synapse with cells in the inner nuclear layer (INL) which, in turn, synapse with ganglion cells at the inner plexiform layer. Ganglion cells project their axons through the optic nerve head to the brain.

Figure 1. Schematic diagram of the different layers of the retina.

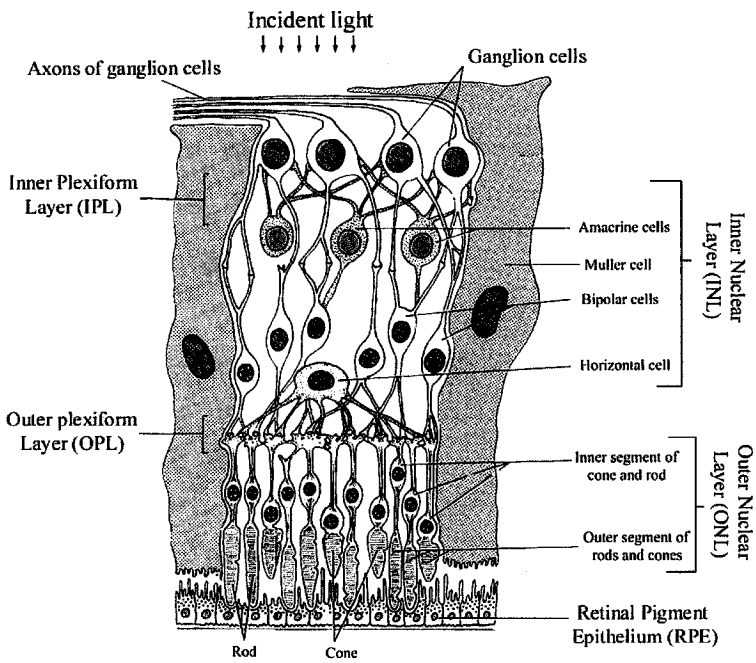
Incident light
Axons of ganglion cells
Ganglion cells
Inner Plexiform Layer (IPL)
Amacrine cells
Muller cell
Bipolar cells
Horizontal cell
Inner Nuclear Layer (INL)
Outer plexiform Layer (OPL)
Inner segment of cone and rod
Outer segment of rods and cones
Outer Nuclear Layer (ONL)
Retinal Pigment Epithelium (RPE)
Rod
Cone

1.2 Retinal Function

Electrophysiological studies over the past five decades have contributed crucial information in regards to the pathophysiology of the diseased or injured retina. Clinical electroretinography has characterized various retinal neuropathologies (Dong CJ and WA Hare, 2002; Neuringer M, 2000). For example, both the a-wave and b-wave are lost irreversibly in patients with Retintis Pigmentosa (RP), a genetic disorder affecting the photoreceptor layer (Van Soest S, et al., 1999). In patients with Central Retinal Vein Occlusion (CRVO), a condition resulting in retinal ischemia, only the b-wave is extinguished (Breton et al., 1991), while the a-wave is maintained. Specifically, the amplitude (microvolts, μV) and latency (milliseconds, ms) of these waves are affected variably. Such variances, therefore, make electroretinography a very useful too in assessing retinal function.

A standard electroretinogram (ERG), which represents the electrical activity in the retina, can be dissected into a negative a-wave followed by a positive b-wave. The a-wave is the sum of the current from the photoreceptors and it is currently believed that ganglion cells and amacrine cells contribute minimally to the b-wave amplitude (Dong C and WA Hare, 2000; Breton ME et al., 1991). The b-wave amplitude is a direct measure of the sum of bipolar cell and Muller cell activity. There are many types of bipolar cells; rod bipolars synapse only with rod photoreceptors and cone bipolar cells synapse with short, medium and long wavelength cone photoreceptors. The rod bipolar cells are on-centre depolarizing bipolar cells while the cone bipolar cells are sub-categorized into both on-centre depolarizing and off-centre or hyperpolarizing neurons. It is believed that the on-centre bipolar cells chiefly contribute to the b-wave (Dong C and WA Hare, 2002;

Dong C and WA Hare, 2000; Ogden TE, 1989), and since bipolar cells synapse with the ganglion cells, changes in b-wave amplitude are also indirectly an indication of ganglion cell activity. When the health of the bipolar cells deteriorates and the synaptic contacts are lost, it stands to reason that the ganglion cells, which are the final step of the visual transduction pathway, will not function.

The retinal ganglion cells, as well as amacrine, horizontal and bipolar cells of the inner nuclear layer are affected the most by a retinal ischemic event, since they are served directly by retinal circulation arising from the ophthalmic (retinal) artery. Conversely, photoreceptors in the outer nuclear layer (ONL) tend to be the last and least affected neurons after ischemic injury to the retina because their blood supply comes from a separate source: the choriocapillaries in the choroid. The majority of the ocular blood flow is through the choroidal circulation (Kuroiwa S et al., 1998; Kohner EM, 1989; Delaey C and J Van de Voorde, 2000).

1.3 Retinal Ischemia

Retinal ischemia is a concern in diabetic retinopathy, in blood diseases such as sickle cell anemia, diseases of the blood vessel wall (e.g. hypertension) and in multifactorial diseases such as central retinal artery occlusion (CRAO) and central retinal vein occlusion (CRVO). Much like cerebral ischemia (stroke), retinal ischemia is the result of an insufficient supply of blood to neurons due to occlusion of blood vessels (Maltson MP et al, 2001; Rosenbaum et al., 1997; Kohner EM, 1989). As a result of this reduction in blood supply, the cells in both retinal and brain tissue undergo hypoxia (lack of oxygen) and are thus metabolically compromised. Consequently, pathophysiological processes occur in the retina such as hypoglycemia, excess calcium influx, glutamate toxicity and the formation of free radicals, which are charged oxygen molecules with unpaired electrons (Luo X et al, 2001; Adachi K et al., 1998; Rosenbaum et al., 1997; Sucher NJ et al., 1997). The end result is damage to the retinal neurons and cell death by apoptosis.

1.4 Apoptosis

Apoptosis is popularly defined as programmed cell death or cell suicide (Salvesen GS and CS Duckett, 2002; Villa P et al., 1997). This organized form of cell death is noted morphologically by cell shrinkage, margination (that is chromatin condensation in the nuclear periphery), and the fragmentation of DNA into fragments approximately 180 base pairs in length. The presence of these DNA fragments makes it possible for one to detect apoptotic activity within the cells. Apoptosis is also noted morphologically when the nucleus breaks off into smaller, membrane-bound pieces and the cell appears to shrink. The shrinkage is due to the cleavage of cytoskeletal proteins that structurally support the cell. Towards the end of apoptosis, fragments of the cell and its contents are blebbed off as apoptotic bodies, which are phagocytosed by macrophages or neighbouring cells (Lam TT et al., 1999; Hengartner MO, 2000; Rosenbaum DM et al., 1998; Xu D et al., 1999). The proteases responsible for the breakdown of cytoskeletal proteins are called cysteine proteases and they cleave after aspartate residues (Huang Y et al., 2003). The cysteine proteases are more commonly referred to as caspases when they are active and pro-caspases when they are dormant. The pro-caspases have three domains: an N-terminal pro-domain, p20 and p10 domains. The pro-caspases are cleaved after the pro-domain to yield active caspases (Hengartner MO, 2000). There are at least ten distinct human caspases, but there are a total of 14 known mammalian caspases. The caspases are subdivided into 2 main categories: initiators and effectors. The initiators are caspases 1, 2, 4, 5, 8, 9 and 10, while the effectors are caspases 3, 6 and 7. (Wong J and MJ Lenardo, 2000; Schulz JB et al., 1999; Villa P et al., 1997). Salvesen and Duckett (2002) summarized both the intrinsic and extrinsic

apoptotic pathways based on current knowledge (Figure 2). The extrinsic pathway is initiated by a receptor-mediated pro-apoptotic signal. One such cell-surface receptor, called Fas, is signaled to recruit a death domain protein called FADD (Fas associated death domain). FADD, in turn, recruits and activates caspase 8, an initiator caspase. Caspase 8 activates effector caspase 3, which activates caspases 6 and 7 (Deveraux, QL et al., 1998).

The intrinsic pathway begins with a pro-apoptotic signal that is triggered by stress (e.g. UV light, chemotherapy, and ischemia). This leads to DNA fragmentation and upregulation of Bax, a pro-apoptotic BCL-2 family member (Kaneda K et al., 1999). The BCL-2 agents heterodimerize to form channels in the outer mitochondrial membrane. It is thought that these channels allow cytochrome C to flow from the mitochondria into the cytoplasm (Hengartner MO, 2000). At this point, both the extrinsic and intrinsic pathways begin to converge into a final common pathway. Cytochrome C binds to Apaf-1 (apoptotic protease-activating factor 1). Caspase 9, another effector caspase, is activated when Apaf-1 and cytochrome C bind with pro-caspase 9 to form the apoptosomal complex. Caspase 9 can also activate caspase 3, hence one of the intermediate steps that lead to the common apoptotic pathway. Caspase activation ensues in the common pathway as a cascade, and morphological changes in the cell occur as described earlier.

Figure 2. A simplified schematic of extrinsic and intrinsic apoptotic pathways. The extrinsic pathway is triggered by a ligand. Although there are several extrinsic pathways, only one is shown here. The intrinsic pathway is triggered by a stress signal (e.g. UV light or ischemia). This signal triggers the translocation of Bax proteins to the mitochondria, which signals the release of cytochrome C. Following this, the caspase activation cascade ensues. The pro-caspase-to-caspase conversion steps were omitted for simplicity.

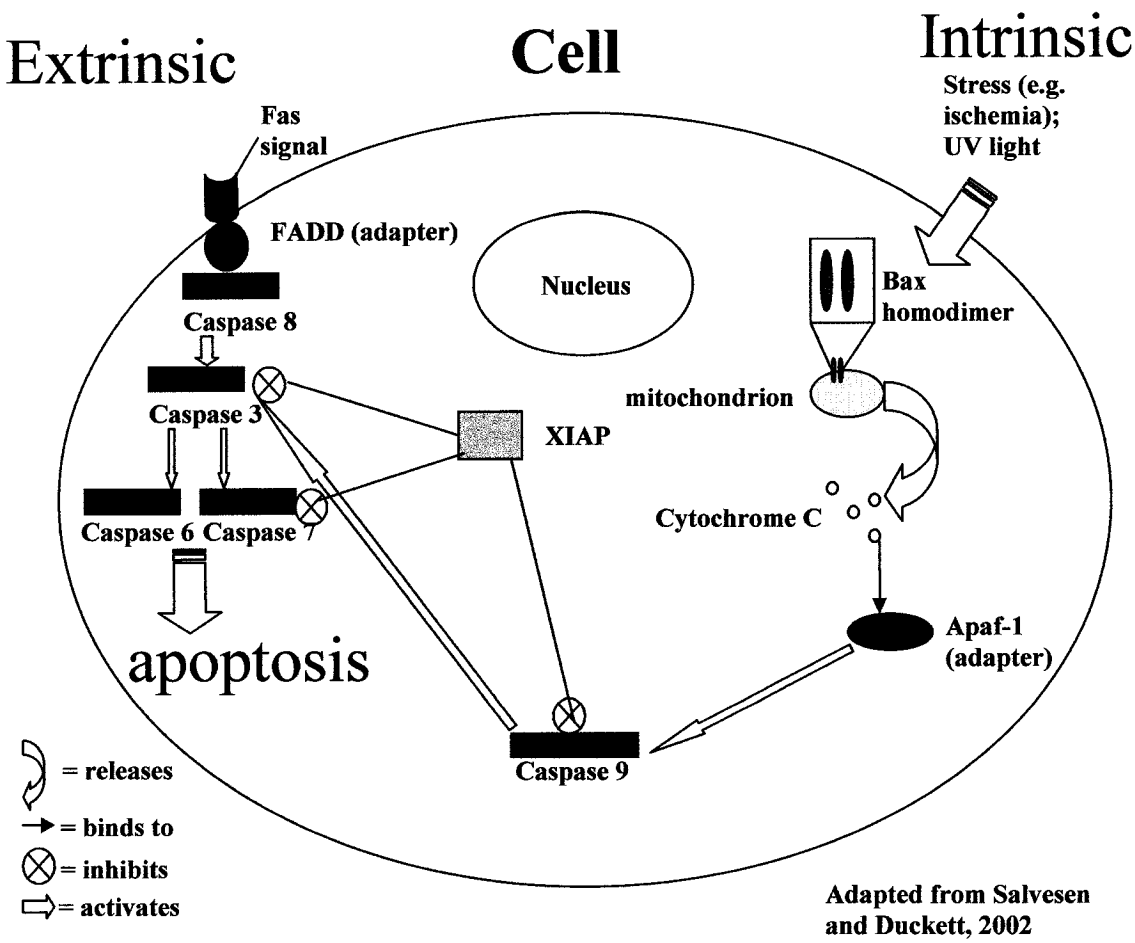
Extrinsic
Cell
Intrinsic
Fas signal
Stress (e.g. ischemia); UV light
FADD (adapter)
Nucleus
Bax homodimer
Caspase 8
Caspase 3
mitochondrion
XIAP
Caspase 6
Caspase 7
Cytochrome C
apoptosis
Apaf-1 (adapter)
Caspase 9
= releases
= binds to
= inhibits
= activates
Adapted from Salvesen and Duckett, 2002

1.5 Retinal Ischemia and Apoptosis

Apoptosis via the intrinsic pathway has been demonstrated as the underlying mechanism of cell death following transient retinal ischemia and brain ischemia (Mattson MP et al., 2001; Katai and Yoshimura, 1999; Lam et al., 1999; Rosenbaum et al., 1997). In these neuropathological cases, apoptosis is triggered by stimuli such as increased calcium ion levels, hypoxia and other processes associated with ischemia (Schulz et al., 1999; Katai N and Yoshimura N, 1999). In retinal ischemia, apoptosis can be initially detected in the GCL at 2 hpi and then in the INL 3 hours later. Apoptosis peaks at 9 hpi in the INL (Kuroiwa S et al., 1998). The key caspases involved are caspases 1, 3 and 7 (Katai and Yoshimura, 1999; Schulz JB et al., 1999). Caspase 1 is an activator protease whereas 3 and 7 are effectors (Schulz JB et al., 1999). Caspase 3 was more highly expressed in the inner nuclear layer (INL) than in the outer nuclear layer (ONL). Therefore, caspase 3 would be a key target for inhibition of apoptosis in an ischemic retina.

1.6 Current Treatments

When untreated, retinal ischemia can lead to irreversible visual loss (Kohner, 1989). Current treatments aim at reestablishing retinal circulation before the damage becomes irreversible. This is attained by a combination of a number of therapeutic regimens, including laser treatment, ocular massage, anticoagulants such as tissue plasminogen activator (t-PA), and vasodilators. However, these treatments have limited effectiveness. Laser treatment must be implemented early enough in diabetic retinopathy to be effective while ocular massage, anticoagulants, and vasodilators are only effective in CRAO patients when applied in combination to have the desired effect (www.cnib.ca; Rumelt S et al., 1999). More recent methods for emergency treatment of both CRAO and CRVO have risks associated with them such as edema, intravitreal hemorrhage, and ocular hypertension (Vallée J et al., 2002). A number of neuroprotective agents have been shown to attenuate cell death in the retina after ischemia. Brimonidine preserves retinal ganglion cells and preserves retrograde axoplasmic transport up to 2 weeks post transient retinal ischemia (2 weeks was the latest time point studied) (Lafuente MP et al., 2002). Aurintricarboxylic acid inhibits glutamate receptors thus reducing glutamate excitotoxicity and essentially apoptosis (Rosenbaum DM et al., 1997). Tumor necrosis factor is one of the many cytokines released shortly after an ischemic attack. Inhibitors of its receptor, Tumor Necrosis Factor receptor 1 (TNF-R1) reduce TNF levels and arrest apoptosis (Fontaine V et al., 2002). Insulin-like growth factor 1 (IGF-I) inhibitors act in a similar manner (Seigel GM et al., 2000). While these agents are effective, they have only been shown to target specific aspects of retinal ischemia. So, in order to rescue retinal neurons from apoptosis

after ischemia, it is most desirable to have a neuroprotectant that directly targets apoptosis itself, since it is the final stage of ischemic cell death.

Researchers have been exploring the application of caspase inhibitors (Lam TT et al., 1999; Schulz JB et al., 1999). There are 3 classes of caspase inhibitors: nuclear phosphoprotein p53, cytokine response modifier A (CrmA) and inhibitors of apoptosis. P53 is from the baculovirus, and CrmA is from the Cow Pox virus, but inhibitors of apoptosis proteins (IAPs) are the only endogenous caspase inhibitors found in a wide variety of multicellular organisms (Huang Y et al., 2003). Although IAPs are effective against their specific target caspases, there are fourteen members of the mammalian caspase family (Schultz JB et al., 1999; Villa P et al., 1997) and some are more prominent than others in different neurodegenerative conditions. Accordingly, multiple types of inhibitors would be required to have a notable effect on apoptosis. It has been demonstrated that caspase expression is cell-specific. For example, Singh and colleagues (2001) showed that caspase 2 is more prominent in the ganglion cell layer (GCL) than in the inner nuclear layer (INL), while caspase 3 was found minimally in the INL after a transient ischemic insult. So, more than one inhibitor would be required to achieve a significant neuroprotective effect in the wake of a transient ischemic insult. Moreover, the therapeutic window (time span form critical insult to the latest time point after which infarction ensues) is short (3-9 hours) for inhibiting caspases (Schultz JB et al., 1999). Therefore, a therapy is required which would either extend the therapeutic window or take full advantage of it.

Recently, inhibitors of apoptosis or IAPs have gained much attention as potential tools for gene therapy because of their impressive ability to inhibit apoptosis. IAPs have

the unique ability as endogenous repressors to inhibit the final common caspase cascade (Holcik M et al., 2001). There are several types of mammalian IAPs, and they are depicted in figure 3. All IAPs have at least one Baculovirus IAP Repeat (BIR) domain, and some have as many as three. It is by their BIR domains that the IAPs bind to and inhibit caspases. Most IAPs share one or both of two other domains: a caspase recruitment domain (CARD) and a Really Interesting New Gene (RING) Zinc finger domain (Salvesen and Duckett, 2002; Holcik M et al., 2001). It has been revealed that the BIR domains and their linker regions (in between the domains) each inhibit a different caspase. (Liston P et al., 2003). The CARD domain has the potential to mediate oligomerization and homodimerization with other CARD-containing proteins (Liston P et al., 2003; Wang J and MJ Lenardo, 2000). The RING zinc finger domain is responsible for protein degradation (via ubiquitination) of XIAP itself and of the caspases it targets (Liston P et al., 2003; MacFarlane M et al., 2002).

X-chromosome-linked inhibitor of apoptosis or XIAP is a 55 kDa protein coded by mRNA that is approximately 9 kilobases in length (Holcik M et al., 2001). XIAP, along with other members of the IAP family, can be antagonized by the second mitochondria-derived activator of caspase (Smac) via ubiquitination (Fulda S et al., 2002; Hengartner, MO, 2000). Also known as BIRC-4 or hILP, XIAP has been demonstrated to be one of the stronger apoptotic inhibitors in the family (Figure 3). It inhibits apoptosis by directly blocking the activity of effector caspases 3 and 7 and initiator caspase 9 via its N-terminal BIR domains (McKinnon SJ et al., 2002; Holcik M et al., 2001; Deveraux QL et al., 1997). The linker region between BIR 1 and BIR 2 in XIAP inhibits caspase 3, BIR 2 complexes with the N-terminus of the small subunit of caspase 7, and BIR 3 inhibits

caspase 9 (Liston P et al., 2003). Deveraux and colleagues (1998) demonstrated that XIAP almost completely prevented pro-caspase 9 processing in cytosolic extracts containing cytochrome c. Addition of cIAP1 and cIAP2 had similar effects but to a lesser extent. *In vivo* studies conducted by Katai and Yoshimura (1999) demonstrated upregulation of caspase 1 and 3 expression after retinal ischemia-reperfusion injury. Caspase 3 was more highly expressed in the inner nuclear layer (INL) than in the outer nuclear layer (ONL). Given the strong anti-apoptotic effect of XIAP against caspases 3, 7 and 9, overexpression of XIAP should be successful in protecting the retina from infarction due to transient ischemia.

Figure 3. A schematic of the IAP family members.

There are several types of IAPs in the mammalian IAP family. The structure that their proteins all have in common is the Baculoviral IAP Repeat (BIR) domain. Some members also have both the CARD domain and the Ring Zinc Finger domain.

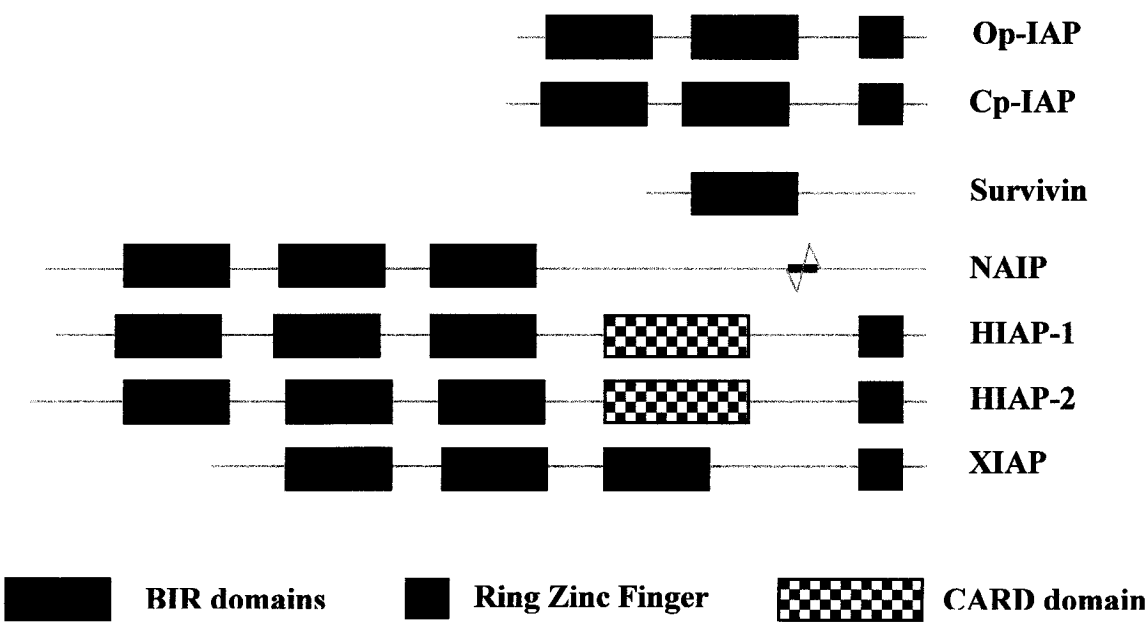
Op-IAP
Cp-IAP
Survivin
NAIP
HIAP-1
HIAP-2
XIAP
BIR domains
Ring Zinc Finger
CARD domain

1.7 XIAP and Ischemia: the precedent

It has been shown that overexpression of XIAP can protect CA1 neurons in the rat hippocampus in a transient forebrain ischemia model (Xu D et al., 1999). AV-XIAP was injected into the dorsal hippocampus of adult Wistar rats five days prior to 4-vessel occlusion (4-VO) surgery. The surgery consisted of cauterizing the vertebral arteries and loosely tying the common carotid arteries with silk ligatures. Seven days later, the transient forebrain ischemia was induced by lifting the ligatures and occluding the common carotid arteries with microaneurysm clips for 12 minutes. At 7 days post 4-VO, neuronal density was higher in the XIAP-treated hippocampus than in the LacZ-treated hippocampus. Xu and his colleagues also demonstrated that apoptosis was actually in effect in their transient forebrain ischemia model. They showed increased levels of effector caspase-3, which preceded evidence of DNA fragmentation, a typical morphological trait of an apoptotic cell. Therefore, Xu and his colleagues were able to show that XIAP attenuates apoptosis in ischemic CA1 neurons of the hippocampus.

McKinnon and colleagues (2002) clearly demonstrated that XIAP can also protect optic nerve axons in a chronic hypertensive model. Adult Norway rats were intravitreally injected in their right eyes with AAV-BIRC4 (also known as AAV-XIAP) or AAV-GFP. One month later, chronic hypertension was induced by injecting hypertonic saline in the limbal area (where the cornea meets the sclera) of the right eye, causing an increase in intraocular pressure (as seen in some human glaucoma patients). Retinal ganglion cell loss was assessed by TUNEL analysis of sectioned retinas and by counting axons in optic nerve cross-sections. While there were many TUNEL positive cells in the AAV-GFP-transduced retinal ganglion cells, there was only background

fluorescence in the retinal ganglion cell layers of the AAV-XIAP-transduced retinas. On average, 50% of the optic nerve axons were protected. Therefore, McKinnon and colleagues showed that overexpression of XIAP protects optic nerve axons from death due to glaucomatous conditions. Overall, both studies showed that when XIAP is overexpressed in degenerating neuronal tissue, cell death is slowed down and the tissue is protected from being seriously compromised further.

1.8 Hypothesis

It has been established that apoptosis is the underlying process for cell death after ischemia in the brain and retina. Moreover, XIAP-mediated gene therapy has been shown to protect brain neurons. Therefore, in principle, XIAP should also protect retinal ganglion cells from ischemic cell death. To prove this, an acute ischemia rat model was designed in which ischemia was induced by increasing intraocular pressure. This led to the collapse of the central retinal artery (CRA). The effects of XIAP-mediated therapy were evaluated in this ischemic model using electrophysiological and histological methods.

Chapter 2. METHODS

2.1 Animals

Male Sprague-Dawley rats (Charles River) were obtained at 75-100 g and maintained in the University of Ottawa Animal Care facility on a 12h light-12h dark cycle. The Association of Research in Vision and Ophthalmology (ARVO) guidelines were adhered to throughout the experiment. The rats were separated into two major groups: those that would receive the gene therapy (XIAP; N=22 rats) and those that would receive the placebo (GFP; N=22 rats). Within each group, three time-points were represented: t = 4 weeks post-ischemia (N=13), t = 24 hours post-ischemia (N=6), and t = 0 hours post-ischemia (N=3). Three additional rats from each group at t = 0 hpi were set aside for Western blot analysis.

2.2 Adeno-associated Virus (AAV)

The adeno-associated viral vectors were prepared by William Hauswirth's lab, Gainesville, Florida. A cDNA construct, coding for the full open-reading frame of XIAP with a hemagglutinin (HA) tag at the N-terminal, was inserted into a pTR vector under the control of the chicken β-actin promoter, which supports XIAP expression in all cell types. Similarly, a GFP construct was generated for use as a negative control. Recombinant AAVs of serotype 2 were packaged, purified, concentrated and titered to between 2 $x10^{13}$ and $4x10^{13}$ physical particles/mL for AAV-GFP and $4x10^{13}$ physical particles/mL for AAV-XIAP. For every 100 particles, approximately one was infectious. A mini-adenovirus helper plasmid, pDG was used to produce AAVs which were free of contaminating adenoviruses or wild-type AAV.

2.3 Intravitreal Injections

Intravitreal injections were done as per the protocol of Timmers (2001). Rat eyes were dilated using a mydriatic: 1% Mydriacyl (Alcon), and vasoconstrictor/mydriatic: 2.5% Mydfrin (Alcon). When the eyes were fully dilated, topical anaesthetic (Alcaine, Alcon) was applied to the right eye. Maxitrol (Alcon), an ophthalmic, anti-inflammatory antibiotic ointment was added to the contralateral eye to keep it hydrated throughout the procedure. The rat was anaesthetized with Halothane in O_2. The cornea of the right eye was punctured with an insulin syringe. The virus was delivered using a blunt-end 33-gauge needle attached to a Hamilton syringe. The needle was maneuvered through the anterior chamber, and around the lens to get to the ventral nasal quadrant of the vitreous humour. 2 μL of the viral mixture (2 μL of fluorescein in 48 μL of virus) was delivered, and the needle was withdrawn. After injection, the right eye was treated with Maxitrol and the animal was left in an oxygenated incubator to recover from anesthesia.

2.4 Transient Retinal Ischemia

Six weeks after the viral injection, ischemia was induced in the right injected eye of each rat. To achieve this, each rat was anesthetized with Halothane in O_2 prior to and during ischemia. Their eyes were dilated with 1% Mydriacyl and 2.5% Mydfrin. Alcaine, a topical anesthetic, was applied to the cornea of the eye. A 30 gauge needle was attached by intravenous tubing to a saline reservoir and a manometer to measure pressure. The anterior chamber of the right eye was cannulated by inserting the 30.5-gauge needle into the anterior chamber, and stabilizing both the tubing and needle with plasticine. The intraocular pressure (IOP) was raised to 110 mm Hg ±2 by raising the saline reservoir and maintained at that level for 60 min. Ischemia was confirmed by loss of redness in vasculature of the iris and in the posterior chamber of the eye. The right eye was kept hydrated using Gonak, a gonioscopic solution from Alcon. Approximately 5 minutes before the end of the 1-hour ischemia, the Halothane was reduced to facilitate a rapid recovery from the anesthetic. After one hour of ischemia, the pressure in the eye was allowed to return to normal and the needle was removed. Maxitrol was applied to the eye and the rat was left to recover in an oxygenated incubator before being returned to the post-operating room.

2.5 Electrophysiology

2.5.1 Scotopic-Photopic Electroretinography

Full-field scotopic-photopic electroretinograms were generated using the Espion system (Diagnosys LLC, Littleton). Rats were dark-adapted overnight. In the dark, rats were injected intraperitoneally with a combination of sedative/analgesic and general anesthetic. Their pupils were dilated by applying Mydriacyl (Alcon) to the corneal surface. The corneal surface was anaesthetized with Alcaine (Alcon). A platinum electrode was applied, touching the center of the cornea of each eye. The ground and reference electrodes were placed in the tail and mouth respectively. The eyes were hydrated and contact between the electrode and cornea was optimized using Gonak (Alcon). The animal's head was positioned beneath a Ganzfeld apparatus. Pulse flashes of white light, four milliseconds in duration, were generated at a frequency of 1 Hz. Responses from the retinal cells were tested at eleven different light intensities: 0.001, 0.0025, 0.006, 0.016, 0.04, 0.1, 0.25, 0.63, 4, 10, and 25 Candela seconds per meter squared ($Cd \bullet s/m^2$). The Espion system (Diagnosys LLC) was used to record the ERG response from the retina to the light stimulus. ERGs were recorded 4 weeks after injection (2 weeks prior to ischemia), and 24 hours, 2 weeks and 4 weeks after ischemia. Five representative ERG traces were obtained and averaged for each luminance step. The a- and b-wave amplitudes were identified by visual inspection and re-selected to ensure both consistency and accuracy. The a-wave amplitude measures the difference in potential between the baseline and the lowest point of the a-wave trough. The a-wave cursor was therefore placed at the lowest point of the a-wave trough following the flash stimulus. The b-wave amplitude measures the difference in potential from the trough of

the a-wave to the peak of the b-wave. For consistency, the b-wave marker was always placed on the 5th oscillatory potential following the a-wave. The peak latency and amplitude of each a- and b-wave was then measured at these points.

2.5.2 30 Hz Flicker Electroretinography

Pulse flashes of white light (6500 Kelvins) were applied at a frequency of 30.03 Hz and an intensity of 5 Cd•s/m^2 only. One tracing was obtained for each rat at each time-point. Response to 30 Hz flickering light was measured in a manner similar to that of the 1-Hz flash for the scotopic-photopic ERG. In essence, the initial trough and peak following stimulus presentation was identified.

2.5.3 Exclusion Criteria

A rat whose right eye did not receive a proper injection (i.e. lens, retina or iris was severely nicked), whose eye did not whiten during the ischemia, or who developed lens or corneal cataracts were excluded. In addition, rats which showed significant differences between the right and left eye based on flicker or full-field ERG, before the ischemia was delivered, were also excluded.

2.6 Perfusion

Rats were given a lethal dose (1 mL) of Somnitol (sedative-anaesthetic, 65mg/mL, MTC-Pharmaceuticals) and the thoracic cavity was opened by first making an incision at the sternum, using surgical scissors. From that incision point, the skin and visceral tissues were cut laterally and then upwards. Using smaller scissors, the diaphragm was cut open, exposing the lungs and the heart. The resulting flap was held back with a hemostat clamp. Then, the descending aorta was clamped with another hemostat clamp to prevent blood from flowing to the lower half of the body. A 23- or 25-gauge needle was attached to an intravenous tube. The tube was threaded through a peristaltic pump and the other end was placed in a 50-mL centrifuge tube filled with 1xPBS (phosphate-buffered saline). The line was flushed through with 1xPBS to ensure that there were no bubbles trapped within. The needle was inserted into the left ventricle of the heart, and a small incision was made in the right atrium using fine surgical scissors. The pump was turned on and approximately 15-20 mL of 1x PBS were pumped through at a flow rate of 5 mL per minute to flush out the blood from the upper body. When the fluid flowing out of the heart was pale pink, it was an indication that all the blood had been flushed out. The tube was placed in a 50-mL centrifuge tube filled with pre-cooled 4% paraformaldehyde (PFA) in 1x PBS and approximately 20 mL were pumped through the upper body also at a flow rate of 5 mL per minute.

2.7 Sampling

Eyes were scored at the nine o'clock position, on the sclera and the cornea (the optic nerve being the six o'clock position) using a hot, 18-gauge needle. Then the eyes were removed by cutting through the conjunctiva and extra-ocular muscles and releasing the eyeball and optic nerve from the distal end of the optic nerve (near the optic chiasm). A small hole was made in the cornea using a needle and a pair of fine surgical scissors to allow penetration of the fixative, and the eyes were placed in labelled cryovials filled with 4% PFA. The optic nerve stalks were removed just below the optic nerve head, leaving a stalk less than 5 mm in length. The optic nerves were sampled only at the 4-week time point. The eyes were fixed in PFA for 1 hour, while the optic nerve stalks were fixed for at least 4 hours. After fixation, the lenses were removed and the eyes were incubated in 30% sucrose overnight. This was followed by incubation in 50:50 OCT: 30% sucrose for 2-3 hours, after which the eyes were oriented in small plastic trays using the score marks, and embedded by freezing in liquid nitrogen. The frozen samples were stored in a - 80°C freezer. Samples were sectioned in the saggital plane using a Shandon Electronic Cryotome at -25 to -28°C. Five sections were obtained per slide, and each section was 10 microns thick.

2.8 Western Blot Analysis

Three rats from the T=0 time point subset of each group, XIAP and GFP, were injected with a fatal dose of Somnitol (between 1 and 2 mL), and asphyxiated in a carbon dioxide chamber. Their eyeballs were clamped at the base of the optic nerve using a hemostat clamp. A small hole was made by piercing the cornea with an insulin syringe, raising the cornea, and cutting underneath the shaft of the needle using corneal scissors. A bit of vitreous was let out by gently squeezing the eye with forceps. The lens was removed using the same forceps, and the retinal tissue (approximately 15 mg) was squeezed out and immediately placed in a frozen culture tube. The culture tubes were kept on dry ice and transported to the -80 °C freezer for storage. The instruments used to extract the retina were sterilized with 100% ethanol and deionized-distilled water prior to extraction from each eye.

The retinal explants were individually homogenized in RIPA Buffer (50 mM Tris HCl at pH 7.4, 150 mM NaCl, 1mM EDTA, 1mM NaF, 1 mM vanadate, 1% Noniodet P-40, 0.25% Na-deoxycholate, 1x Leupeptin, 1x Aprotinin, 1x PMSF) using a sonicator set at 20% amplification. The homogenates were placed in their respective 1.5 mL eppendorf tubes, rocked for 1 hour at 4°C, and then centrifuged for 15 minutes at 4°C and 13 000 RPM. The supernatant, which contained the total protein, was collected. The protein concentration of each sample was determined using the DC assay. Total protein (40 μg) and Precision Plus Dual Color Standard (BIORAD) were run on a 10% sodium dodecyl sulfate-polyacrylamide gel electrophoresis (SDS-PAGE) gel at 50 mAmps until the dye front ran off the gel. GFP samples were re-run alone on a 12% gel (20 μg per sample). The protein was then transferred onto immobilon-P membranes

(polyvinylidene difluoride, PVDF membranes from Millipore). The membrane was probed with primary antibodies to GFP (rabbit anti-GFP IgG, Molecular Probes), or XIAP (rabbit GST-XIAP), both courtesy of Dr. Peter Liston. The secondary antibodies used were goat anti-rabbit IgG peroxidase (Jackson ImmunoResearch Laboratories) and donkey anti-rabbit-horseradish peroxidase (courtesy of Dr. Peter Liston) respectively. All of the above antibodies were diluted 1:2000. Protein detection was achieved using an enhanced chemiluminescence (ECL) detection kit (Amersham Biosciences).

2.9 Histochemical Analysis

2.9.1 Haematoxylin and Eosin Staining

Haematoxylin and Eosin staining was conducted on cryosections of rat eyes (four slides were selected per sample). Briefly, the frozen slides were brought to room temperature by leaving the slide boxes on the bench for 30 minutes. Then the slides were selected, quickly dipped in distilled water and air-dried for 2 minutes. Then the sections were fixed for 3 minutes in 4% PFA in 1x PBS. The fixative was washed out using running tap water for 5 minutes. The sections were then stained in filtered Harris Haematoxylin (acidified) (ThermoShandon, #6765004)) for 30 to 45 seconds, depending on how many times that stain had been used previously. The slides were then rinsed in running tap water for approximately 2 minutes, and dipped in 70% ethanol with hydrochloric acid (5 drops of glacial HCl for every 250 mL of 70% ethanol) 3 times to differentiate. The ethanol or anhydrous ethyl alcohol (4L) was obtained from Commercial Alcohols Inc., Brampton ON. Then the slides were dipped in tap water 3-5 times, dipped in Lithium carbonate (3g in 300 mL of deionized distilled water, diluted 1:2 in deionized distilled water) 3-5 times to differentiate the tissue by changing the colour of the haematoxylin. The slides were rinsed in tap water for 10 minutes and then stained for 1 minute in Eosin. Eosin stain was prepared by combining 1g Eosin Y with 200 mL of deionized-distilled water and 0.5 mL of glacial acetic acid (BDH, Toronto ON) for every 100mL of stain. Following the Eosin stain, the sections were dehydrated in 50% ethanol for 1 minute, 70% ethanol for another minute, and dipped 3 times in 95% ethanol. Then the sections were further dehydrated by dipping the slides 5 times in 100% ethanol, and immersing them twice more in 100% ethanol (2 x 1 minute). Finally,

the slides were immersed in Xylenes (histology grade, EMD, #XX0060-4) 3 times (1 x 1minute, and 2 x 2minutes), mounted in Permount (Fisher Scientific) and cover-slipped. Images of the retinas were obtained at approximately 440 and 1320 microns from the optic nerve head at 40x magnification using a Zeiss Axioskop light microscope with a Zeiss AxioCam HRc camera. The inner nuclear layer (INL) and ganglion cell layer (GCL) cells were counted by four unbiased, independent observers.

2.9.2 TUNEL Analysis

TUNEL (TdT-dUTP terminal Nick End Labelling) analysis was conducted on eye sections at 24 hours post ischemia (hpi). Slides were selected appropriately and then dipped into distilled water and air-dried for 2 minutes. The cryosections were then fixed in 1% PFA in 1x PBS (diluted from 4% PFA) for 10 minutes at room temperature. The slides were then rinsed 1xPBS (2 x 5 minutes), and post-fixed in pre-cooled (-20°C) Ethanol: Glacial Acetic Acid (2:1) for 5 minutes. Then, the slides were incubated in Proteinase K (20 ug/mL) for 15 minutes at room temperature. The remnant proteinase K was rinsed out with 1xPBS (3 x 1 minute). The slides were then incubated in terminal transferase reaction mixture for 1 hour at 37°C (approx. 50 uL per slide; slides were covered with plastic coverslips). The terminal transferase reaction mixture consisted of the following: 2 uL of Terminal Deoxynucleotidyl Transferase (TdT), recombinant (10533-065, 500 U, 15 U/uL. Invitrogen), 0.25 uL Digoxygenin-11-dUTP (1 093 088, 25 nmol/25uL, 1mM, Roche), 20 uL 5x Buffer (included in TdT kit), and 70 uL of distilled water. After 1 hour, the TdT reaction was stopped by washing the slides for 10 minutes in 1xPBS at room temperature. The slides were then incubated in Anti-digoxygenin

fluorescein (#1 207 741, 200 ug, Roche; diluted 1:100) for 30 minutes at room temperature. The anti-digoxygenin bound to the digoxygenin-tagged dUTPs that were added to the ends of the fragmented DNA (Kuroiwa S et al., 1998). This was followed by four 2-minute rinses in 1xPBS to remove any unbound anti-digoxygenin antibodies. The sections were then counter-stained for 3 minutes, at room temperature, with 4', 6-Diamindino-2-phenylindole dihydrochloride (DAPI) (D9542, Sigma-Aldrich) diluted that had been diluted 1:750 000 with 1xPBS. This was followed by two 5-minute washes with 1xPBS. The slides were mounted with Antifade (50:50 1xPBS:Glycerol, BDH, B10118-76 and 1% N-propyl gallate). Slides of right eye sample tissue that were treated without the TdT enzyme served as negative controls for TUNEL assays. Slides of left eye tissue samples treated with the complete TUNEL reaction mixture served as negative controls for ischemia-induced apoptosis.

2.9.3 1% Toluidene Blue Staining of Optic Nerve Cross-sections

Optic nerve stalks from animals sacrificed 4 weeks post ischemia were fixed in 4 % PFA for at least 4 hours, rinsed in 1x PBS and treated with osmium tetraoxide (OsO_4). The stalks were embedded in Epon and sectioned at 0.5 microns. Five sections were obtained per slide, one slide for each sample. The sections were stained with 1% Toluidene Blue and coverslipped. Sections were viewed at 10x, 40x and 63x magnification under the Zeiss Axioskop light microscope. Images were obtained using a Zeiss AxioCam HRc camera. The optic nerve cross sections were semi-quantitatively analyzed using a method developed by Dr. Balwantray Chauhan and his associates (unpublished). This method is described in the results. The areas of the cross-sections

were also calculated. The cross-sectional shape of each optic nerve was treated as an ellipse.

2.10 Statistical Analysis

Student's T-Test was used to compare the electrophysiology data as well as mean axon counts from histological analysis of optic nerve cross-sections. A one-tailed distribution curve for comparing groups of unequal sample variance was applied and a P values less than 0.05 were considered significant. Comparisons were made between the experimental and control group. One-way analysis of variance (ANOVA) was conducted on the cell counts obtained from histological analyses of retinal cross-sections. The standard error of the mean (SEM) was obtained for all averages. Naka-Rushton analysis was conducted on the electrophysiology data as well to evaluate the responsiveness (Rmax) of the retina. One-way analysis of variance (ANOVA) was conducted on Rmax ratios (right eye versus left eye).

Chapter 3. RESULTS

3.1. Verification of Overexpression

Western analysis of retinal protein extracts show that the chicken-beta actin-driven AAV vector overexpresses XIAP in the rat retina. In figure 4, this is shown by the higher intensity of the signal in the lane representing the XIAP-treated eye relative to those representing a GFP-treated and non-injected eyes, and contralateral (non-ischemic) controls. In other words, exogenous XIAP was overexpressed above endogenous levels. Expression of GFP in retinal protein extracts was also verified by Western immunoblot analysis (not shown). The presence of GFP protein in the GFP-treated retinas, and the lack thereof in the control retinas (left eyes) indicated that the GFP transgene was being expressed. Expression of GFP was also driven by the chicken-beta actin promoter.

Figure 4. Western blot of total protein extracted from rat retina. Protein extract from a XIAP-treated, GFP-treated and non-treated rat are presented below. Equal amounts of total protein (40 ug) were loaded into each lane. The membrane was probed with a rabbit anti-GST-XIAP antibody, which annealed to both the AAV-XIAP transgene as well as the endogenous rat IAP (RIAP3). Overexpression is indicated by the higher intensity of the band in the lane representing the AAV-XIAP-injected eye relative to the control eye. Tx = treatment. Relevant bands are indicated by a black arrow.

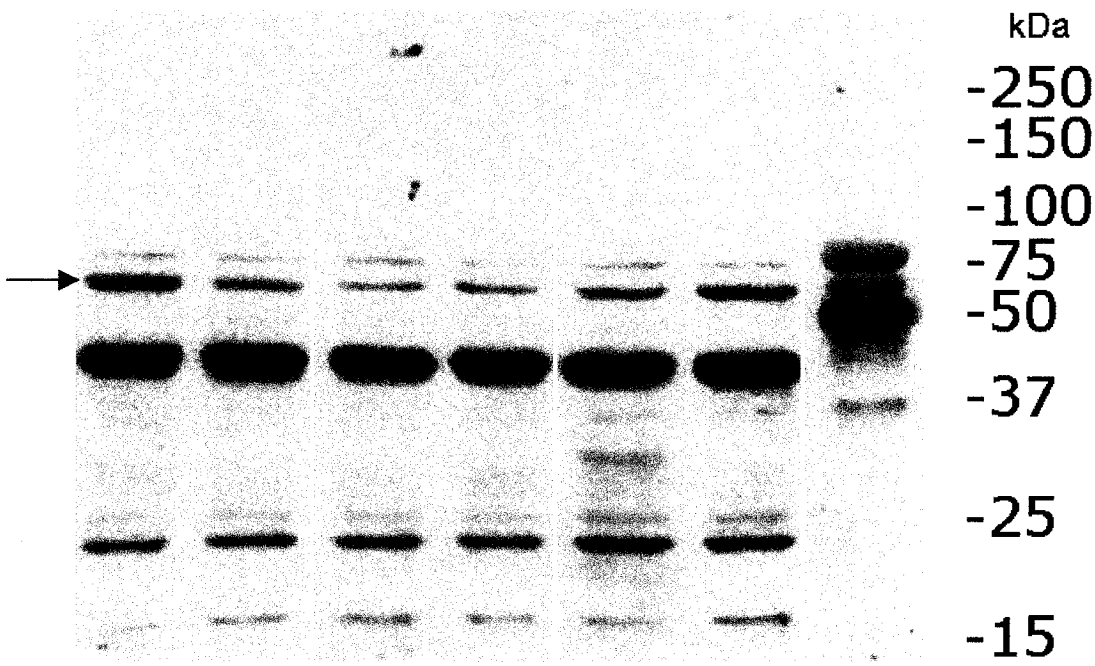
kDa
-250
-150
-100
-75
-50
-37
-25
-15

3.2 Electrophysiology

There are two main components to a full-field, light evoked electroretinogram or ERG: a negative a-wave followed by a positive b-wave (figure 5). Hyperpolarization of the rod and cone photoreceptors generates the negative a-wave. Depolarization of the bipolar cells and Müller cells contributes to the positive b-wave (Ogden TE, 1989). Oscillatory potentials are found on the ascending limb of the b-wave. These are indicated by dotted arrows in figure 5. Bipolar cells have been hypothesized as the most likely generators of oscillatory potentials (Wachtmeister L, 1998). Together, these components contribute to the ERG waveform.

Scotopic-Photopic ERGs were performed bilaterally on rats in both the XIAP and GFP groups prior to ischemia (Baseline or T=0), 24 hours post ischemia (hpi), 2 weeks post ischemia (wpi) and 4 wpi. "Scotopic-Photopic" indicates that the retina was tested in both dim and bright conditions respectively. Light intensity varied as follows: 0.001, 0.0025, 0.006, 0.016, 0.04, 0.1, 0.25, 0.63, 4, 10, and 25 Candela-seconds per meter squared ($Cd \bullet s/m^2$). The left eye was used as an internal/contralateral control since it was neither injected nor rendered ischemic. On average, 5 traces were obtained and the mean trace was taken for each luminance step.

When a retina which has received an ischemic insult is tested by electroretinography (ERG), the a-wave is maintained while the b-wave is markedly reduced or extinguished (Figure 5). Figure 6 depicts the ERGs of two sample rats at 4 wpi: a GFP-treated rat (figure 6A) and a XIAP-treated rat (Figure 6B). Note that the

Figure 5. Scotopic-photopic ERG traces of a GFP-treated rat at 24 hours post-ischemia. The right eye (OD) is represented by a blue trace while the left eye (OS) is represented by a red trace. These traces were obtained at a light intensity of 0.25 Candela- seconds per m^2. The a-wave amplitude was measured from baseline (0 μV), which was the first data point in the series, to the lowest point of the trough (indicated by solid arrow). The b-wave was measured from the bottom of the a-wave to the peak of the 5th oscillatory potential (indicated by dashed black arrow). Two oscillatory potentials are indicated by dotted arrows. Amplitude is measured in microvolts (μV), while latency is measured in milliseconds (ms).

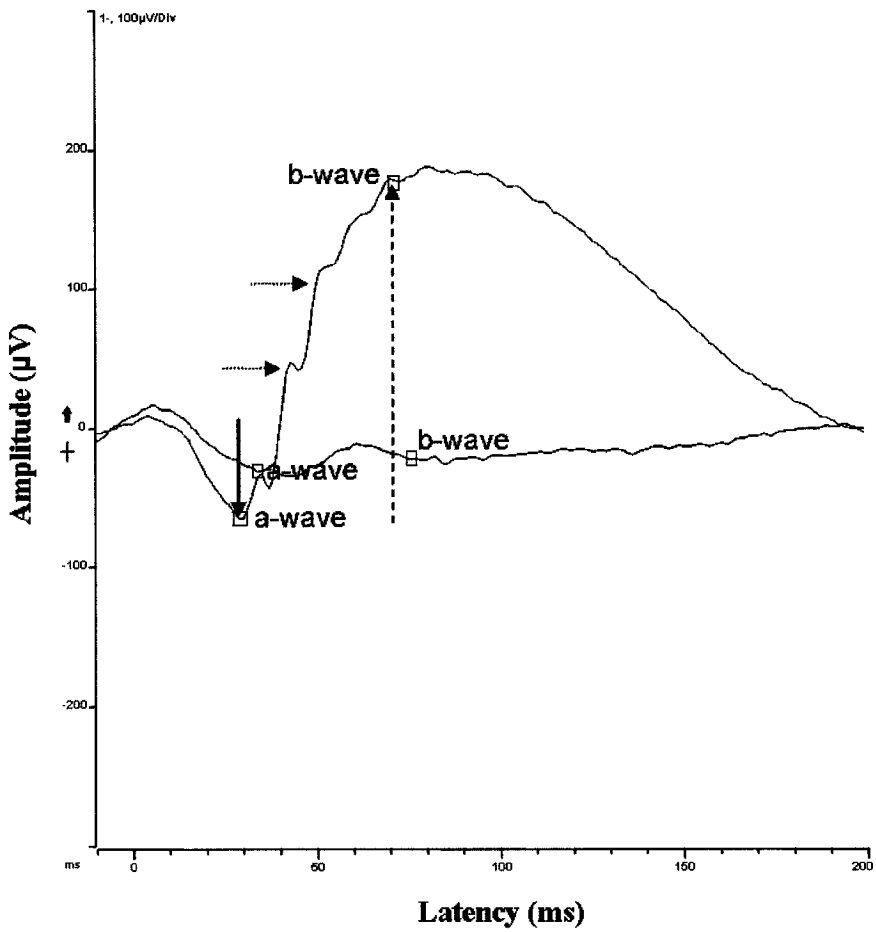
1-, 100µV/Div
200
100
0
-100
-200
ms
0
50
100
150
200
b-wave
b-wave
a-wave
a-wave
Amplitude (µV)
Latency (ms)

Figure 6. Scotopic-photopic ERG traces of a XIAP- and a GFP-treated rat. The ERGs for the GFP-treated rat are represented in (A), and those of the XIAP-treated rat are in (B). Both sets of traces were obtained at 4 weeks post-ischemia. The luminance (or light intensity) was measured in Candela-seconds per meter squared (Cd•s/m2). The latency was measured in milliseconds (50 ms per division on axis). OD = right eye; OS = left eye.

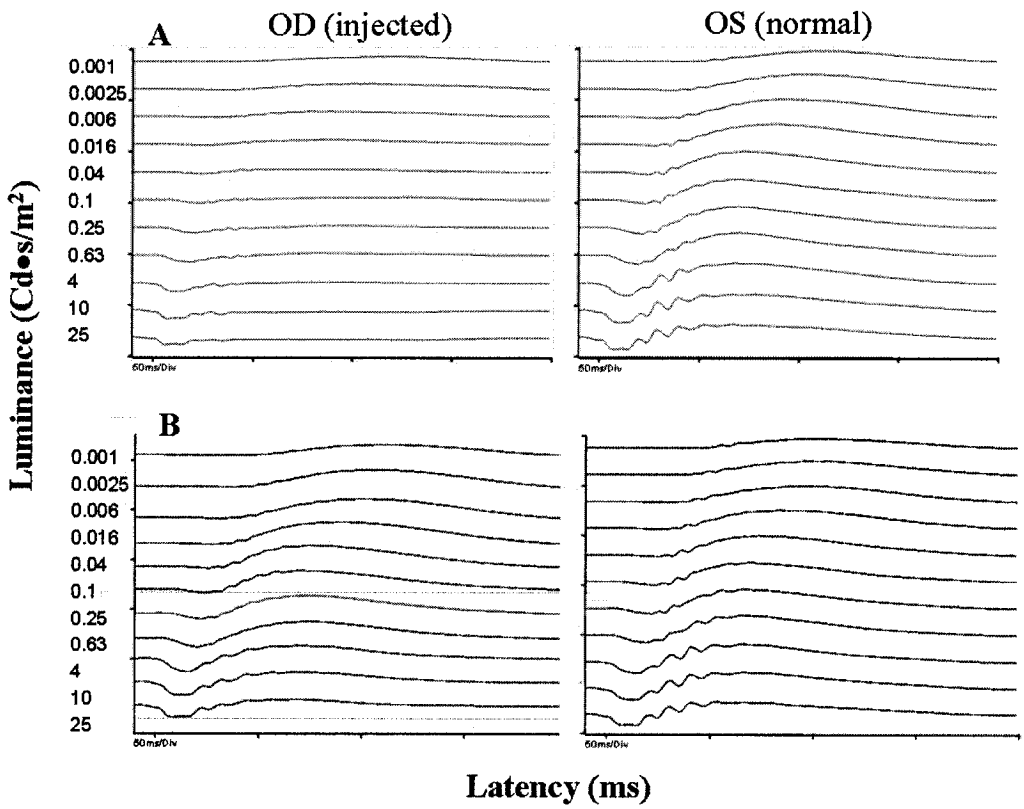
A
OD (injected)
OS (normal)
0.001
0.0025
0.006
0.016
0.04
0.1
0.25
0.63
4
10
25
50ms/Div
B
Luminance (Cd•s/m²)
Latency (ms)

GFP-injected right eye (OD) responds poorly at all light intensities. The a-wave appears normal but the b-wave is extinguished compared to the normal eye (OS). The XIAP-injected eye (see Figure 6B), on the other hand, showed a prominent b-wave similar to the control eye.

To statistically determine how well the b-wave amplitude was preserved, the b-wave amplitude of the treated eye (conventionally the right eye) was divided by that of the contralateral eye to give a b-wave amplitude ratio (OD:OS). The closer the ratio was to 1.0 the better the preservation of the b-wave amplitude in the XIAP-treated eye. These ratios were averaged across groups of animals and plotted against light intensity. Figure 7 shows these plots at 24 hours post-ischemia (hpi), 2 weeks post-ischemia (wpi) and 4 wpi. ERG amplitude ratios for the lowest light intensity were omitted due to variability in those ERG waveforms produced from low-level stimulation. At 24 hpi (Figure 7A) we observed that the XIAP-treated eyes possessed b-wave amplitude ratios that were closer to 1.0 in comparison to the GFP-treated controls. The two groups were significantly different for all except the lowest three intensities: 0.001, 0.0025, and 0.006 $Cd \bullet s/m^2$. At 2 wpi (Figure 7B), while the trend was similar to that found at 24 hpi, the two groups were not significantly different. At 4 wpi, the average b-wave amplitude ratio of the XIAP-treated group was significantly higher than that of the control group at the two highest light intensities (Figure 7C). Again, the trend noted in two previous graphs was maintained. Therefore, over increasing luminance, the XIAP-injected eye responded relatively better compared to the contralateral eye as demonstrated by the higher b-wave amplitude ratios relative to those of the GFP-injected eyes, which did not respond very well.

Figure 7. Comparison of average b-wave amplitude ratios. B-wave amplitudes at 24 hours (A), 2 weeks (B) and 4 weeks (C) post-ischemia were averaged for each eye of each rat in both groups (XIAP and GFP). The ratios were obtained by dividing the average value for the ischemic eye (conventionally the right eye) by that of the normal eye. The ratios were pooled and means (error bars = ± 1SEM) were calculated for each luminance step within each group. Student's T-test was conducted between the XIAP and GFP groups at each time point. Significant differences at $P<0.05$ are indicated by a star. Luminance steps 2 through 11 (inclusive) represent light intensities 0.0025, 0.006, 0.016, 0.04, 0.1, 0.25, 0.63, 4, 10, and 25 Candela seconds per meter squared ($Cd \bullet s/m^2$). The first luminance step (0.001 $Cd \bullet s/m^2$) was omitted due to high variability.

A

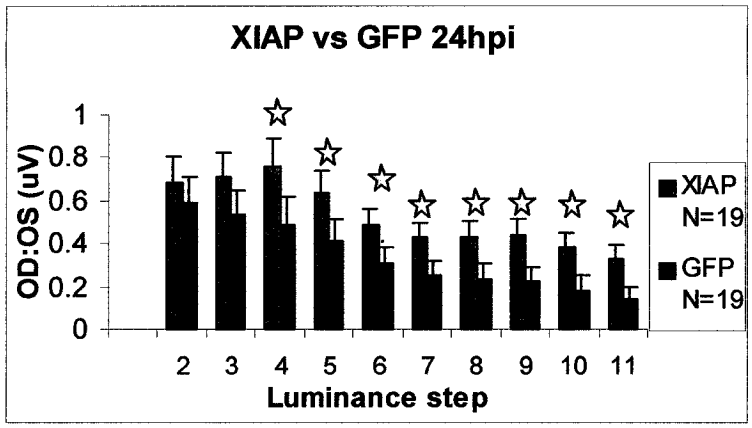
XIAP vs GFP 24hpi
OD:OS (uV)
1
0.8
0.6
0.4
0.2
0
2 3 4 5 6 7 8 9 10 11
Luminance step
XIAP N=19
GFP N=19

B

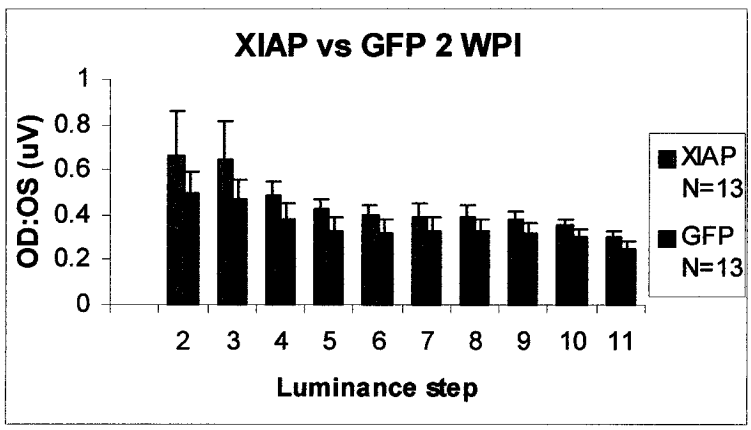
XIAP vs GFP 2 WPI
OD:OS (uV)
1
0.8
0.6
0.4
0.2
0
2 3 4 5 6 7 8 9 10 11
Luminance step
XIAP N=13
GFP N=13

C

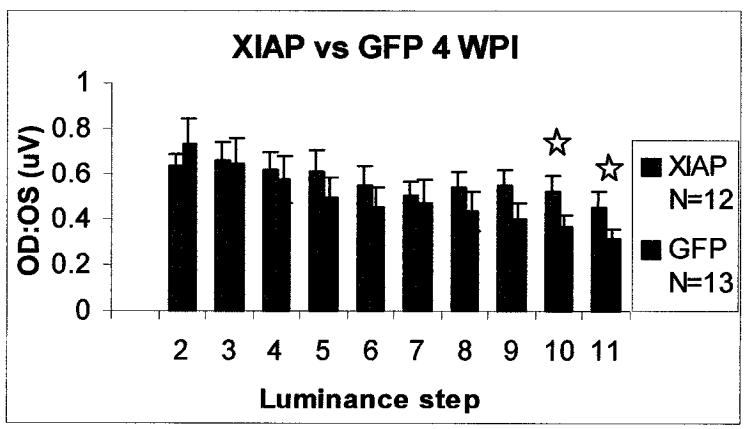
XIAP vs GFP 4 WPI
OD:OS (uV)
1
0.8
0.6
0.4
0.2
0
2 3 4 5 6 7 8 9 10 11
Luminance step
XIAP N=12
GFP N=13

A related test, called the flicker ERG, was also performed. The protocol followed was the same as that for the scotopic-photopic ERG with a couple of exceptions. First, only one level of light intensity was applied: 5 $Cd \bullet s/m^2$. Second, the frequency at which the light was flashed was 30.03 Hz, which was 30 times greater than the frequency of the scotopic-photopic ERG flash. The ratios (OD:OS) of flicker ERG amplitude, as well as those of latency, were plotted over time: baseline (T=0), 24 hpi, 2 wpi, and 4 wpi. These ratios are depicted in Figure 8. Although the amplitude ratio (μV) was substantially lower 24 hours following ischemia in all the rats, when compared to the baselines, the ratios increased over time (figure 8A). There was no significant difference between the two groups at any of the time points studied.

The latencies were compared in a similar manner. The average latency for the XIAP-treated group at 24 hpi was lower relative to the GFP-treated group, suggesting a better response from the XIAP-treated retinas. In other words, the GFP-treated retinas exhibited a slight delay in response relative to the XIAP-treated retinas. This difference, however, was statistically insignificant (Figure 8B). Nevertheless, the latencies for both groups remained stable. When the flicker data were compared between the time points, however, there was a significant increase in average amplitude ratio for the XIAP group from 24 hpi to 4 wpi.

Figure 8. Ratios of flicker ERG amplitudes and latencies. Amplitude (A) was measured in milliseconds and latencies (B) were measured in microvolts at 24 hours post-ischemia (hpi), 2 weeks post-ischemia (2 wpi), and 4 wpi. Error bars = ± 1SEM. A yellow star denotes significance ($P<0.05$). Flashes of white light were applied at a frequency of 30.03 Hz with an intensity of 5 candelas seconds per m^2. Because of the high frequency and light intensity, flicker ERG tests were performed immediately after the scotopic-photopic ERGs were obtained. XIAP: Baseline N=19, 24 hpi N=14, 2 wpi N=13, and 4 wpi N=12. GFP: Baseline N=19, 24 hpi N=15, 2 wpi N =13, and 4 wpi N=13. Student's T-test was applied to determine significance between the XIAP and GFP groups as well as between time points within each group. Significance difference at $P<0.05$ is indicated by a star.

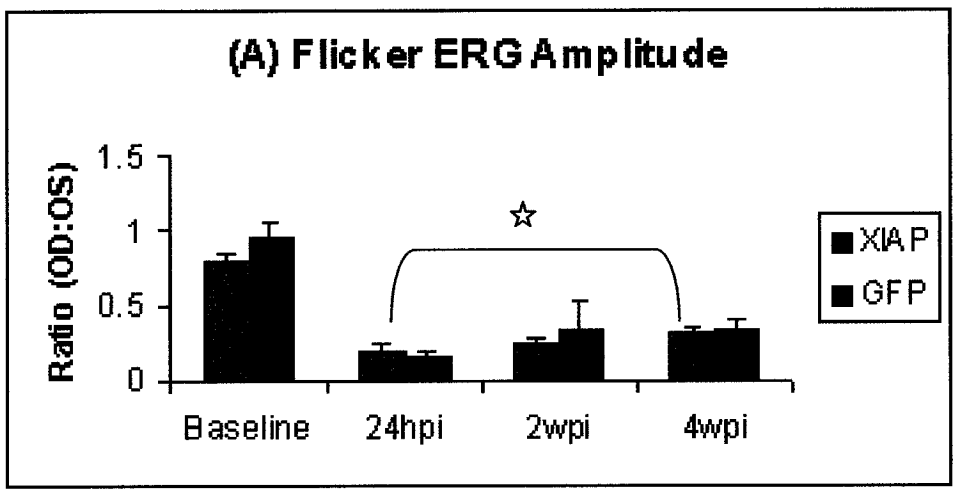
(A) Flicker ERG Amplitude
Ratio (OD:OS)
1.5
1
0.5
0
Baseline
24hpi
2wpi
4wpi
XIAP
GFP

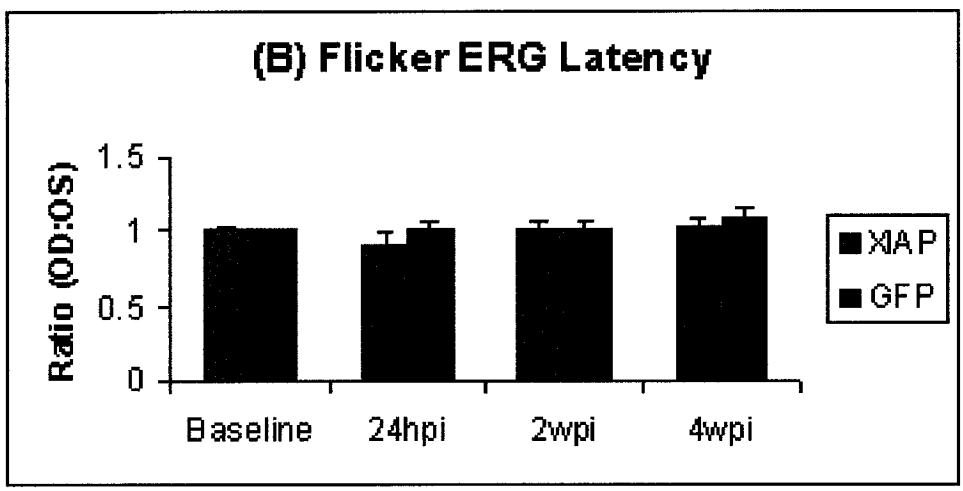
(B) Flicker ERG Latency
Ratio (OD:OS)
1.5
1
0.5
0
Baseline
24hpi
2wpi
4wpi
XIAP
GFP

3.3 Naka-Rushton Analysis

The Naka-Rushton fit is a non-linear regression analysis that mathematically models the relationship between retinal responsiveness/sensitivity and light intensity. A standard Naka-Rushton fit takes on a sigmoid shape with three main parameters: Rmax, K, and n, which are depicted in Figure 9A. Rmax represents the maximum electrical response obtainable from the retina and the minimum light intensity required for that response. K is a constant that represents the intensity at half saturation (i.e. the semi-saturation constant). The n represents the slope of the curve at that mid-point (Breton ME at al., 1991). This analysis was conducted on the average b-wave amplitudes from both XIAP and GFP groups at all four time points (T=0, 24hpi, 2wpi and 4wpi). Figure 9B and C depict the responsiveness and sensitivity of a XIAP- and a GFP-injected retina respectively over time. In Figure 9B, the baselines of both the left and right eyes of each animal show that there is little difference between the two eyes. When the baseline plots were compared to those at 24 hpi, it was evident that the responsiveness decreased substantially for these two particular animals shortly after ischemia. However, at 2 wpi and then at 4wpi, the response improved in the XIAP-treated eye as evidenced by proximity of the respective plots to the baselines. A return to baseline values was not seen in the GFP-injected retina (Figure 9C). Inset in figures 9B and 9C are tables that indicate the Rmax that correspond to the Naka-Rushton plots.

The Rmax values were averaged for the XIAP- and GFP-treated groups, and one-way ANOVA was conducted for all the time points. In figure 10, it appears that both groups experienced a reduction in responsiveness over the 4-week period following

Figure 9. Naka-Rushton plots. A, B and C are Naka-Rushton plots of a normal rat, a XIAP-treated rat, and a GFP-treated rat respectively. In graphs B and C, data was obtained at T=0 (baseline), 24 hpi, 2 wpi, and 4 wpi. Rmax is the maximum responsiveness, K is the intensity of light required to elicit half the maximum response, and n is the slope of the fitted curve. The tables at the bottom left of each graph are the actual Rmax values for each animal at each time point. Note that the baseline Rmax values for the right and left eyes for each animal are similar. There is a marked reduction in responsiveness (Rmax) at 24 hours, which improves over time.

A

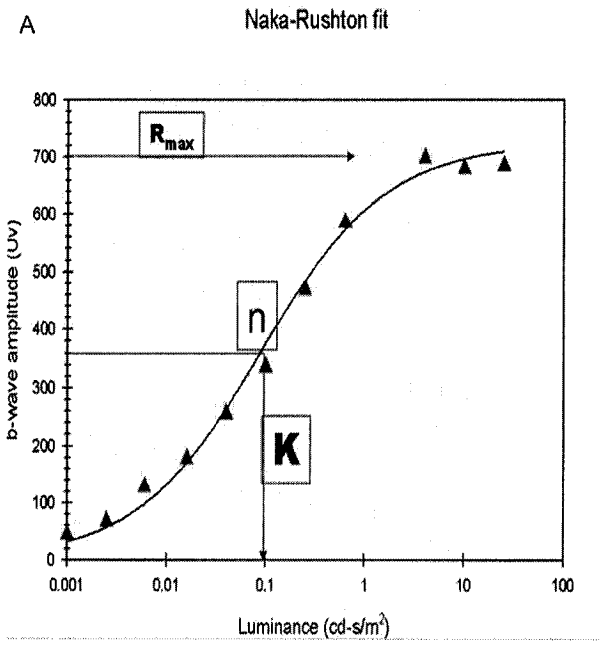

B

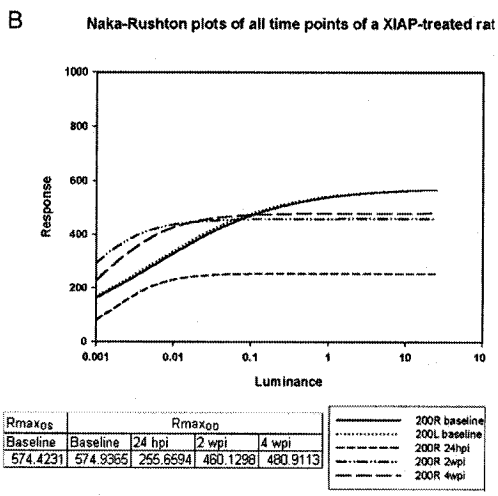

$Rmax_{OS}$	$Rmax_{OD}$			
Baseline	Baseline	24 hpi	2 wpi	4 wpi
574.4231	574.9365	255.6594	460.1298	480.9113

C

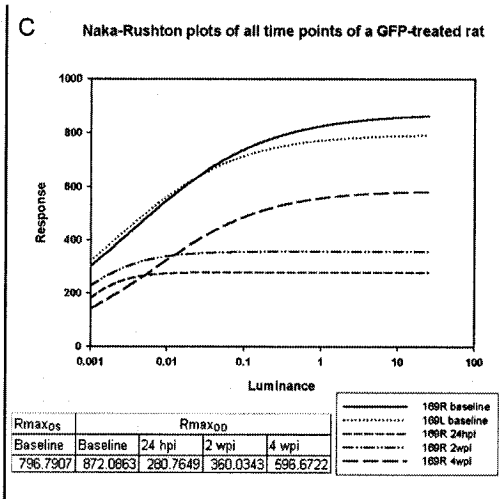

$Rmax_{OS}$	$Rmax_{OD}$			
Baseline	Baseline	24 hpi	2 wpi	4 wpi
796.7907	872.0863	260.7649	360.0343	596.6722

ischemia. The average R max ratio (OD:OS) for the GFP group, however, was significantly lower than that of the XIAP group at 24 hours post-ischemia. This suggests a reduction in responsiveness (Rmax) in the GFP-injected retinas relative to XIAP-injected retinas at 24 hours post-ischemia. Flat Naka-Rushton plots made it difficult to determine K values. Therefore, no comparison of sensitivity was made between the XIAP and GFP groups.

Figure 10. A comparison of average responsiveness between the experimental group and the control group. The responsiveness (Rmax) values were obtained from the Naka-Rushton analysis and compared between the XIAP and GFP groups. One-way ANOVA was conducted and $P<0.05$ was considered significant. Significant differences are indicated by a star. Mean ± 1 SEM. N=19 at baseline and 24 hpi. N=13 at 2 wpi and 4 wpi. One data point was omitted from the XIAP group at 4 wpi due to the presence of a cataract, therefore, N=12 for the XIAP group at 4 wpi.

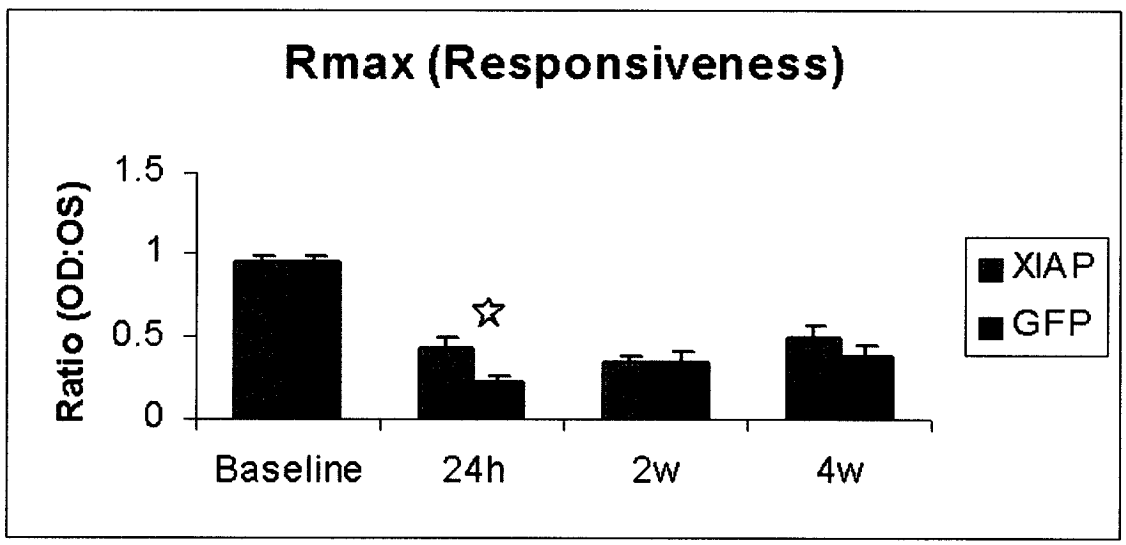
Rmax (Responsiveness)
Ratio (OD:OS)
1.5
1
0.5
0
Baseline
24h
2w
4w
XIAP
GFP

3.4 Histological Analysis

3.4.1 Haematoxylin and Eosin Staining

Using the Zeiss Axioskop fitted with the Zeiss AxioCam HRC camera, images were taken of the retinal tissue sections where the optic nerve head transected the retina. The images were taken at 40x magnification, approximately 440 and 1320 μm from the optic nerve head. The image contrast and brightness were modified using Adobe Photoshop 7.0 and the images were printed in colour (Figure 11). At 24 hpi, there was no evident reduction in the thickness of the XIAP-treated or GFP-treated retinas (Figure 11 A,B,E,F,I and J). However, at 4 wpi, there was a reduction in thickness of the para-papillary retina (approximately 440 microns from the optic nerve head) in the right eye of a GFP animal in comparison to the contralateral, control eye of that same animal (compare figures 11G and 11C). At 4 wpi, there was also a reduction in thickness of the retina in the right eye of the GFP-treated animal (Figure 11 G) relative to that of the XIAP-treated animal (Figure 11 H). At the mid-peripheral retina (approximately 1320 microns from optic nerve head) there was a similar reduction in thickness of a GFP-treated retina (Figure 11K) relative to a XIAP-treated retina (Figure 11L), but to a lesser extent.

Figure 11. Haematoxylin and Eosin stained cryosections of rat retinas. A,C,E, I, and K are samples of GFP-treated retinas while B, D, F, H, J, and L are XIAP-treated retinas. Samples were obtained at 24 hours post-ischemia (hpi) and 4 weeks post-ischemia (wpi). The samples are identified by 3-digits (rat#), the eye sampled (L, left or R, right) and then the location (distance in microns from optic nerve head). Cross-sections were 10 microns thick and images were taken at 40x magnification in the parapapillary region (440 microns from optic nerve head) and in the mid-periphery (approximately 1320 microns from the optic nerve head). Scale bar = 75 microns. GCL = ganglion cell layer; IPL = inner plexiform layer; INL = inner nuclear layer; OPL = outer plexiform layer; ONL = outer nuclear layer.

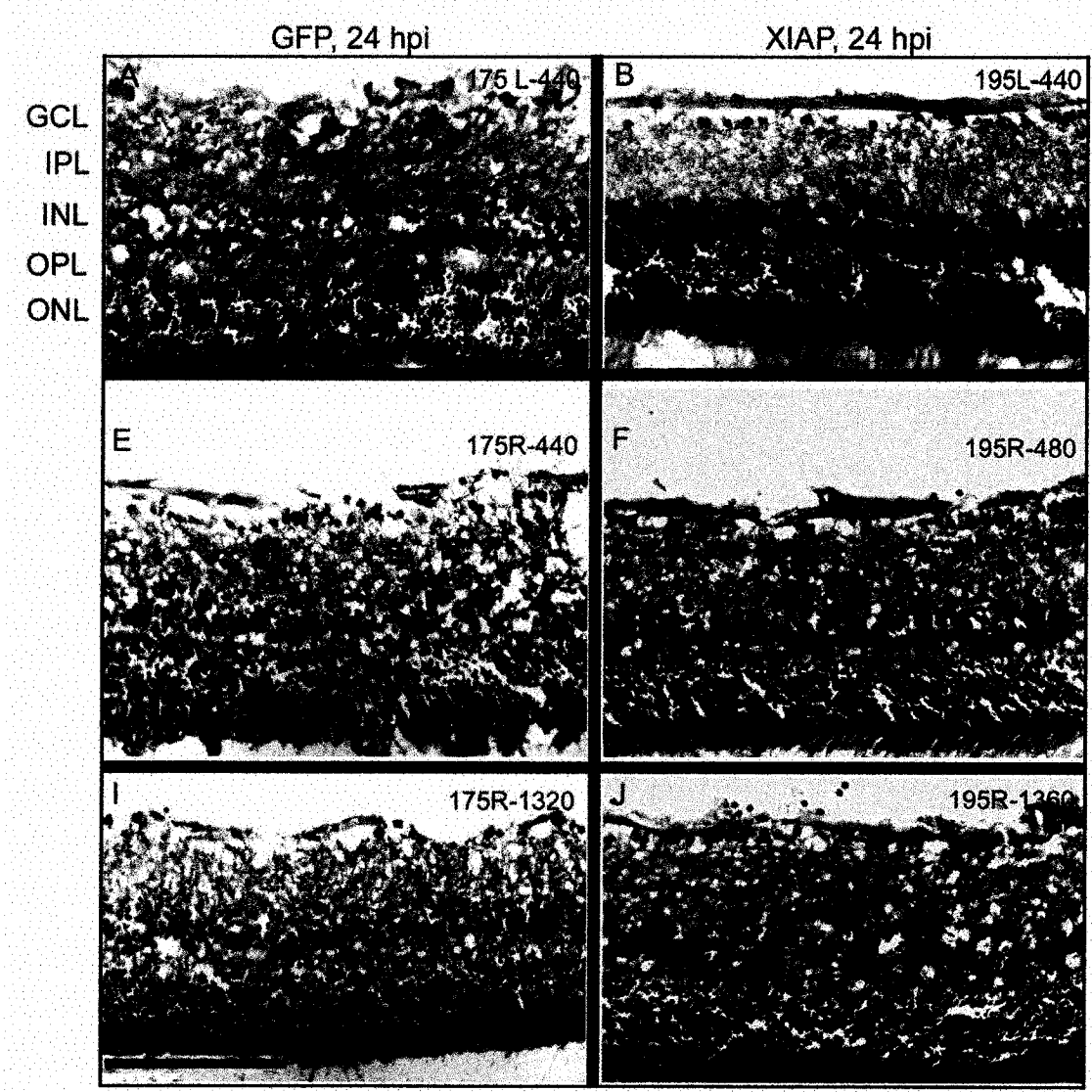
GFP, 24 hpi
XIAP, 24 hpi
GCL
IPL
INL
OPL
ONL
A
175 L-440
B
195L-440
E
175R-440
F
195R-480
I
175R-1320
J
195R-1360

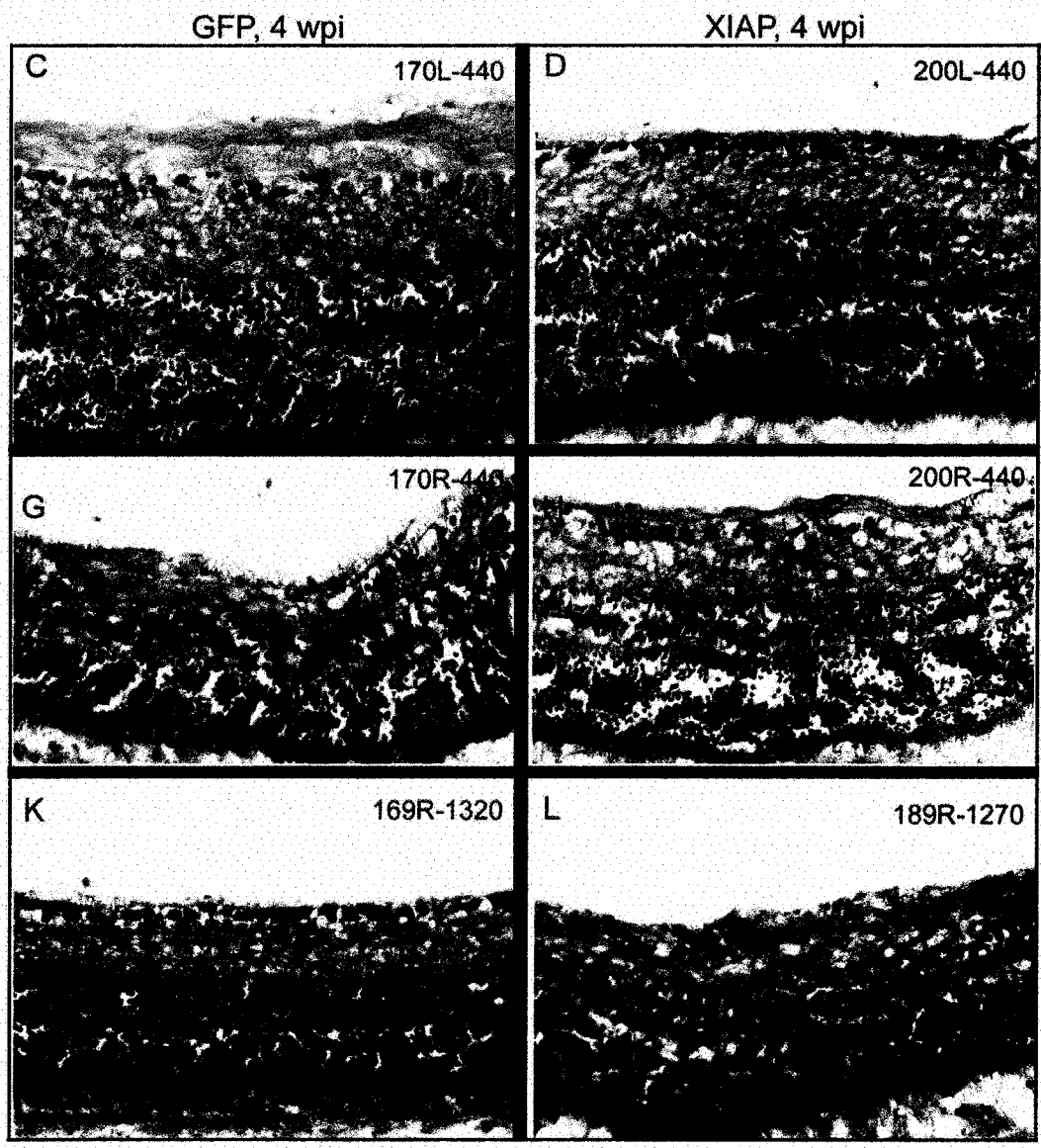
GFP, 4 wpi
XIAP, 4 wpi
C
170L-440
D
200L-440
G
170R-440
200R-440
K
169R-1320
L
189R-1270

3.4.2 Statistical Analysis of Cell Counts

Cell counts were conducted on the images of the retinas that had been stained with haematoxylin and eosin. For the purpose of an unbiased analysis, the images were not identified by experimental group, but instead were assigned a number and a letter at random (e.g. 1a, 1b, 2a, 2b, etc.). The cells in the ganglion cell layer (GCL) and inner nuclear layer (INL) were counted and the ratios of the counts were calculated for right eye (OD) versus left eye (OS). The average ratios for the para-papillary and mid-peripheral retina of each group are presented in Figure 12. One-way ANOVA was carried out to determine if there was a difference between the mean cell counts in right eyes and left eyes as well between the treatment groups. $P<0.05$ was considered significant.

The cell count ratios (OD:OS) were compared between the XIAP and GFP groups at 24 hpi and 4 wpi. At 24 hpi, there were significantly more inner nuclear layer (INL) cells in XIAP-treated retinas than in control (GFP-treated) retinas in both the para-papillary and mid-peripheral regions. A similar trend was observed in the GCL at 24 hours, but the difference was not significant between the GFP and the XIAP groups. At 4 weeks post-ischemia (wpi), there was no difference between the XIAP-treated group and the control group in regards to the number of INL cells in either the para-papillary or mid-peripheral areas. Neither was there a difference in the number of GCL cells at 4 wpi although there seemed to be a reversal in the trend in both the para-papillary and mid-peripheral areas. In other words, the GCL cell counts appeared to be greater in the GFP-treated retinas relative to the XIAP-treated retinas. Be that as it may, it should be noted that there was a great degree of variability between animals (see Table 1).

Figure 12. Inner nuclear layer and ganglion cell layer cell counts in XIAP- and GFP-injected rat retinas. Cryosections taken through the parapapillary (optic nerve head) area and mid-periphery were fixed in 4% PFA and stained with Haematoxylin and Eosin. Cells were counted by four independent individuals. Ratios were calculated for right versus left eye. The means of the ratios were calculated for each group at each time point. Error bars = ± 1SEM. Significant difference at $P<0.05$ is indicated by a star. INL = inner nuclear layer; GCL = ganglion cell layer.

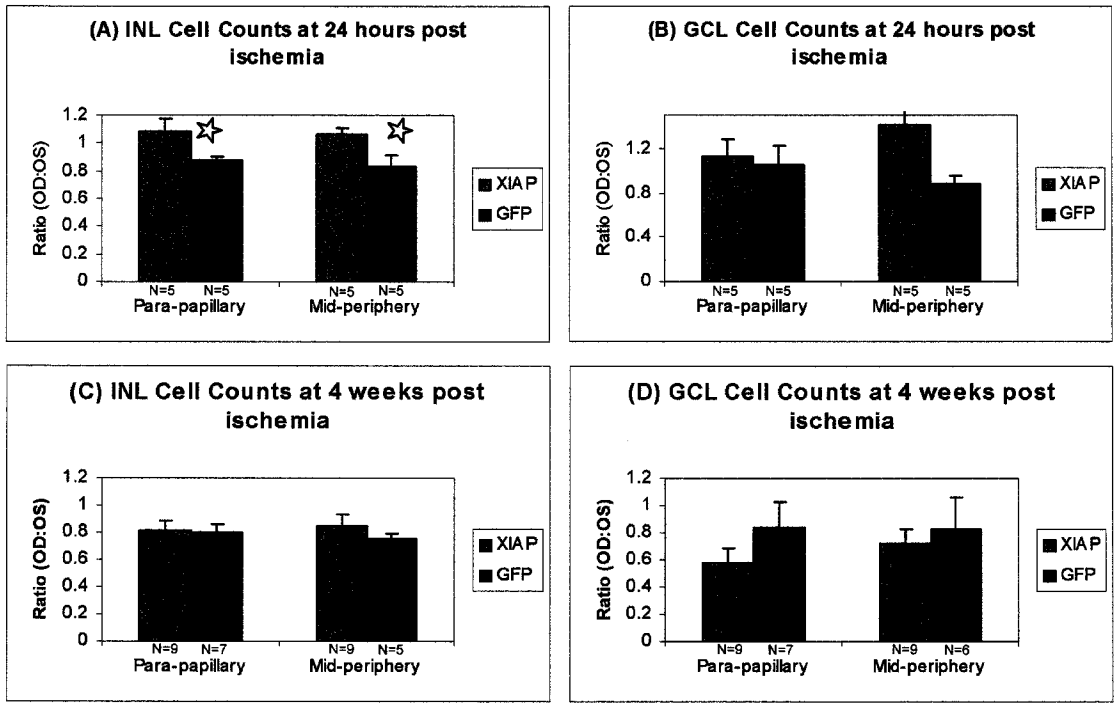
(A) INL Cell Counts at 24 hours post ischemia
Ratio (OD:OS)
1.2
1
0.8
0.6
0.4
0.2
0
N=5 N=5
N=5 N=5
Para-papillary
Mid-periphery
XIAP
GFP
(B) GCL Cell Counts at 24 hours post ischemia
Ratio (OD:OS)
1.2
0.8
0.4
0
N=5 N=5
N=5 N=5
Para-papillary
Mid-periphery
XIAP
GFP
(C) INL Cell Counts at 4 weeks post ischemia
Ratio (OD:OS)
1.2
1
0.8
0.6
0.4
0.2
0
N=9 N=7
N=9 N=5
Para-papillary
Mid-periphery
XIAP
GFP
(D) GCL Cell Counts at 4 weeks post ischemia
Ratio (OD:OS)
1.2
1
0.8
0.6
0.4
0.2
0
N=9 N=7
N=9 N=6
Para-papillary
Mid-periphery
XIAP
GFP

Table 1. Averages of cell counts. Raw counts obtained by each observer for the para-papillary (p) and mid-peripheral (m) regions of the retina (see also pages 131-134) were averaged for the XIAP (Table A) and the GFP (Table B) groups. Some specimens were not matched with contralateral counterparts because those counterparts were either poor samples, which could not be quantitatively analyzed properly, or they were unobtainable. Therefore, some ratios were incalculable.

Table 1A

Slide #	INL avg p	INL avg m	GCL avg p	GCL avg m
35L	143.333	163.333	22	16.66667
36L	206.333	244.667	28.6667	21
183L	277	220.5	23	29
185L	286	302	55.5	39
186L	225.5	249	30.5	33.5
187L	310	202	45	36.5
188L	268.5	244.5	45	27
190L	308	316	35	38.5
191L	239.667	206.5	32.3333	25
200L	275	255.333	28	20.66667
AVG 4 wpi OS	**251.593**	**238.722**	**35.2222**	**29.57407**
35R	162.333	184.333	10.5	16.66667
36R	230	181.333	13.6667	11
183R	249.5	255	27.5	39.5
185R	237	183	29	26
187R	215.5	200	30.5	19
188R	163.5	209	12.5	22
189R	217	249	44	34
190R	173	158	7	10
191R	149.667	162	12.5	16.5
200R	223.333	196	18.6667	12
AVG 4 wpi OD	**199.722**	**197.963**	**20.7963**	**21.62963**
194L	247.5	204	24.5	16.5
195L	224	187.333	22.3333	38.33333
197L	220.667	243.333	27.3333	27
199L	256.333	257.667	34	14
201L	273	248.333	27	20.33333
AVG 24 hpi OS	**244.3**	**228.133**	**27.0333**	**23.23333**
194R	227.5	251	37.5	17
195R	224	224.333	23	19.66667
197R	315	255	22.3333	33.33333

Table 1A (cont'd)

Slide #	INL avg p	INL avg m	GCL avg p	GCL avg m
199R	242.333	248.333	23.3333	37.33333
201R	316	248	39.3333	24.66667
AVG 24 hpi OD	**264.967**	**245.333**	**29.1**	**26.4**
192L	250.333	253.667	29.6667	31.66667
196L	279.667	226.667	32.3333	25
203L	321.667	292.667	37.6667	46.33333
AVG 0 hpi OS	**283.889**	**257.667**	**33.2222**	**34.33333**
192R	234.667	263	27.3333	31
203R	285	237.333	25	12
AVG 0 hpi OD	**259.833**	**250.167**	**26.1667**	**21.5**

Table 1B

Slide #	INL avg p	INL avg m	GCL avg p	GCL avg m
52L	200	243.3333	24	14.66667
61L	310	268.6667	39.66667	26.33333
162L	245.3333	198	29	24.33333
164L	260.3333	199.6667	32.66667	19.33333
166L	232.6667	213.6667	13.66667	14.33333
167L	294	226.6667	30.66667	14.66667
168L	227.6667	249.3333	23.33333	25
169L	235.3333	252.6667	20.33333	20
170L	230.6667	329.3333	25	38.66667
172L	268	322.6667	34	29.33333
Avg 4 wpi OS	**250.4**	**250.4**	**27.23333**	**22.66667**
52R	155	148	11.66667	13.66667
61R	185.3333	144	15	13
162R	194.3333	N/A	21.66667	N/A
164R	196.5	164	21.5	8.333333
165R	198	235.6667	16.33333	22
166R	181.3333	168.3333	22	16.66667
168R	212	222.3333	10.66667	8
169R	248	176.6667	31	30.66667
170R	135	159.6667	17.33333	10
Avg 4 wpi OD	**189.5**	**177.3333**	**18.57407**	**15.29167**
173L	226.3333	208	33	32.33333
175L	293.3333	363.6667	26.33333	24.33333
176L	234.3333	185.3333	24.33333	9
177L	245.6667	244	27	20
179L	248	232	38.33333	29.66667
Avg 24 hpi OS	**249.5333**	**246.6**	**29.8**	**23.06667**

Table 1B (cont'd)

Slide #	INL avg p	INL avg m	GCL avg p	GCL avg m
173R	186.3333	220.3333	26.66667	30.33333
175R	237.6667	236	33.66667	20.66667
176R	205	193.6667	32.33333	8.333333
177R	243	144	21	17.66667
178R	272	183	34.5	16
179R	229.6667	137	26.33333	18
Avg 24 hpi OD	**228.9444**	**185.6667**	**29.08333**	**18.5**
51L	202	177.6667	23.66667	29.66667
53L	201.3333	134	60	26.33333
180L	206	198	20	25.33333
182L	247	237.3333	36.33333	25.33333
Avg 0 hpi OS	**214.0833**	**186.75**	**35**	**26.66667**
53R	244.6667	158.6667	24	23.33333
180R	209.5	192.6667	16	23
Avg 0 hpi OD	**227.0833**	**175.6667**	**20**	**23.16667**

3.4.3 TUNEL Analysis

TdT-dUTP terminal deoxynucleotidyl transferase nick end labelling (TUNEL) assays allow for the identification of apoptotic cells. The principle behind it is based on one of the key characteristics of apoptosis: DNA cleavage (Katai and Yoshimura, 1999). The cleavage of DNA during apoptosis yields multiple fragments approximately 180 base pairs in length. Terminal deoxynucleotidyl transferase (TdT) facilitates the addition of deoxyuracil triphosphates (dUTPs) to the 3' OH ends of the DNA fragments. For the current study, dUTPs were tagged with digoxygenin prior to use. An antibody to digoxygenin, which was conjugated with fluorescein, was applied to facilitate visualization of cells containing the fragmented DNA. The tissue was counterstained with DAPI to identify nuclei. TUNEL-positive cells were identified as pale green to whitish (due to blue overlapping green). A subset of TUNEL images is presented in figure 13, panels A-F. At 24 hpi, there appeared to be more TUNEL-positive INL and/or GCL cells in the GFP-treated cells (Figure 13 A, C, and E) compared to the XIAP-treated group (Figure 13 B,D,F) in both the para-papillary and mid-peripheral regions.

For each sample, the number of TUNEL-positive cells was expressed as a percentage of the total number of cells at 24 hpi. These percentages were averaged and plotted (Figure 13 G). One-way ANOVA was carried out to determine if there was a difference between the XIAP and GFP groups. There were significantly more TUNEL-positive cells in the para-papillary region of the INL in the GFP-treated retinas compared to the XIAP-treated retinas. However, there were no significant differences between the two groups in the para-papillary region of the GCL. Moreover, there was no significant difference between the XIAP-treated and GFP-treated retinas in the mid-periphery (1320

microns from optic nerve head) or in the region 880 microns from the optic nerve head (not shown).

Figure 13. Fluorescent TUNEL assay on cryosections of rat retinas at 24 hours post-ischemia. A, C and E are GFP-treated samples while B, D, and F are XIAP-treated samples. Cross-sections were 10 microns thick and images were taken at 20x magnification in the following areas: the parapapillary region (440 microns from optic nerve head), the mid-periphery (approximately 1320 microns from optic nerve head), and 880 microns from the optic nerve head. Some of the TUNEL-positive cells are indicated by white arrows. In the INL and GCL of each sample, the number of TUNEL-positive cells was expressed as a percentage of the total number of cells. The means of the percentages were calculated for each group at 24 hpi and plotted on a bar graph (G). GFP N=6 and XIAP N=5. Error bars = ± 1SEM. Significant difference is indicated by a star ($P < 0.05$). GCL = ganglion cell layer; IPL = inner plexiform layer; INL = inner nuclear layer; OPL = outer plexiform layer; ONL = outer nuclear layer. R, OD= right eye; L, OS= left eye. Scale bar = 140 microns.

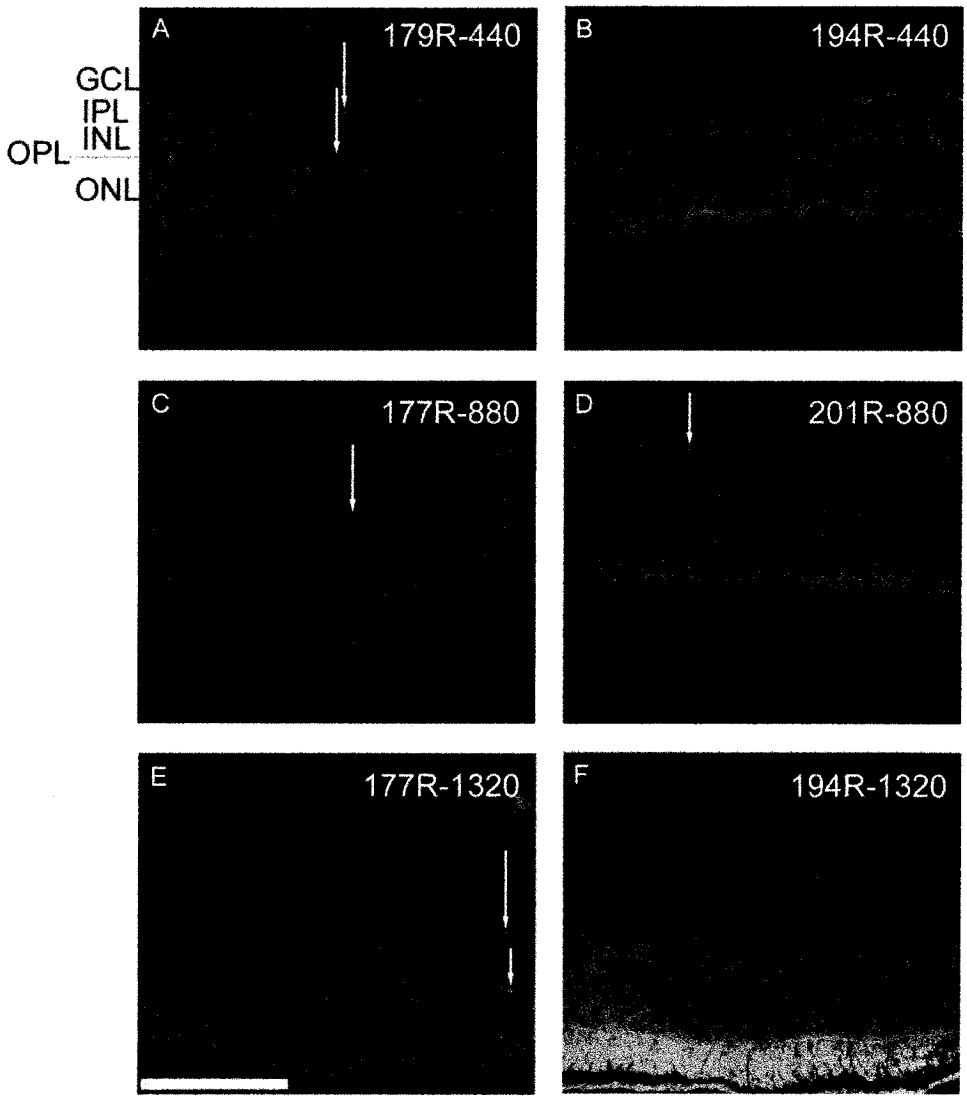

(Figure continues on next page...)

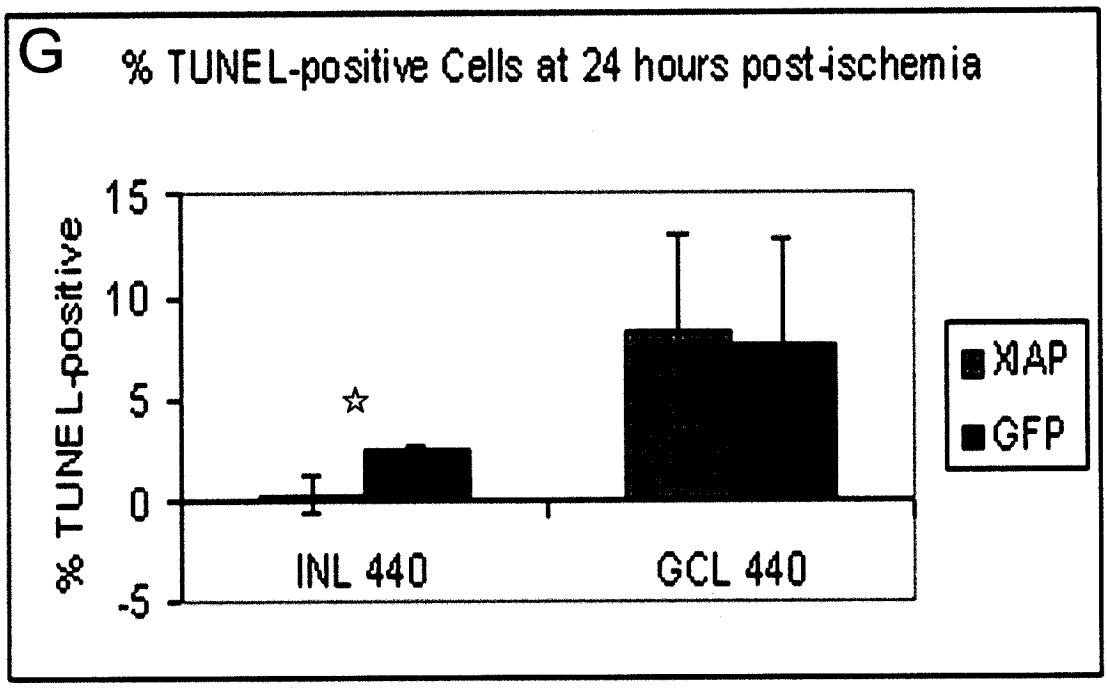
G
% TUNEL-positive Cells at 24 hours post-ischemia
% TUNEL-positive
15
10
5
0
-5
INL 440
GCL 440
XIAP
GFP

3.4.4 Analysis of Optic Nerve Cross-sections

At 4 weeks post-ischemia, the optic nerve stalks were cut, detached from the eyes and fixed in 4% PFA in 1xPBS for at least four hours. The stalks were then embedded in plastic and sectioned at 0.5 microns. The sections were stained with 1% Toluidene Blue and cover-slipped. Images of the cross-sections were taken at 10x and 63x magnification on a Zeiss Axioskop light microscope (Figure 14, panels A-H). There appeared to be a marked reduction in size and a change in shape (right, R versus left, L) in the GFP-treated samples relative to the XIAP-treated samples. In figure 14, panels I, J and K are magnified versions (63x magnification) of panels A, B and H respectively. Compared to a cross-section of a normal optic nerve (Figure 14 I) there were many dying axons found in the ischemic optic nerve cross-section (Figure 14 J). These were characterized by an unhealthy myelin sheath which was either very thick or very thin. When the myelin sheath was very thin, the roundness normally associated with a healthy axon was absent. In addition, some dying axons exhibited moderate to heavy discolouration.

A semi-quantitative analysis was conducted on the optic nerve cross-sections. This semi-quantitative analysis was based on a method developed by Dr. Balwantray Chauhan and his colleagues (unpublished). Briefly, one or two representative sections from each optic nerve sample were observed under a Zeiss Axioskop light microscope at 40x magnification so that each entire section could be seen at once. Based on the size of the dying population, the section was assigned a score between 0 and 1. A rating of 0.1 meant that 10% of the section contained damaged axons. The average ratings were plotted in a bar graph (Figure 14 L). Overall, damage never exceeded 30% of an

Figure 14. Analysis of optic nerve cross-sections. Optic nerve stalks were extracted 4 weeks post-ischemia (wpi), sectioned at 0.5 microns and stained with 1% Toluidene Blue. A-D are GFP-treated samples while E-H are XIAP-treated samples. Images are at 10x magnification (scale bar = 620 microns). I and J are images of optic nerve cross-sections of GFP-treated rat #162 at 63x magnification (scale bar = 5 microns). The right ischemic eye (J) shows characteristics of dying axons: axoplasm/contents condense, axons shrink and myelin thickens (red arrow) or axon expands and myelin thins (black arrow). K is a magnified cross-section of an optic nerve from a XIAP-treated animal. H has fewer of the characteristics associated with dying axons. L is a graph representing the results of the semi-quantitative analysis. Student's T-Test was conducted on the results. No significance was found even though GFP-treated optic nerves (N=8) showed more damage than XIAP-treated optic nerves (N=7).

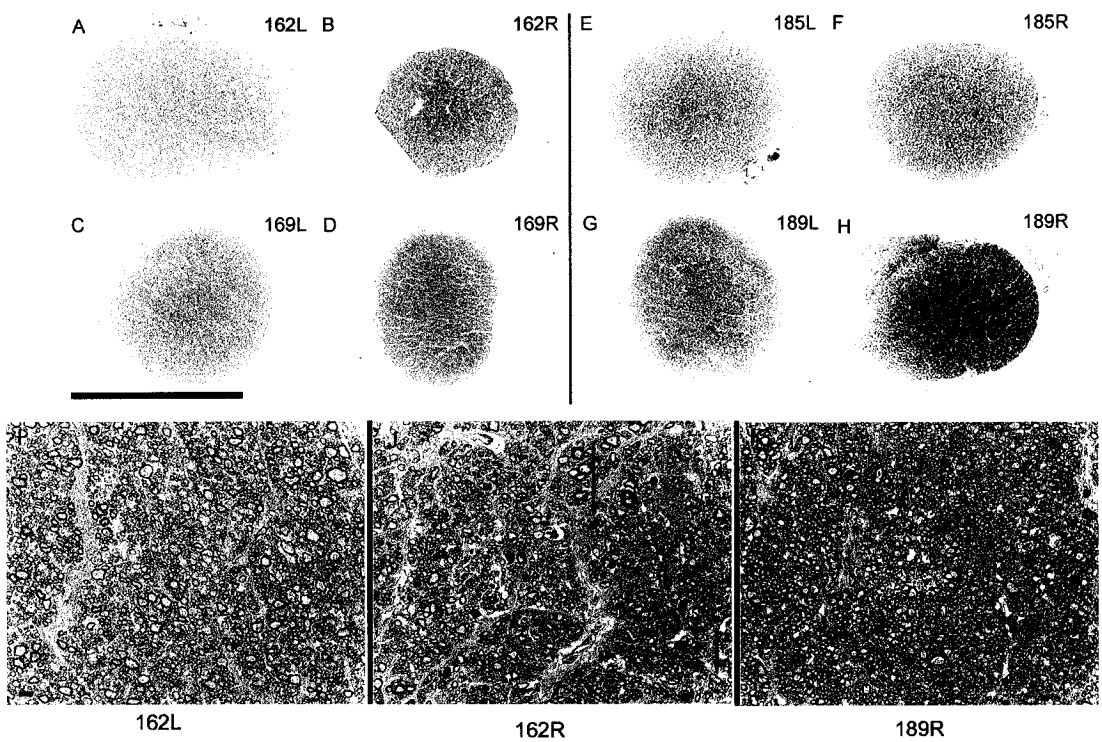
A
162L
B
162R
E
185L
F
185R
C
169L
D
169R
G
189L
H
189R
162L
162R
189R

L

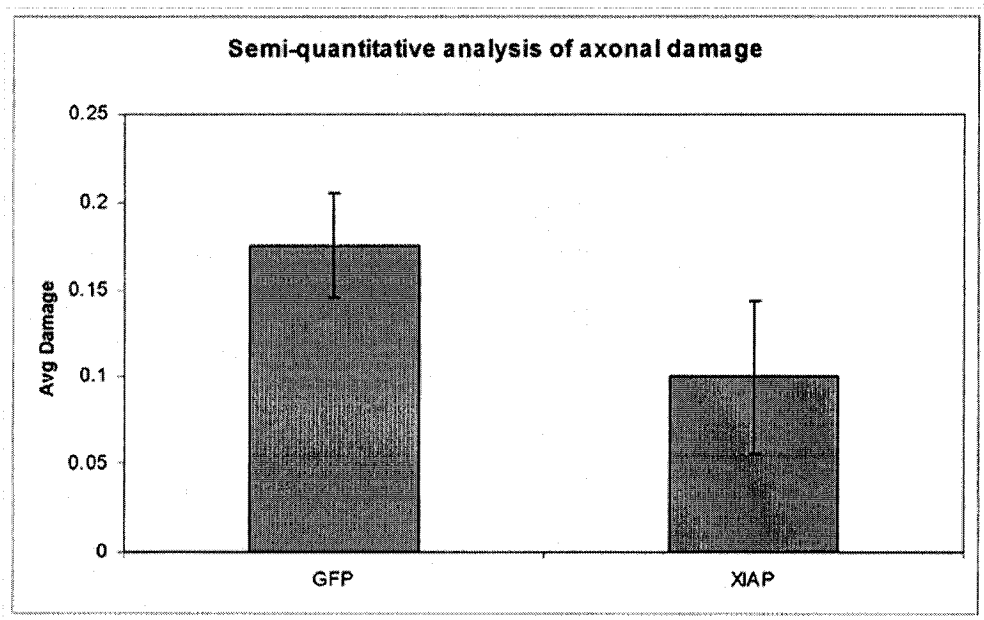
Semi-quantitative analysis of axonal damage
Avg Damage
0.25
0.2
0.15
0.1
0.05
0
GFP
XIAP

entire cross-section. There was no significant difference in overall damage between the XIAP- and GFP-treated groups. However, the GFP group showed more overall damage than the XIAP group, as shown in Table 2.

When the optic nerve cross-sections were analyzed qualitatively, the cross-sectional areas of the ischemic samples appeared to be reduced compared to the normal samples. This prompted a series of measurements of the cross-sectional areas. The shape of each cross-section was elliptical (oval). Therefore, two diameters were measured for each sample. The ratios of the areas, right eye versus left eye (OD:OS) were averaged for the XIAP- and GFP-treated groups, and a Student's T-Test was conducted. There was no significant difference found between the two groups at $P>0.05$ (not shown). When only the right optic nerves were compared between groups, there was again no significant difference (Figure 15). However, in both instances the trends appeared to corroborate the trend seen in the semi-quantitative analysis results. The cross-sections of XIAP-treated optic nerves appeared to be larger than those of the GFP-treated optic nerves.

Table 2. Raw scores from semi-quantitative analysis of optic nerve cross sections.

GFP $_{OD}$	Rating	Avg Damage
162	3	0.3
164	2	0.2
165	1	0.1
166	2.5	0.25
168	2.5	0.25
169	1	0.1
170	1	0.1
172	1	0.1
Average		**0.175**

XIAP $_{OD}$	Rating	Avg Damage
185	0	0
186	0	0
187	2	0.2
188	1	0.1
189	1	0.1
191	3	0.3
200	0	0
Average		**0.1**

Figure 15. Cross-sectional areas of optic nerves. Right eye optic nerve stalks were obtained at 4 wpi, and sectioned at 0.5 microns. Sections were observed at 10x magnification. Sections were treated as ellipses, therefore two diameter measurements were taken. The area (μm^2) was calculated for each specimen. The areas were averaged for the XIAP (N=7) and GFP (N=8) groups. $P<0.05$ was considered significant. Mean ± 1SEM.

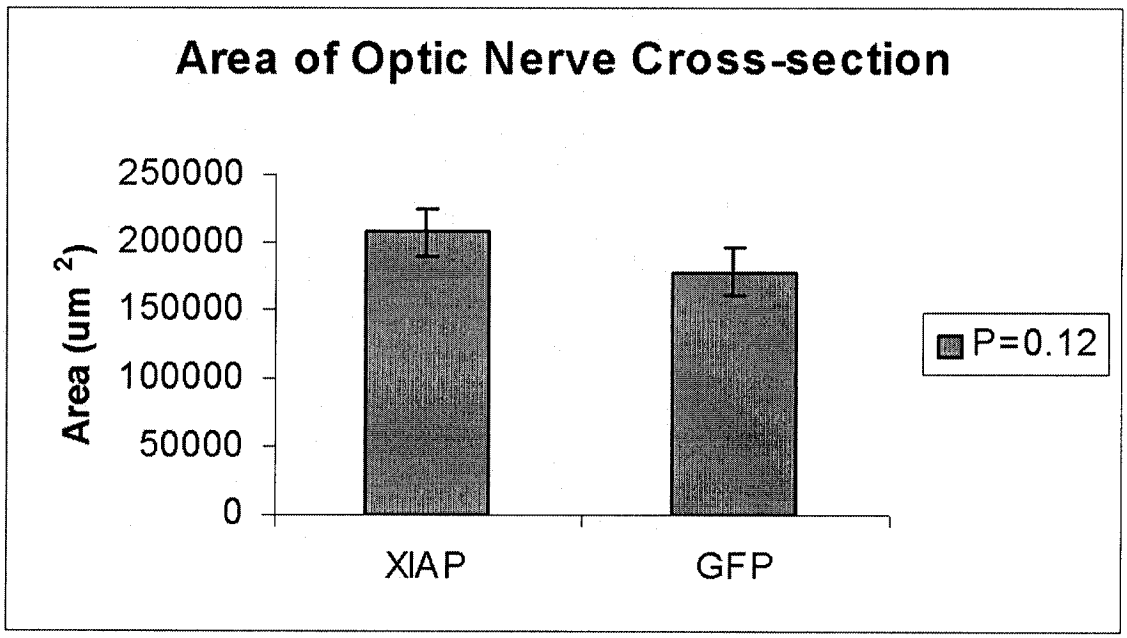
Area of Optic Nerve Cross-section
Area (um 2)
250000
200000
150000
100000
50000
0
XIAP
GFP
P=0.12

Chapter 4. DISCUSSION

Scotopic-Photopic ERG

The preservation of the b-wave amplitude due to XIAP-mediated gene therapy over a 4-week period suggests that XIAP is rescuing the ischemic neural retina from complete infarction. At 24 hpi and 4 wpi, the b-wave amplitude ratios of the XIAP-treated group are significantly higher than the GFP-treated group. At 2 wpi, although the trend matches that found at 24 hpi and 4 wpi, the differences are not significant. This could be a temporary adaptive response on the part of the ischemic retina.

Bertoni-Freddari and colleagues (2002) proposed such an explanation in their study on young spontaneous hypertensive rats. Transient ischemia was induced in these rats by four-vessel occlusion (previously described). The right hippocampus tissue was explanted from each ischemic and non-ischemic rat. The hippocampus explants were sectioned and assessed quantitatively. Numeric density or Nv (the number of synaptic profiles per μm^3 of tissue) was measured. Average synaptic area (S) and synaptic density or Sv (overall area of the synaptic contact zones per μm^3 of tissue) were estimated. Despite the significantly decreased Nv and Sv, the ischemic rats exhibited a non-significant increase in S. Bertoni-Freddari and colleagues suggested that this may have been due to a "reactive phenomenon purported to counteract" the heavy loss of synaptic junctions. They based their interpretation on a theory of synaptic remodeling which proposes that sustained stimulation can cause synaptic apposition, which can lead to an increase in synaptic area. The expanded area, hypothetically, may then undergo perforation and result in the division of large synapses into smaller ones, which may enlarge and split further or regress. In other words, the mild and temporary but

insignificant recovery of the hippocampus from an ischemic insult may have been due to reorganization of synapses.

In the current study, since the non-significant difference in b-wave amplitude ratios of the XIAP- and GFP-treated groups is only at the intermediary time point, this reactive phenomenon can only be interpreted as temporary. It may very well be that sub-populations of INL cells are more sensitive and thus more affected than other sub-populations. In studies on larval salamanders, it was found that certain subsets of ganglion cells were differentially sensitive to hypoxia and that other subsets were compensating for the affected ganglion cells (Gross et al., 1999). So it is possible that certain types of INL cells of the ischemic rat may be compensating for the affected cells by way of synaptic remodelling (plasticity). Moreover, perhaps this synaptic remodelling may be limited and therefore insufficient in the face of the aggressive ischemia being generated in both the XIAP- and GFP-treated retinas but may be sufficient to allow a limited "regaining" of function at the 4-week time point in XIAP-treated retinas. Studies have also shown that certain INL cell types are more susceptible to ischemia than others (Singh M et al., 2001; Winkler BS et al., 2000; Chun M et al., 1999). This also supports the idea that less susceptible cell types may be compensating for the more vulnerable ones.

Flicker ERG

Flicker ERG data did not reveal any significant differences between XIAP and GFP groups. However, both groups exhibited some recovery of the flicker ERG amplitude over time. This supports the previous conclusions regarding the scotopic-

photopic ERG – namely that some degree of synaptic remodeling may be occurring in the damaged inner nuclear layer which is allowing some recovery by 4 weeks post ischemia.

Histological Analysis

Two separate circulations are involved in supplying the retina with nutrients: the retinal and choroidal circulations. The GCL and INL draw their blood supply from the ophthalmic (retinal) artery, while the ONL derives its blood supply from the cilliary arteries which feed into the choroid. It is also important to note that the ophthalmic (retinal) circulation is slower and requires more oxygen than the choroidal circulation. In other words, the inner retina has a higher oxygen demand than the outer retina. Therefore, in the event of an ischemic insult, the GCL and INL tend to be more affected by an ischemic event than the outer nuclear layer (Delaey C and J Van de Voorde, 2000; Kohner, 1989), and (2) (Delaey C and J Van de Voorde, 2000). Accordingly, an acute ischemic insult due to occlusion of the central retinal artery would have a greater impact on the INL and GCL cells than on the ONL cells. This is further supported by an ultrastructural study conducted by Rosenbaum and colleagues (1998), which revealed that the entire retinal thickness was reduced following transient ischemia. Both the GCL and INL were significantly affected. However, the inner segments of the photoreceptors (ONL) and the outer segments were only mildly affected (Rosenbaum DM et al., 1998).

After an ischemic episode, if the structure of the retina is adversely affected, i.e. many cells are lost, retinal function may only be minimal. In other words, the more cells that are structurally preserved, the better the chances of retinal function being

maintained. The ganglion cell layer, inner nuclear layer and outer nuclear layer were studied histologically at 24 hpi and 4 wpi to determine if XIAP structurally protects the retina.

Structural rescue of retinal neurons is evident in the XIAP-treated retinas. INL cell counts in retinal cross-sections of the XIAP-injected eyes were higher than the GFP controls at 24 hpi in both the pare-papillary region and the mid-periphery. There was, however, no significant difference at 4 wpi. These results suggest temporary structural protection. However, qualitative observation of the retinas at 4 wpi also suggests that retinal thickness is preserved to a certain extent in the XIAP-treated retinas. A closer look revealed that the inner plexiform layer (IPL) diminished very much in GFP-treated retinas, and to a lesser extent in the XIAP-treated retinas, suggesting degeneration of the INL cell and ganglion cell axons. This supports the idea of synaptic reorganization between the two layers, which was proposed earlier in relation to the functional analysis. As mentioned earlier, studies have also shown that the rat retina has selective vulnerability to transient ischemia via increased IOP. Horizontal and Müller cells are resistant or mildly susceptible, while the amacrine and ganglion cells were more susceptible (Singh M et al., 2001; Winkler BS et al., 2000; Chun M et al., 1999).

The GCL counts were somewhat difficult to interpret. While the XIAP group appeared to have higher counts in both the para-papillary and mid-peripheral regions at 24 hpi, this trend appeared to reverse at 4 wpi, with the GFP group having higher counts. This might be due to extremely high variability in the counts. Anywhere from 8 to 50 cells were counted in a region spanning 440 μm. So, before any conclusions can be drawn, additional experiments will need to be performed. Studies have shown that

amacrine cells can migrate into the GCL (Haverkamp S and H Wässle, 2000). In addition, as cells degenerate, macrophages migrate into a damaged area to phagocytose the remaining debris. Without immunohistochemistry to identify the cell types in the GCL, conclusions cannot be made about what cell types are present. To resolve this issue, cross-sections of ischemic retinas will have to be immunoassayed with anti-Thy-1 antibody. Thy-1 is an antibody that is specific for ganglion cells. A recent study showed that Thy-1 levels decrease in ischemic retinas (Chidlow and Osbourne, 2003). Statistical analysis on samples immunoassayed with anti-Thy-1 will give a clearer picture of how overexpression of XIAP affects the ischemic retinal ganglion cells.

TUNEL analyses

To verify that cell loss was due to apoptosis, TUNEL analysis was performed on cross-sections of GFP- and XIAP-treated retinas at 24 hpi. There were significantly more TUNEL positive cells in the inner nuclear layer of the GFP-treated retinas than in the XIAP-treated retinas at 24 hpi. This suggests that XIAP-mediated gene therapy rescued the retinal neurons from apoptotic cell death. TUNEL analysis did not reveal significant difference between the GCL in XIAP-treated retinas and that of the GFP-treated retinas. This may be due to the timing of the TUNEL assay. Since apoptosis peaks at 9 hours in the GCL (Kuroiwa S et al., 1998), it stands to reason that the GCL would be greatly reduced by 24 hpi.

Optic Nerve Cross-sections

Dudus and colleagues (1999) demonstrated that intravitreal injection of AAV-GFP in mice and dogs persisted for more than 7 months in both the ganglion cells and the INL cells throughout the entire retina, as well as up to 6 months in the optic nerves. Guy and colleagues (1999) showed that, in guinea pigs, intravitreally injected AAV-GFP lead to expression that persisted for up to one year, albeit to a lesser extent towards the end of that period. Accordingly, it was deemed useful to observe the effects of overexpressed XIAP on the optic nerve in the retinal ischemia model. Qualitative analysis of optic nerve cross sections at 4 wpi revealed characteristics of dying axons that appeared to be consistent with those of Wallerian degeneration. Axon degeneration can differ based on the size of the axon and even the type of injury/neuropathy involved (Marques SA et al., 2003; Narciso MS et al., 2001). Wallerian degeneration begins with granular disintegration and ends with condensed material. Granular disintegration occurs when both axoplasmic microtubules and neurofilaments become amorphous and granular material. In the central nervous system (CNS), this can be achieved in two ways: dark degeneration and watery degeneration. Dark degenerating axons have dark, dense axoplasm, and very dark myelin sheaths. Watery degeneration, on the other hand, involves the displacement of axoplasm by amorphous granular material, or the axoplasm loses mitochondria, microtubules, and neurofilaments. Therefore, those axons look pale and large, or "watery" (Marques SA et al., 2003; Narciso MS et al, 2001). To verify that Wallerian degeneration is in fact occurring in the optic nerve following retinal ischemia, the optic nerve cross-sections would need to be immunoassayed with an anti-neurofilament protein antibody. It has been shown that neurofilament proteins play a

role in dark degeneration of rat optic nerve axons that has been induced by enucleating of the eye (Adriani S et al., 2003). So there could be a similar marker in rat optic nerve axons that are degenerating due to an acute increase in IOP.

A semi-quantitative analysis of damaged axons at 4 wpi uncovered no significant difference between the XIAP and GFP groups. However, further qualitative analysis of the optic nerve cross-sections revealed that the sizes of the cross-sections from the ischemic optic nerves were reduced. Because of axonal loss, it made sense that the entire optic nerve would shrink resulting in the decrease in cross-sectional area. Accordingly, the area of each section was calculated. Most of the sections were elliptical in shape so the areas were calculated accordingly. When the areas were averaged for the right eye of each group, there was again no significant difference ($P>0.05$), but the general trends were maintained: XIAP-treated optic nerves appeared to be thicker than GFP-treated optic nerves. Using a rat ocular hypertensive model, McKinnon and colleagues studied the effects of XIAP on the rat retinal ganglion cell survival, 12 weeks after the intraocular pressure was initially elevated. They found significantly higher axonal loss in their GFP treated group compared to their XIAP-treated group. The pattern, however, differed from that found in our retinal ischemia model in that they saw more loss in the centre of the cross-sections. Since a pattern of axonal loss had not been fully characterized for the increased-IOP retinal ischemia model, it was difficult to discern whether the diffuse axonal loss pattern seen at 4 wpi was complete. Further study at earlier and later time points would allow characterization of this "diffuse" axonal loss.

Summary

Overall, functional and structural analysis of both the GFP-treated and XIAP-treated retinas suggests that overexpression of XIAP rescued retinal neurons up to 4 weeks post-ischemia (wpi). The rescue efforts appeared to be strong at 24 hours post ischemia (hpi) and more moderate at 4wpi. This suggests that overexpression of XIAP has the potential to both structurally and functionally rescue retinal neurons for the long-term under severe ischemic conditions. Therefore, XIAP-mediated gene therapy holds promise as a therapy in the clinic. It is important to note, however, that gene therapy in retinal ischemia using AAV vectors will provide valuable information on the efficacy of XIAP as a neuroprotective agent, but will not be immediately applicable to human disease. Arterial occlusion in the retina occurs acutely, often without warning, and requires rapid treatment. So, AAV vectors would be ineffective in therapeutic strategies. Nevertheless, the experiments employing AAV vectors constitute important preclinical proof of principle for XIAP cytoprotection in the eye. If nearly full neuroprotection can be achieved by XIAP in this model, after further experimentation, then different strategies for the rapid upregulation of XIAP will need to be explored. In other words, an alternative delivery system would be required, one in which transgene expression is more tightly controlled. One way of controlling the expression of a gene would be using an inducible system (Auricchio A et al., 2002; Pollock R et al, 2000) combined with a pharmacological agent (i.e. a drug). This system would consist of a vector containing the activator domain of a pharmacological agent fused to a promoter that drives not only the expression of the transgene but of the factor that responds to the pharmacological agent as well. Such an approach has recently been tested with a single AAV and the

tetracycline (Tet)-dependent system in rats (Chtarto A et al., 2003). After being injected with the AAV-GFP virus, the rats were fed doxycycline with their meals. The inducible AAV vector was successful as evidenced by the transduction of the brain neurons with GFP.

Since one cannot predict when a transient retinal ischemic event may occur, a rapidly inducible system would be effective in increasing XIAP expression. This new approach to AAV therapy may prove particularly effective in upregulation of XIAP in the immediate period following surgery to treat retinal ischemia. However, the current model consists of an injection prior to ischemia. Therefore, the results suggest that XIAP-mediated gene therapy could be useful as a preventative measure in combination with methods that detect warning signs of impending retinal ischemic events.

References

Adachi K, S Kashii, H Masai, M Ueda, C Morizane, K Kaneda, T Kume, A Akaike and Y Honda (1998). "Mechanism of the pathogenesis of glutamate neurotoxicity in retinal ischemia." Graefe's Arch Clin Exp Ophthalmol. **236**: 766-774

Auricchio A, V M Rivera, T Clackson, EE O'Connor, AM Maguire, MJ Tolentino, J Bennett and JM Wilson (2002). "Pharmacological regulation of protein expression from adeno-associated viral vectors in the eye." Mol Ther. **6** (2): 238-242.

Bertoni-Freddari C, P Fattoretti, U Caselli, C De Angelis and E Perna (2002). "Transient Ischemia Associated with Hypertension Significantly Affects Synaptic Plasticity in Young Rats." Ann N.Y. Acad. Sci. **977**: 123-128.

Breton ME, DP Montzka, AJ Brucker and GE Quinn (1991). "Electroretinogram interpretation in Central Retinal Vein Occlusion." Ophthalmology **98**: 1837-1844.

Buchi, ER (1992). "Cell death in the rat retina after a pressure-induced ischaemia-reperfusion insult: an electron microscopic study. I. Ganglion cell layer and inner nuclear layer." Exp Eye Res **55**(4): 605-13.

Chidlow, G and NN Osborne (2003). "Rat retinal ganglion cell loss caused by kainate, NMDA and ischemia correlates with a reduction in mRNA and protein of Thy-1 and neurofilament light." Brain Res. **963** (1-2): 298-306.

Chtarto A, HU Bender, CO Hanemann, T Kemp, E Lehtonen, M Levivier, J Brotchi, T Velu and L Tenenbaum (2003). "Tetracycline-inducible transgene expression mediated by a single AAV vector." Gene Therapy **10**: 84 - 94

Chun M, I Kim, W Ju, K Kim, M Lee, C Joo and J Chung (1999). "Horizontal cells of the rat retina are resistant to degenerative processes induced by ischemia-reperfusion." Neurosci Lett. **260**:125-128.

Deveraux QL, R Takahashi, GS Salvesen, JC Reed (1997). "X-linked IAP is a direct inhibitor of cell-death proteases." Nature. **388** (6639): 300-304.

Deveraux QL, N Roy, HR Stennicke, T Van Arsdale, Q Zhou, SM Srinivasula, ES Alnemri, GS Salvesen and JC Reed (1998). "IAPs block apoptotic events induced by caspase-8 and cytochrome c by direct inhibition of distinct caspases." EMBO J **17**(8): 2215-2223.

Delaey C and J Van de Voorde (2000). "Regulatory mechanisms in the retinal and choroidal circulation." Ophthalmic Res. **132** (6): 249-56.

Dong, CJ and WA Hare (2000). "Contribution to the kinetics and amplitude of the electroretinogram b-wave by third-order retinal neurons in the rabbit retina." Vision Res. **40** (6): 579-89.

Dong, CJ and WA Hare (2002). "GABAc feedback pathway modulates the amplitude and kinetics of ERG b-wave in a mammalian retina in vivo." Vision Res. **42** (9): 1081-7.

Dudus L, V Anand, GM Acland, S Chen, JM Wilson, KJ Fisher, AM Maguire and J Bennett (1999). "Persistent transgene product in retina, optic nerve and brain after intraocular injection of rAAV." Vis Res. **39**: 2545-2553.

Fontaine V, S Mohand-Said, N Hanoteau, C Fuchs, K Pfizenmaier, and U Eisel (2002). "Neurodegenerative and Neuroprotective Effects of Tumor Necrosis Factor (TNF) in Retinal Ischemia: Opposite Roles of TNF Receptor 1 and TNF Receptor 2." J Neurosci. **22**: 1-7.

Fulda S, W Wick, M Weller and K Debatin (2002). "Smac agonists sensitize for Apo2L/TRAIL- or anticancer drug-induced apoptosis and induce regression of malignant glioma in vivo." Nat Med. **8** (8): 808-815.

Gross RL, Hensley SH, Gao F, Wu SM. (1999). "Retinal ganglion cell dysfunction induced by hypoxia and glutamate: potential neuroprotective effects of beta-blockers." Surv Ophthalmology **43** (Suppl 1): S162-70

Guy J, X Qi, N Muzyczka and WW Hauswirth (1999). "Reporter Expression Persists 1 Year After Adeno-Associated Virus-Mediated Gene Transfer to the Optic Nerve." Arch Ophthalmol. **117**: 929-937.

Haverkamp S and H Wässle (2000). "Immunocytochemical analysis of the mouse retina." J Comp Neurol. **424**: 1-23.

Hengartner, MO (2000). "The biochemistry of apoptosis." Nature **407**: 770-776.

Holcik M, H Gibson and RG Korneluk (2001). "XIAP: Apoptotic brake and promising therapeutic target." Apoptosis **6**: 253-261.

http://www.cnib.ca/eng/eye_con/cospubs/diabetes.htm

Huang Y, RL Rich, DG Myszka, and H Wu (2003). "Requirement of both the second and third BIR domains for the relief of X-linked inhibitor of apoptosis protein (XIAP)-mediated caspase inhibition by Smac." J Biol Chem. **278** (49): 49517-49522.

Kaneda, K., S. Kashii, T. Kurosawa, S. Kaneko, A. Akaike, Y. Honda, M. Minami and M. Satoh (1999). "Apoptotic DNA fragmentation and upregulation of Bax induced by transient ischemia of the rat retina." Brain Res. **815** (1): 11-20.

Katai, N. and N. Yoshimura (1999). "Apoptotic retinal neuronal death by ischemia-reperfusion is executed by two distinct caspase family proteases." Invest Ophthalmol Vis Sci. **40** (11): 2697-705.

Kohner, E. (1989). "Retinal Ischemia." Retina **2**: 89-97.

Kuroiwa, S., N. Katai, H. Shibuki, T. Kurokawa, J. Umihira, T. Nikaido, K. Kametani and N. Yohsimura (1998). "Expression of cell cycle-related genes in dying cells in retinal ischemic injury." Invest Ophthalmol Vis Sci. **39** (3): 610-7.

Lafuente MP, MP Villegas-Perez, I Selles-Navarro, S Mayor-Torroglosa, J Miralles de Imperial, and M Vidal-Sanz (2002). "Retinal ganglion cell death after acute retinal ischemia is an ongoing process whose severity and duration depends on the duration of the insult." Neuroscience. **109** (1):157-168.

Lam TT, AS Abler, MOM Tso (1999). "Apoptosis and Caspases after Ischemia-Reperfusion Injury in Rat Retina." Invest Ophthalmol Vis Sci. **40** (5): 967-975.

Liston P, W Fong, and RG Korneluk (2003). "The inhibitors of apoptosis: there is more to life than Bcl2." Oncogene **22**: 8568-8580.

Luo, X., G. N. Lambrou, et al. (2001). "Hypoglycemia induces general neuronal death, whereas hypoxia and glutamate transport blockade lead to selective retinal ganglion cell death in vitro." Invest Ophthalmol Vis Sci. **42** (11): 2695-705.

MacFarlane M, W Merrison, SB Bratton and GM Cohen (2002). "Proteasome-mediated degradation of Smac during apoptosis: XIAP promotes Smac ubiquitination *in vitro*." J Biol Chem. **277** (39): 36611-36616.

Marques SA, M Taffarel, AM Blanco Martinez (2003). "Participation of neurofilament proteins in axonal dark degeneration of rat's optic nerves." Brain Res. **969**: 1-13.

Mattson MP, W Duan, WA Pedersen and C Culmsee (2001). "Neurodegenerative disorders and ischemic brain diseases." Apoptosis **6**: 69-81.

McKinnon SJ, DM Lehman, NG Tahzib, NL Ransom, HA Reitsamer, P Liston, E LaCasse, Q Li, RG Korneluk and WW Hauswirth (2002). "Baculoviral IAP repeat-containing-4 protects optic nerve axons in a rat glaucoma model." Mol Ther. **5**(6): 780-787.

Neuringer M (2000). "Infant vision and retinal function in studies of dietary long-chain polyunsaturated fatty acids: methods, results and implications." Am J Clin Nutr. **71** (1): 256-267.

Ogden TE (1989). "Clinical Electrophysiology." Retina **1**: 285-296.

Pollock R, R Issner, K Zoller, S Natesan, VM Rivera and T Clackson (2000). "Delivery of a stringent dimerizer-regulated gene expression system in a single retroviral vector." Proc Natl Acad Sci U S A. **97** (24): 13221-13226.

Rosenbaum DM, PS Rosenbaum, A Gupta, MD Michaelson, DH Hall, JA Kessler (1997). "Retinal Ischemia Leads to Apoptosis Which is Ameliorated by Aurintricarboxylic Acid." Vision Res. **37** (24): 3445-3451.

Rosenbaum DM, PS Rosenbaum, H Gupta, M Singh, A Aggarwal, DH Hall, S Roth and JA Kessler (1998). "The role of the p53 protein in the selective vulnerability of the inner retina to transient ischemia." Invest Ophthalmol Vis Sci. **39**(11): 2132-9.

Ross MH, LG Romrell and GI Kaye. Histology: a text and atlas. 3rd ed. 1995, Baltimore: Williams and Wilkins.

Rumelt S, Y Dorenboim and U Rehany (1999). "Aggressive systematic treatment for central retinal artery occlusion." Am J Ophthalmol. **128**:733-738.

Salvesen GS and CS Duckett (2002). "IAP proteins: blocking the road to death's door." Nat Rev Mol Cell Biol. **3**: 401-409.

Seigel, G. M., L. Chiu and A. Paxhia (2000). "Inhibition of neuroretinal cell death by insulin-like growth factor-1 and its analogs." Mol Vis. **6**: 157-63.

Schulz JB, M Weller and MA Mosckowitz (1999). "Caspases as Treatment Targets in Stroke and Neurodegenerative Diseases." Ann Neurol. **45**: 421-429.

Singh M, SI Savitz, R Hoque, G Gupta, S Roth, PS Rosenbaum and DM Rosenbaum (2001). "Cell-specific caspase expression by different neuronal phenotypes in transient retinal ischemia." J Neurochem. **77**: 466-475.

Singh M., S. I. Savitz, et al. (2001). "Cell-specific caspase expression by different neuronal phenotypes in transient retinal ischemia." J Neurochem. **77**(2): 466-75.

Sucher NJ, SA Lipton, and EB Dreyer (1997). "Molecular Basis of Glutamate Toxicity in Retinal Ganglion Cells." Vision Res. **37** (24): 3483-3493.

Timmers AM, H Zhang, A Squitieri and C Gonzalez-Pola (2000). "Subretinal injections in rodent eyes: Effects on electrophysiology and histology of rat retina." Mol Vis. **7**: 131-7.

Vallée J, M Paques, A Aymard, P Massin, P Santiago, P Adeleine, A Gaudric, J Merland (2002). "Combined Central Retinal Arterial and Venous Obstruction: Emergency Ophthalmic Arterial Fibrinolysis." Radiology **223**: 351-359.

Van Soest S, A Westerveld, PTVM De Jong, EM Bleeker-Wagemakers and AAB Bergen (1999). "Retinitis Pigmentosa: Defined from a Molecular Point of View." Surv Ophthalmol. **43**(4): 321-334.

Villa P, SH Kaufmann and WC Earnshaw (1997). "Caspases and caspase inhibitors." TIBS **22**: 388-393.

Wachtmeister, L. (1998). "Oscillatory potentials in the retina: what do they reveal." Prog Retin Eye Res. **17**(4): 485-521.

Wang J and MJ Lenardo (2000). "Roles of caspases in apoptosis, development, and cytokine maturation revealed by homozygous gene deficiencies." J Cell Sci. **113**: 753-757.

Winkler, B. S., M. J. Arnold, M.A. Brassell and D.G. Puro (2000). "Energy metabolism in human retinal Muller cells." Invest Ophthalmol Vis Sci. **41**(10): 3183-90.

Xu D, Y Bureau, DC McIntyre, DW Nicholson, P Liston, Y Zhu, W Fong, SJ Crocker, RG Korneluk, and GS Robertson (1999). "Attenuation of Ischemia-induced Cellular and Behavioral Deficits by X-chromosome-linked Inhibitor of Apoptosis Protein Overexpression in the Rat Hippocampus." J Neurosci **19** (12): 5026-5033.

Appendices

Appendix 1: Scotpic-photopic ERG B-wave amplitudes, means and ratios

XIAP Baseline B-wave Amplitudes

OD Step	183	185	186	187	188	189	190	191	200	194	195	197	199	201	35	36	40	49
1	356.6	289.8	175	279.8	375.9	202	280.6	254.3	135.1	318.8	315.8	199.3	328.8	226.6	113.3	282.4	158.1	250.6
2	508.3	395.5	236.8	357.6	492	294.4	404.7	381.2	252.5	425.4	357.6	280.7	444.3	346.5	175.3	327.5	248.8	297.3
3	582.1	476.8	256.9	485.6	537	333.7	509.5	438.2	309.9	494.5	397.2	332.2	499.3	394.1	228.4	445.8	355.5	425.5
4	623.2	536.8	343.8	541.3	569.8	358.7	572.8	452.3	381	524.8	444.9	377.4	569.7	406.3	265.7	525.8	441.8	451.2
5	646.8	558.5	375.9	591.3	610.9	374.7	608.4	474.3	398.6	550.1	529.1	390.8	578.6	444.8	276.7	583.1	495.8	524.3
6	679.1	606.9	403.7	634.8	696.6	399.6	700.9	550.3	420.2	625.9	573.8	443.7	654.7	486.3	274.4	639.4	548.5	582.3
7	791.5	681.4	450.2	721.2	777.4	446.1	777.3	625	525.3	730.3	694.8	524.7	795	575.2	302.5	713.4	605.3	721.5
8	817.5	744.9	464.6	788.2	821.3	499.8	871.5	633.4	549.8	779.6	770.9	575.7	851.8	621.8	447.7	759.9	718	923.4
9	832.1	745.8	568.4	824.5	751	532.2	957.8	585.7	640.9	747.9	782.4	555.2	866.5	588.7	514.1	898.9	835.8	738
10	719.3	649.5	563.7	749.9	656.4	456.6	913.8	480.1	571.7	652.1	726	502.7	745	529.3	501.7	817.5	820.7	665.4
11	605.2	538.3	521.8	642	521.7	408.8	784.2	375.4	488.7	526.6	641.4	420.4	634.7	468.5	478.6	680.9	772.3	564.2

OS Step	183	185	186	187	188	189	190	191	200	194	195	197	199	201	35	36	40	49
1	257.6	183.6	239.6	225.2	281	163.4	198.4	164.3	149.2	210.6	253.8	199.7	228.6	186.3	64.93	230.7	226.9	157.9
2	426.1	268.9	323.8	312.2	408.7	226.2	309.9	260.4	268.6	451	372.2	292.3	370.7	274.2	104.1	298.8	329.2	203
3	562.3	364.6	374.9	491.5	498.4	310.7	484.5	361.9	302.9	551.3	393.7	355.5	442.1	395.7	153.1	384.8	400.2	308.6
4	652.1	485	450.7	588.4	595.4	360.2	561.2	423.8	375.2	602.1	476.3	375.6	516.7	437.6	187.2	518.5	443.4	361
5	739.4	549.4	478.8	680.3	714.1	428.7	632.3	447.9	418.1	626.1	571.8	410.4	596.1	472.7	193	587.4	471.7	399.5
6	633.8	560.6	523.9	688.7	755.4	420.7	724.5	481	425.3	675.5	593.7	435	620.3	488.5	197	642.7	509.1	435.7
7	686.1	591.6	534.2	756.4	817.5	444.3	781.8	520.7	527.7	774.5	713.5	507.1	757.5	581.4	237.1	689.9	554.4	509.9
8	779.6	709.2	518.5	837.1	945.9	533.2	890.8	580.9	589.8	859.3	790	546	852.8	668.4	351	763.3	631.4	637.3
9	941.8	777.6	587.4	956.3	1049	615.9	1023	634.4	635.4	857.9	814.9	544	897	662.1	453	912.2	669.1	788.2
10	903.8	728	565.5	905.8	996	549.8	1000	578.5	549.7	784.6	756.6	489.7	822.6	598.3	497.5	851.8	620.1	838.6
11	803.4	622.9	513.2	805.8	898.2	517.4	897.4	504.7	493.4	652.9	674.3	430.4	729.6	555.6	505.8	777.4	559.7	753.2

XIAP 24 hpi B-wave Amplitudes

OD Step	183	184	185	186	187	188	189	190	191	194	195	197	199	200	201	35	36	40	49
1	147.6	46.05	34.81	39.21	14.84	32.72	65.3	11.11	28.71	116.2	156.9	144.3	51.41	93.17	180	81.22	13.69	71.56	34.04
2	255.6	129	57.95	89.36	38.43	77.45	182.7	29.54	52.07	172.1	237	209.8	114.2	145.8	248.6	184	27.01	137.8	50.25
3	355.8	133.2	71.68	154.8	58.82	107.1	209.3	53.61	43.65	287.1	253.7	269.1	129.6	202.6	324.6	181.1	45.81	214	98.59
4	383.6	179.5	137.3	180.5	97.17	146.8	260.9	50.13	53.91	291	313.8	242.4	165.8	266.3	352.8	339.1	54.44	242.7	137.7
5	356.4	154.4	165.1	167.8	92.31	187.4	224	63.54	42.64	330.2	249.3	227.5	130.1	285.2	339.1	335.5	103.7	269.2	125.4
6	345.2	108.7	141.1	144	54.57	150.3	174.4	50.29	24.17	308.4	196.6	199.3	116.1	263.8	297.5	289.6	49.93	240	82.34
7	361.1	77.31	128.4	109.2	35.02	159.9	160	51.58	21.46	288.1	206.8	246.2	95.6	241.2	327.2	214.4	77.99	226.7	77.91
8	388.1	93.8	157.5	127.9	54.49	174.2	166.9	43.1	13.41	308.1	223.2	231.3	100.1	249.1	348.4	277.4	53.18	233.4	82.3
9	449.5	116.7	160.8	152.3	62.11	195.2	166.9	83.74	17.72	336.8	225.9	202.5	103.6	278.3	363.7	308.5	104.9	267.2	107.5
10	380	69.44	156.8	96.49	26.77	146.5	107.7	45.86	20.91	298.5	182.7	132.5	71.16	253.9	328.3	262.6	68.94	196.2	76.74
11	361.8	69.33	125.8	49.76	15.03	121	58.33	11.38	16.33	262.2	149.5	95.6	20.91	202.5	278.9	152.9	28.47	168.1	35.9

OS Step	183	184	185	186	187	188	189	190	191	194	195	197	199	200	201	35	36	40	49
1	81.56	135.1	138.4	136.7	98.95	126.1	32.41	181.6	191.5	280.7	139.6	131.1	115.1	269.6	160.5	58.59	88.77	102.6	100.2
2	167.4	238.5	191.3	169.9	199.3	180.7	158.2	323.7	282.1	403.8	191	206.1	165.2	401.2	195.7	106.6	145.9	160.9	169.6
3	273.2	321.8	257.2	254	266.7	232.6	168.3	411.6	288.6	464	207.4	283.2	184	479.8	214	105.9	174.4	227.1	255.8
4	341.2	380.3	294.5	288.3	320.9	288.1	280.1	475.1	297.1	500.2	259.8	323.5	225.1	518.6	262.3	129.9	199.3	223.2	274
5	343.1	446.6	385.5	338.2	363.2	341.1	348.9	506.8	294	578.5	256.9	425.8	251.3	542.2	305.4	166.1	221.1	281.8	274.3
6	465.4	541.3	400	355.5	360.6	382.5	406.9	600.6	280.5	628.4	272.5	437.8	289.9	543.7	342.4	183.9	188.8	320.5	275.1
7	474.3	563.1	452.1	392.9	406	437.5	407.6	661.6	284.3	648.1	283	498.4	316.2	562.7	347.1	192.3	250.9	317.6	292.7
8	494.9	588.9	524.6	436.8	487.6	480.7	460.2	705.2	288	672.8	268.9	569.8	329.8	584.6	382.6	225.5	213.7	341	320.3
9	605.5	653	527.6	501.5	561	460.4	577.6	801.3	259.8	637	266.8	707.6	393.1	649.1	411.2	256.2	268.9	357.9	337.6
10	607.4	581.4	475	461.4	522.5	386.5	556.5	716	225.2	564.9	235.2	680.6	383.6	605.9	384.2	240.6	250.4	296.9	301.4
11	613.5	526.6	395	388.6	462.5	329	486.5	595.7	196.9	467.7	234.8	637.3	332.2	493.9	358.3	177.6	196.8	251.9	250.2

XIAP 2 wpi B-wave Amplitudes

OD Step	183	185	186	187	188	189	190	191	200	35	36	40	49
1	146.6	123.8	195	85.33	209.6	130.5	72.7	59.2	298.8	7.834	96.47	151.5	37.12
2	200.7	138.2	242.7	138.2	279.9	119.2	116.8	87.08	365.3	41.87	129.9	279.2	68.78
3	233	158.4	247.8	157.3	308.6	185.1	129	116.7	443.6	136.8	140.4	343.7	74.55
4	223.7	174.4	224.1	181.2	335.9	199.2	141.1	120	439.1	123.1	187.3	365	116.1
5	225.2	221.5	220.2	167.9	322	194.8	128.7	110.3	433.3	181.1	148.3	382.2	107.7
6	264.4	235	262.3	150.2	336.1	203.8	103.1	89.93	450	180.2	117	368.5	110.3
7	309.7	228.4	330.5	159.1	387.2	227.2	108	63.56	520.2	186.2	124.7	423.6	84.64
8	344.3	251.2	347.4	167.3	415.3	230.9	162.3	81.3	548.8	203.2	188.4	453.4	96.26
9	355.1	324.4	338.6	209.6	394.7	247.3	193.6	128.1	517.5	206.9	214.4	480.5	123.3
10	302.1	263.2	242.2	172.1	303.3	202.7	178.6	104.5	438.7	209.1	180.5	393.3	137.1
11	261.5	205.8	180.1	125.9	149	143.3	113.1	113.5	302	165.6	149.7	338.4	110

OS Step	183	185	186	187	188	189	190	191	200	35	36	40	49
1	210.4	259	50.13	342.8	234.8	216.3	253.7	170.5	341.4	63.68	241.3	215	150
2	297.6	373.1	85.38	503.2	339.1	244.1	353.2	228.9	476.9	122.4	335.6	370.4	291.6
3	343.8	438.4	95.95	567.3	420.7	349.5	484.9	286	629.7	223.7	418.3	483.9	343.1
4	384.7	496.3	216	618.2	484	398.7	586.5	427.7	676.1	224.2	552.8	643.6	432.8
5	487.4	591.3	371	655	603	420	674.5	450.9	757.3	257.2	501.3	706.8	463.8
6	517.1	632.9	460	704.9	629.7	463.2	684.4	394.3	783.3	278.3	548.6	733.9	506.7
7	539.8	680.1	546.6	768.7	697	487.3	741.5	487.7	886.7	307.9	611.5	799.7	529.3
8	603.9	710.7	538.5	781.3	797.4	541.5	920	455.2	1006	388.8	693.9	918.1	611.3
9	661.1	785.1	684.5	768.4	861	553	985.7	475.6	1070	439.5	829.9	1025	612.6
10	621.1	673.4	708.3	686.2	778.8	494.9	932.7	486.5	1001	402.8	801.4	878.7	562.6
11	565	564.1	727.7	544.7	631	447.8	776.6	480.9	878.3	345.4	706.6	828.5	455.3

XIAP 4 wpi B-wave Amplitudes

OD Step	185	186	187	188	189	190	191	200	35	36	40	49
1	138	109.3	136.1	151.9	171.7	147.7	111.7	230	54.38	91.36	158.2	103.7
2	209.9	218.2	202.2	203.3	223.6	194.8	140.6	336.3	47.69	129	229.7	129.5
3	273.1	242.3	244.8	233.7	212	218	148	387.5	96.07	170.9	234.9	135.4
4	291.8	292.1	264	304.5	223.6	198.1	162.9	449.8	131.6	164.1	267.2	164.9
5	285.3	293.4	249.5	318	203.7	181.6	148	473.4	164.7	198.1	264.5	141.7
6	294.4	278	225.7	315.1	235.7	199.6	132.7	455.1	178.4	149.6	247.1	131.6
7	327.6	309.3	225.4	324.6	265.1	222.5	168.5	486.4	111.5	153.8	241.4	124.8
8	359.3	349	258.9	363.1	275.5	269.2	193.3	532.4	170.8	170.7	305.4	151.9
9	347	415	301.4	377.7	271.4	279.2	185.1	539.3	174.2	202.6	274.4	159.8
10	305.4	391.4	277.3	316.2	193.9	231.1	152.2	482	167.9	164	240	178.9
11	244	363.5	210.6	229.9	153.9	180.5	109.6	373.1	86.32	139.9	179.1	130.8

OS Step	185	186	187	188	189	190	191	200	35	36	40	49
1	272	263.1	233	324.5	244.8	293.4	302	199.2	41.6	157	267.1	124.4
2	371.1	325.6	331.6	400.8	357.8	444.5	390	289.5	67.96	253.6	382	157
3	424.1	339.7	433	480.5	394	545.9	438.8	327.9	82.53	314.9	440.6	156.9
4	457.1	379.8	519.5	539.8	461.9	622	528.5	398	131.7	327.9	518.5	228.8
5	478.2	374.7	565.9	583.2	504.8	676.4	549.1	437.5	116.7	429.5	575.3	248.7
6	507.9	389.6	593.7	639.3	549.3	737.3	596.8	471.4	137.4	384.8	567.3	316.5
7	566.8	430.5	636.7	723	612.2	810.1	683.1	506.2	131	437.4	606.1	299.7
8	603.9	470.7	709.2	783.6	667.6	935	746.1	564.7	152.2	465.8	704.4	353.6
9	574.9	470.2	750.9	747.6	699.3	972.1	730.6	594.8	169.1	450	720.5	362.7
10	522.6	436	718.4	652.8	631.1	935.7	639	563.8	173.7	383.5	618.6	371
11	435.7	402.1	640.4	507.8	570.2	824.6	524.8	476.2	151	334	529.8	322.9

B-wave amplitude ratios - XIAP

XIAP 24 hpi

OD:OS Step	183	184	185	186	187	188	189	190	191	194	195	197	199	200	201	35	36	40	49
1	1.81	0.341	0.252	0.287	0.15	0.259	2.015	0.061	0.15	0.414	1.124	1.101	0.447	0.346	1.121	1.386	0.154	0.697	0.34
2	1.527	0.541	0.303	0.526	0.193	0.429	1.155	0.091	0.185	0.426	1.241	1.018	0.691	0.363	1.27	1.726	0.185	0.856	0.296
3	1.302	0.414	0.279	0.609	0.221	0.46	1.244	0.13	0.151	0.619	1.223	0.95	0.704	0.422	1.517	1.71	0.263	0.942	0.385
4	1.124	0.472	0.466	0.626	0.303	0.51	0.931	0.106	0.181	0.582	1.208	0.749	0.737	0.513	1.345	2.61	0.273	1.087	0.503
5	1.039	0.346	0.428	0.496	0.254	0.549	0.642	0.125	0.145	0.571	0.97	0.534	0.518	0.526	1.11	2.02	0.469	0.955	0.457
6	0.742	0.201	0.353	0.405	0.151	0.393	0.429	0.084	0.086	0.491	0.721	0.455	0.4	0.485	0.869	1.575	0.264	0.749	0.299
7	0.761	0.137	0.284	0.278	0.086	0.365	0.393	0.078	0.075	0.445	0.731	0.494	0.302	0.429	0.943	1.115	0.311	0.714	0.266
8	0.784	0.159	0.3	0.293	0.112	0.362	0.363	0.061	0.047	0.458	0.83	0.406	0.304	0.426	0.911	1.23	0.249	0.684	0.257
9	0.742	0.179	0.305	0.304	0.111	0.424	0.289	0.105	0.068	0.529	0.847	0.286	0.264	0.429	0.884	1.204	0.39	0.747	0.318
10	0.626	0.119	0.33	0.209	0.051	0.379	0.194	0.064	0.093	0.528	0.777	0.195	0.186	0.419	0.855	1.091	0.275	0.661	0.255
11	0.59	0.132	0.318	0.128	0.032	0.368	0.12	0.019	0.083	0.561	0.637	0.15	0.063	0.41	0.778	0.861	0.145	0.667	0.143

XIAP 2 wpi

OD:OS Step	183	185	186	187	188	189	190	191	200	35	36	40	49
1	0.697	0.478	3.89	0.249	0.893	0.603	0.287	0.347	0.875	0.123	0.4	0.705	0.247
2	0.674	0.37	2.843	0.275	0.825	0.488	0.331	0.38	0.766	0.342	0.387	0.754	0.236
3	0.678	0.361	2.583	0.277	0.734	0.53	0.266	0.408	0.704	0.612	0.336	0.71	0.217
4	0.581	0.351	1.038	0.293	0.694	0.5	0.241	0.281	0.649	0.549	0.339	0.567	0.268
5	0.462	0.375	0.594	0.256	0.534	0.464	0.191	0.245	0.572	0.704	0.296	0.541	0.232
6	0.511	0.371	0.57	0.213	0.534	0.44	0.151	0.228	0.574	0.648	0.213	0.502	0.218
7	0.574	0.336	0.605	0.207	0.556	0.466	0.146	0.13	0.587	0.605	0.204	0.53	0.16
8	0.57	0.353	0.645	0.214	0.521	0.426	0.176	0.179	0.546	0.523	0.272	0.494	0.157
9	0.537	0.413	0.495	0.273	0.458	0.447	0.196	0.269	0.484	0.471	0.258	0.469	0.201
10	0.486	0.391	0.342	0.251	0.389	0.41	0.191	0.215	0.438	0.519	0.225	0.448	0.244
11	0.463	0.365	0.247	0.231	0.236	0.32	0.146	0.236	0.344	0.479	0.212	0.408	0.242

XIAP 4 wpi

OD:OS	185	186	187	188	189	190	191	200	35	36	40	49
Step												
1	0.507	0.415	0.584	0.468	0.701	0.503	0.37	1.155	1.307	0.582	0.592	0.834
2	0.566	0.67	0.61	0.507	0.625	0.438	0.361	1.162	0.702	0.509	0.601	0.825
3	0.644	0.713	0.565	0.486	0.538	0.399	0.337	1.182	1.164	0.543	0.533	0.863
4	0.638	0.769	0.508	0.564	0.484	0.318	0.308	1.13	0.999	0.5	0.515	0.721
5	0.597	0.783	0.441	0.545	0.404	0.268	0.27	1.082	1.411	0.461	0.46	0.57
6	0.58	0.714	0.38	0.493	0.429	0.271	0.222	0.965	1.298	0.389	0.436	0.416
7	0.578	0.718	0.354	0.449	0.433	0.275	0.247	0.961	0.851	0.352	0.398	0.416
8	0.595	0.741	0.365	0.463	0.413	0.288	0.259	0.943	1.122	0.366	0.434	0.43
9	0.604	0.883	0.401	0.505	0.388	0.287	0.253	0.907	1.03	0.45	0.381	0.441
10	0.584	0.898	0.386	0.484	0.307	0.247	0.238	0.855	0.967	0.428	0.388	0.482
11	0.56	0.904	0.329	0.453	0.27	0.219	0.209	0.783	0.572	0.419	0.338	0.405

Mean B-wave amplitudes - XIAP

XIAP
OD Avg

Step	Base	24 hpi	2 wpi	4 wpi
1	252.38	71.728	124.19	133.67
2	345.91	128.35	169.83	188.73
3	416.79	168.11	205.77	216.39
4	465.96	205.04	217.71	242.88
5	500.71	202.57	218.71	243.49
6	551.17	170.33	220.83	236.92
7	636.56	163.48	242.54	246.74
8	702.21	175.05	268.47	283.29
9	720.33	194.94	287.23	293.93
10	651.19	153.79	240.57	258.36
11	559.65	117.04	181.38	200.1

XIAP
OS Avg

Step	Base	24 hpi	2 wpi	4 wpi
1	201.21	135.21	211.46	226.84
2	305.57	213.53	309.34	314.29
3	396.48	266.82	391.17	364.9
4	467.24	309.55	472.43	426.13
5	523.21	351.09	533.81	461.67
6	545.08	382.96	564.41	490.94
7	610.31	409.92	621.83	536.9
8	693.58	440.84	689.74	596.4
9	767.73	485.95	750.11	603.56
10	724.27	446.08	694.49	553.85
11	649.74	389.21	611.68	476.63

Mean B-wave amplitude ratios – XIAP

	XIAP 24 hpi N=19			XIAP 2 wpi N=13			XIAP 4 wpi N=12		
Step	**MEAN Ratio**	**STDEV**	**SE**	**MEAN Ratio**	**STDEV**	**SE**	**MEAN Ratio**	**STDEV**	**SE**
1	0.655	0.592	0.136	0.753	0.974	0.27	0.668	0.292	0.084
2	0.685	0.499	0.114	0.667	0.684	0.19	0.631	0.207	0.06
3	0.713	0.488	0.112	0.647	0.611	0.169	0.664	0.274	0.079
4	0.754	0.57	0.131	0.489	0.227	0.063	0.621	0.249	0.072
5	0.64	0.436	0.1	0.42	0.165	0.046	0.608	0.337	0.097
6	0.482	0.347	0.08	0.398	0.173	0.048	0.549	0.309	0.089
7	0.432	0.296	0.068	0.393	0.198	0.055	0.503	0.228	0.066
8	0.433	0.317	0.073	0.39	0.173	0.048	0.535	0.269	0.078
9	0.443	0.307	0.07	0.382	0.123	0.034	0.544	0.257	0.074
10	0.385	0.296	0.068	0.35	0.112	0.031	0.522	0.253	0.073
11	0.327	0.275	0.063	0.302	0.103	0.029	0.455	0.217	0.063

GFP baseline B-wave amplitudes

OD Step	162	164	165	166	167	168	169	170	172	173	175	176	177	178	179	52	54	59	61
1	199.5	186.6	300.3	227.6	224.8	218.6	294.8	286.4	474.8	312.3	191.7	117.3	92.89	144.3	166.8	54.88	87.35	108.3	128.2
2	243.3	249.5	411.6	320.7	315.1	306.7	431.3	394.5	669.8	532.2	262.1	148.9	129.9	200.6	177.9	98.52	137.1	214.3	215.3
3	319.8	281.7	510.4	413.9	314.8	361.8	526.2	428.1	770.3	659.8	290.9	164.8	195.4	295.1	299.1	183.9	147.2	249.9	315.2
4	374.1	325.6	522	428	373.7	384.6	566.1	476.2	854.8	763.4	290.3	193.6	270.3	331.8	407.9	251	201.3	335.7	404.5
5	388.6	320.2	542.5	500.2	355.7	421.1	628	508.1	977.6	778.9	304	194.7	379.4	448.5	426.7	282.9	280.2	479.9	479.7
6	456.6	385.5	582.7	550.4	413.6	443	672.6	553.8	1067	843.3	298.2	193	395	462.9	475	375.7	286	549.2	503.4
7	496.6	423	640.1	670.4	465.8	495.5	827.7	653.7	1270	1021	343.1	218.4	435.4	499.6	487.1	398.5	344.4	663.7	528
8	537.2	452.3	664.8	758.1	500.6	550.9	944.5	745.9	1353	1141	378	235.4	500.1	571.4	578.6	440.2	407.6	805.7	597.3
9	553.5	479.6	749.3	849.4	550.7	550.6	917.4	718.4	1247	1061	386.6	256.6	596.9	695.2	651	598.9	477	928.5	745.1
10	472.1	422.7	724.5	773.9	472.9	480.7	834.7	657.5	1150	986.5	331.1	230.6	610.7	701.6	635.1	651.5	448	919.3	722.4
11	417	492.9	621.7	694.4	414	429.4	747.6	487.2	874.9	855.4	310.2	220.5	585	671.4	583.7	669.1	490.9	866.8	719.4

OS Step	162	164	165	166	1667	168	169	170	172	173	175	176	177	178	179	52	54	59	61
1	103.4	111.5	246.8	259.1	255.7	245.8	302.7	279.4	289	310.5	234	125.3	376.6	295.7	404.9	69.17	88.14	115.2	138
2	170.5	164.7	350.6	374.2	398.3	361.6	452.9	412	437.1	474.9	314.4	163	502.2	387.2	511.8	117.9	137.8	213.8	220.4
3	228.5	199.3	478.2	476.5	420.5	476.3	548.7	470.5	571.1	578.5	333	192.8	581.9	426.8	601.8	240.9	156.6	255.2	301.4
4	276.1	243	500.8	512.9	544	518.2	566.2	553.8	706.5	681.7	348.9	202	589.5	452.4	634.7	322	190.3	376.9	423.5
5	290.6	285.6	609	601	522.5	582.9	634.6	622.3	847.7	684.4	369.7	189.8	650.9	508.9	665.5	337.1	280.6	579.9	413.7
6	347.5	441.3	631.2	647.9	607.4	614.3	667.7	632.9	881.4	716.5	360.8	204	739.1	582.8	755.6	412.6	277.5	596	436.5
7	349.5	446.1	689.5	708.2	682.3	663.3	778.7	710.2	1020	813.6	390.6	217	825.9	683.9	809.4	412.5	322.5	715	485.2
8	376.1	452.3	743	772.3	739.5	732.5	872.3	853.7	1171	905.9	428.6	240.9	884.8	723.9	853.7	473.8	386.8	864.1	575.2
9	419.1	574	806.3	834.7	803.9	768.2	847.2	915.5	1203	991.9	448.3	247.2	818.7	629.6	812.5	632.2	498.5	982.1	736.2
10	387.1	567.5	778.3	787.8	708.4	705.5	769.8	858.9	1162	935.5	375	217.6	690.1	553.7	706.6	662.6	484.8	968.4	703.2
11	342.7	547.9	697	725.2	644.4	649.1	689.9	716	954.5	808.2	324.9	207.6	549.9	486	552.3	663.4	512	892.5	693.6

GFP 24 hpi B-wave Amplitudes

OD Step	162	164	165	166	167	168	169	170	172	173	175	176	177	178	179	52	54	59	61
1	6.722	122.8	91.01	88.69	48.33	18.43	175.2	18.2	126.9	116.8	45.76	7.253	35.16	15.58	4.101	29.92	6.438	11.52	26.24
2	36.9	185.9	131.1	174.9	71.55	104.6	245.4	40.41	193.7	223.7	97.78	76.56	107.2	17.7	42.3	35.26	33.1	3.976	52.34
3	54.86	243.9	195.8	258.6	100.8	150.1	294.1	63.24	233.8	253.4	104.2	122.6	163.6	14.98	4.5	76.48	41.48	53.08	54.58
4	70.87	271.7	188.3	253.1	123.7	167.7	381.7	86.87	223.3	261.6	147.2	81.47	129.8	41.76	23.71	106.6	95.68	70.81	135.3
5	47.96	306.4	218.6	265.2	182.8	174	317.4	101.7	172	223.9	108.7	98.72	76.52	66.25	46.14	131.1	115.1	72.16	128.8
6	15.65	267.9	162.9	221.6	153.2	159.7	282.9	26.3	191.5	209.6	76.31	58.41	63.43	22.77	52.17	117.9	95.34	87.58	108.2
7	7.518	225	162.9	258.4	128.9	125.4	299.6	8.8	192.7	206.3	56.28	70.59	66.24	2.517	11.58	104.6	67.09	42.52	95.16
8	11.54	242.3	178.3	244.9	118.7	96.67	330.5	17.75	189.7	227.6	73.14	67.42	77.44	35.6	11.67	73.61	66.69	28.26	93.96
9	2.707	271.3	204.4	235.5	134.4	173	272.7	65.36	134.2	205.6	87.18	45.78	59.89	34.94	4.231	110.1	100.3	107.4	103
10	7.76	201.4	130.8	193.3	119	171.9	216.2	39.58	94.85	159.5	52.87	22.55	32.36	49.81	2.467	98.4	49.82	84.86	94.03
11	1.815	129.3	104.4	165.6	110.5	95.44	126.3	35.54	35.12	110.3	45.37	10.93	21.39	14.27	1.93	57.56	35.06	60.65	90.28

OS Step	162	164	165	166	167	168	169	170	172	173	175	176	177	178	179	52	54	59	61
1	79.39	94.48	99.22	155.8	164.9	82.33	155.3	134.9	159.8	59.09	179.7	147.4	78.18	36.81	199.2	90.7	64.96	59.56	37.18
2	147.5	123.5	157.2	267.5	240.3	218	214.1	232.1	269.7	116.9	243.4	238.7	165.4	90.6	370.4	116.4	126	80.18	52.12
3	210.6	188.5	280.3	391.4	309.1	340	270.4	319.7	420.5	162.1	297.6	333.3	285	142.4	372.2	205	269.3	152.5	71.57
4	283.2	228.5	341.2	488.5	400.4	409.6	381.3	391.2	534.1	225.4	379.8	331.3	414.8	225.4	457.6	251.5	353.1	167.5	148.9
5	312.2	317	425.5	600.9	538.7	484.9	418.7	451	562.6	224.1	427.5	394.4	461.6	234.2	499.7	282.2	404.4	202.3	189.8
6	352.7	365.1	426	642	578.3	544.8	456.3	470.2	632.5	288.9	482	440.4	491.6	250.6	550.4	306.4	407.7	227.4	229.4
7	382.1	381.5	513.7	680	564.8	573.8	533.7	538.9	678	332.8	485.4	488.6	564.4	308.4	606.6	305.7	431.1	249.8	224.7
8	396.9	419.5	520.5	723.7	653.2	595.9	602.5	626.8	768.1	392.8	562.2	512	593.9	387.9	666.4	312.5	464.5	265.6	234.9
9	485	514.2	677.6	887.7	823.5	786.8	632.3	703.9	844.1	452.9	658.9	502	772.3	404.5	666.9	381.2	568.2	317.4	254.8
10	465.5	512.3	634.4	883	809.8	786.8	591.2	622.7	780.8	455.7	620.4	440.1	820.5	403.7	574.4	344.9	421.7	303.7	274.5
11	447.3	442.1	596.7	809.4	781.1	680	493.6	552.9	682.7	433.4	557.9	381.4	795.5	331.4	522.1	316.9	510.1	267.2	255.5

GFP 2 wpi B-wave Amplitudes

OD Step	162	164	165	166	167	168	169	170	172	52	54	59	61
1	69.09	195.8	128.4	281.3	136.1	139	239.8	50.72	168.4	9.136	39.27	18.62	4.862
2	82.61	277.3	196.8	370.4	187	238.6	260	49.25	205.3	77.28	15.8	29.34	16.01
3	79.04	283.6	205.9	354	164.1	244.7	361.9	75.86	302.6	56.66	61.24	45.97	0.679
4	50.24	308.1	216	361	210.2	244.3	349.6	39.8	303.3	36.02	44.13	80.47	19.84
5	56.63	291.5	218.4	338.3	252.4	294.6	334.8	56.43	279.6	24.74	48.76	30.34	24.55
6	31.19	338.3	241.7	386.9	241.3	290.7	336.7	44.11	282.1	34.22	41.46	31.2	38.05
7	78.89	315.2	309.5	426.6	271.7	316.8	428.2	54.61	365	41.9	27.95	16.03	12.41
8	99.75	319.4	322.4	441.7	280.2	340.7	459.5	94.27	376.9	55.62	51.74	62.62	37.29
9	92.26	310.6	331.9	433.5	317	329.3	398.9	107.4	352.6	49.57	66.49	116.2	78.36
10	80.61	290.3	283.4	341.6	292.6	297	304.4	130.2	288.1	33.67	78.54	89.12	89.22
11	67.47	187	183.7	247.3	225.7	236.9	238.5	72.47	231.5	28.26	57.28	68.46	70.76

OS Step	162	164	165	166	167	168	169	170	172	52	54	59	61
1	185.5	203.6	171.5	202.3	169.3	298.9	266.8	251.8	357.3	16.58	101.8	152.6	109.1
2	271.1	335.1	290.4	294.8	241.3	454.2	304	327.7	515.8	217.9	121.8	259.5	207.9
3	344.7	371.8	325.7	296.5	284.8	485.5	394.1	371.6	619.1	244.8	299.3	363	214.3
4	363.2	441.8	441.6	437.5	338.3	521.8	488.3	418.2	774.8	266.4	265.2	469.3	350.8
5	436.6	544.5	510.2	491.5	420.8	632	533	518.6	788	282.9	311.8	414.8	456.6
6	410.7	604.3	548.2	543.1	467	648.6	540.8	528.7	807.3	326.7	312.7	561.4	522.9
7	506.4	637.4	615.5	589.8	507.6	722.6	647.6	576.8	882.8	350.5	334.5	571.5	549.6
8	575.5	684.6	659.9	675.9	571.4	787.4	727.7	645.3	950.4	377.8	393.6	648.3	701.3
9	628.5	748.2	739.1	742.2	631.9	767	751.2	644.1	933.7	428.2	451.3	723.8	747.5
10	597.4	751.1	716.5	705.4	592.7	697.9	669.4	607.3	793.6	408.7	412.2	690.1	705.7
11	544.3	643.8	644.9	604.4	531.2	612.3	608.5	471.1	699.2	363.6	396.8	624.6	642.6

GFP 4 wpi B-wave Amplitudes

OD Step	162	164	165	166	167	168	169	170	172	52	54	59	61
1	79.25	132.1	133.6	360.1	0	256.3	403.4	95.68	241.3	18.18	46.1	14.8	12.73
2	108.2	177.1	166.9	447.1	206.9	343.2	579.2	131.1	312.1	61.23	52.78	21.08	25.12
3	95.69	189.5	196.5	505	242.6	363	603.4	129.1	329.8	69.09	103.3	13.72	22.93
4	90.95	182.5	175.9	549.6	259.4	378.5	583.3	114.2	341.2	81.95	106.6	62.17	30.65
5	69.55	184.9	182.5	583.8	307.1	406.6	564	99.62	317	106.1	116.9	46.32	37.59
6	66.43	186.9	158.7	612.9	280.2	433.7	612.5	95.78	327	111.2	85.8	30.82	27.73
7	96.92	190.9	175	711.4	277.2	439.6	667.1	126.8	377.4	48.18	101.3	14.97	18.72
8	97.1	180.6	180.4	747	314.9	480.8	699.6	171.7	424.2	64.8	80.03	25.86	33.76
9	108.1	192.2	162	692.9	321.3	449.4	639.7	183.3	312.4	75	127.2	50.91	48.89
10	96.12	184.1	126.2	554.8	294.7	374.5	513.7	123.5	258.4	96.09	98.68	59.93	37.62
11	70.29	123.1	102.4	419.5	248.6	236.2	356.7	105	149.1	78.15	110.9	56.71	42.02

OS Step	162	164	165	166	167	168	169	170	172	52	54	59	61
1	122.3	103.7	205.8	227.6	229.7	341.8	221.4	213.6	382.7	24.3	18.7	43.88	47.12
2	177.2	148	279	320.7	339.9	441.2	382.2	316.8	549.2	107.6	62.54	80.59	165.2
3	187.3	168.6	433.4	413.9	429.4	536.6	441.4	373.5	671.9	184.8	103.3	110.3	203
4	195.1	214.9	497.9	428	500.3	652	480.1	427.1	849.4	245.8	126.6	231	294
5	205	322.9	597.5	500.2	580.4	717.7	502	459.5	883	294.6	208.5	241.4	370.3
6	211.4	378.5	625.5	550.4	666.7	768.8	532.7	477.5	918.6	356.7	193.9	224.6	386.5
7	234.7	189	683	670.4	758.1	812.7	589.5	545.2	1025	289.6	224.3	250.5	318.6
8	252.1	287.9	748.7	758.1	820.7	933.5	651	617.3	1138	340	209.2	289.9	239.4
9	285.8	386.4	817	849.4	783.9	953	681	639.2	1099	377.4	296.6	377.9	250.9
10	286.3	405.9	769.7	773.9	711.7	884.3	640.4	563.7	1004	388.5	263	392.7	222
11	245.4	395.2	693.1	694.4	613.2	735	556.2	509.1	878.5	372.8	297.8	376.8	212

B-wave amplitude ratios – GFP

GFP 24 hpi

OD:OS Step	162	164	165	166	167	168	169	170	172	173	175
1	0.084671	1.299746	0.917255	0.569255	0.293087	0.223855	1.128139	0.134915	0.794118	1.976646	0.254647
2	0.250169	1.505263	0.833969	0.653832	0.297753	0.479817	1.146193	0.174106	0.718205	1.913601	0.401726
3	0.260494	1.293899	0.698537	0.660705	0.326108	0.441471	1.087648	0.19781	0.556005	1.563233	0.350134
4	0.250247	1.189059	0.551876	0.518117	0.308941	0.409424	1.001049	0.22206	0.418087	1.160603	0.387572
5	0.153619	0.966562	0.513749	0.441338	0.339335	0.358837	0.758061	0.225499	0.305723	0.999108	0.254269
6	0.044372	0.733772	0.382394	0.345171	0.264914	0.293135	0.619987	0.055934	0.302767	0.725511	0.15832
7	0.019675	0.589777	0.317111	0.38	0.228222	0.218543	0.561364	0.01633	0.284218	0.619892	0.115946
8	0.029075	0.577592	0.342555	0.3384	0.181721	0.162225	0.548548	0.028318	0.246973	0.57943	0.130096
9	0.005581	0.527616	0.301653	0.265292	0.163206	0.219878	0.431283	0.092854	0.158986	0.453963	0.132311
10	0.01667	0.393129	0.206179	0.218913	0.14695	0.21848	0.365697	0.063562	0.121478	0.350011	0.085219
11	0.004058	0.292468	0.174962	0.204596	0.141467	0.140353	0.255875	0.064279	0.051443	0.254499	0.081323

OD:OS Step	176	177	178	179	52	54	59	61
1	0.049206	0.449731	0.423255	0.020587	0.329879	0.099107	0.193418	0.705756
2	0.320737	0.648126	0.195364	0.114201	0.302921	0.262698	0.049588	1.004221
3	0.367837	0.574035	0.105197	0.01209	0.373073	0.154029	0.348066	0.76261
4	0.24591	0.312922	0.185271	0.051814	0.423857	0.270971	0.422746	0.908664
5	0.250304	0.165771	0.282878	0.092335	0.464564	0.284619	0.356698	0.678609
6	0.132629	0.129028	0.090862	0.094786	0.384791	0.233848	0.385136	0.471665
7	0.144474	0.117364	0.008161	0.01909	0.342166	0.155625	0.170216	0.423498
8	0.13168	0.130392	0.091776	0.017512	0.235552	0.143574	0.106401	0.4
9	0.091195	0.077548	0.086378	0.006344	0.288825	0.176522	0.338374	0.404239
10	0.051238	0.039439	0.123384	0.004295	0.2853	0.118141	0.27942	0.34255
11	0.028658	0.026889	0.04306	0.003697	0.181635	0.068732	0.226984	0.353346

GFP
2 wpi

OD:OS	162	164	165	166	167	168	169	170	172	52	54	59	61
Step													
1	0.3725	0.9617	0.7487	1.3905	0.8039	0.465	0.8988	0.2014	0.4713	0.551	0.3858	0.122	0.0446
2	0.3047	0.8275	0.6777	1.2564	0.775	0.5253	0.8553	0.1503	0.398	0.3547	0.1297	0.1131	0.077
3	0.2293	0.7628	0.6322	1.1939	0.5762	0.504	0.9183	0.2041	0.4888	0.2315	0.2046	0.1266	0.0032
4	0.1383	0.6974	0.4891	0.8251	0.6213	0.4682	0.716	0.0952	0.3915	0.1352	0.1664	0.1715	0.0566
5	0.1297	0.5354	0.4281	0.6883	0.5998	0.4661	0.6281	0.1088	0.3548	0.0875	0.1564	0.0731	0.0538
6	0.0759	0.5598	0.4409	0.7124	0.5167	0.4482	0.6226	0.0834	0.3494	0.1047	0.1326	0.0556	0.0728
7	0.1558	0.4945	0.5028	0.7233	0.5353	0.4384	0.6612	0.0947	0.4135	0.1195	0.0836	0.028	0.0226
8	0.1733	0.4665	0.4886	0.6535	0.4904	0.4327	0.6314	0.1461	0.3966	0.1472	0.1315	0.0966	0.0532
9	0.1468	0.4151	0.4491	0.5841	0.5017	0.4293	0.531	0.1667	0.3776	0.1158	0.1473	0.1605	0.1048
10	0.1349	0.3865	0.3955	0.4843	0.4937	0.4256	0.4547	0.2144	0.363	0.0824	0.1905	0.1291	0.1264
11	0.124	0.2905	0.2849	0.4092	0.4249	0.3869	0.3919	0.1538	0.3311	0.0777	0.1444	0.1096	0.1101

GFP
4 wpi

OD:OS	162	164	165	166	167	168	169	170	172	52	54	59	61
Step													
1	0.648	1.2739	0.6492	1.5822	0	0.7499	1.822	0.4479	0.6305	0.7481	2.4652	0.3373	0.2702
2	0.6106	1.1966	0.5982	1.3941	0.6087	0.7779	1.5154	0.4138	0.5683	0.5691	0.8439	0.2616	0.1521
3	0.5109	1.124	0.4534	1.2201	0.565	0.6765	1.367	0.3456	0.4908	0.3739	1	0.1244	0.113
4	0.4662	0.8492	0.3533	1.2841	0.5185	0.5805	1.215	0.2674	0.4017	0.3334	0.842	0.2691	0.1043
5	0.3393	0.5726	0.3054	1.1671	0.5291	0.5665	1.1235	0.2168	0.359	0.3601	0.5607	0.1919	0.1015
6	0.3142	0.4938	0.2537	1.1136	0.4203	0.5641	1.1498	0.2006	0.356	0.3117	0.4425	0.1372	0.0717
7	0.413	1.0101	0.2562	1.0612	0.3657	0.5409	1.1316	0.2326	0.3682	0.1664	0.4516	0.0598	0.0588
8	0.3852	0.6273	0.241	0.9854	0.3837	0.5151	1.0747	0.2781	0.3728	0.1906	0.3826	0.0892	0.141
9	0.3782	0.4974	0.1983	0.8158	0.4099	0.4716	0.9394	0.2868	0.2843	0.1987	0.4289	0.1347	0.1949
10	0.3357	0.4536	0.164	0.7169	0.4141	0.4235	0.8022	0.2191	0.2574	0.2473	0.3752	0.1526	0.1695
11	0.2864	0.3115	0.1477	0.6041	0.4054	0.3214	0.6413	0.2062	0.1697	0.2096	0.3724	0.1505	0.1982

GFP vs. XIAP T-Tests

Step	24 hpi	2 wpi	4 wpi
1	0.233793	0.268817	0.150659
2	0.286737	0.217516	0.223584
3	0.11343	0.18357	0.441537
4	0.043841	0.145451	0.359146
5	0.031941	0.140832	0.196564
6	0.036231	0.180907	0.219968
7	0.016005	0.239281	0.397056
8	0.011727	0.222338	0.197267
9	0.004701	0.147046	0.085881
10	0.005348	0.170917	0.050867
11	0.00499	0.1326	0.03679

Mean B-wave amplitudes-GFP

Step	Base OD	24 hpi OD	2 wpi OD	4 wpi OD
1	200.9	52.37	113.9	138
2	287.3	98.65	154.3	202.5
3	354.1	130.7	172	220.3
4	408.2	150.6	174.1	227.5
5	457.7	150.2	173.2	232.5
6	500.4	124.9	179.8	233.1
7	572.7	112.2	205	249.7
8	640.1	115	226.3	269.3
9	684.9	123.8	229.5	258.7
10	643.5	95.87	199.9	216.8
11	586.9	65.88	147.3	161.4

Step	Base OS	24 hpi OS	2 wpi OS	4 wpi OS
1	223.7	109.4	191.3	167.9
2	324.5	182.6	295.5	259.2
3	396.8	264.3	355	327.5
4	454.9	337.5	429	395.6
5	509.3	391.1	487.8	452.5
6	555.4	428.6	524.8	484
7	617	465.5	576.4	507
8	686.9	510.5	646.1	560.4
9	735.2	596.5	687.4	599.8
10	685.4	565.6	642.2	562
11	613.5	518.8	568.3	506.1

Mean B-wave amplitude ratios-GFP

	GFP 24 hpi N=19			GFP 2 wpi N=13			GFP 4 wpi N=13		
Step	**MEAN Ratio**	**SDEV**	**SE**	**MEAN Ratio**	**STDEV**	**SE**	**MEAN Ratio**	**STDEV**	**SE**
1	0.5235	0.5122	0.1175	0.5706	0.3642	0.101	0.8942	0.6998	0.1941
2	0.5933	0.5006	0.1149	0.4957	0.3364	0.0933	0.7316	0.4126	0.1144
3	0.5333	0.4084	0.0937	0.4673	0.3155	0.0875	0.6434	0.4093	0.1135
4	0.4863	0.333	0.0764	0.3824	0.2533	0.0703	0.5757	0.3676	0.1019
5	0.4154	0.2611	0.0599	0.3315	0.2079	0.0577	0.4918	0.3271	0.0907
6	0.3078	0.213	0.0489	0.3212	0.2217	0.0615	0.4484	0.3334	0.0925
7	0.249	0.1963	0.045	0.3287	0.2078	0.0576	0.4705	0.3697	0.1025
8	0.2327	0.1829	0.042	0.3313	0.1756	0.0487	0.4359	0.3021	0.0838
9	0.2222	0.1553	0.0356	0.3177	0.1516	0.0421	0.403	0.2414	0.067
10	0.1805	0.1265	0.029	0.2985	0.122	0.0338	0.3639	0.2041	0.0566
11	0.1368	0.1063	0.0244	0.2491	0.1096	0.0304	0.3096	0.162	0.0449

Appendix 2: Flicker ERG Latencies and Amplitudes: values, ratios, means and T-tests

Flicker ERG Data

XIAP	latency		amplitude	
Baseline	OD	OS	OD	OS
35	39	37	20.25	21.23
36	39	35	27.15	39.53
40	38	37	32.82	27.31
49	36	37	16.9	32.68
183	38	36	25.85	48.65
184	36	38	21.22	20.3
185	37	36	21.36	28.4
186	34	35	27.48	22.5
187	38	37	29.76	34.76
188	41	38	13.77	34.98
189	38	38	10.13	15.78
190	39	38	19.4	26.95
191	41	40	8.105	17.72
194	39	40	10.63	16.53
195	38	38	19.15	21.07
197	46	39	5.818	6.168
199	43	41	19.66	26.97
200	39	39	10.9	9.932
201	39	40	12.24	15.76

XIAP	Latency		Amplitude	
24 hpi	OD	OS	OD	OS
35	27	35	0.254	11.13
36	50	36	3.793	12.54
40	28	37	1.656	19.77
49	45	39	1.354	17.3
183	42	35	10.4	31.65
184	50	39	6.537	23.9
185	25	38	0.128	15.91
186	25	37	0.373	8.967
187	25	38	0	13.01
188	25	40	0	6.171
189	25	39	0	16.26
190	31	42	0.475	11.16
191	40	36	5.481	6.906
194	26	39	1.555	12.52
195	29	34	2.448	8.264
197	48	40	5.027	24.14
199	49	41	3.1	20.53
200	31	39	4.245	13.75
201	50	37	3.173	16.56

Flicker ERG Data - cont'd

XIAP	Latency		Amplitude	
2 wpi	OD	OS	OD	OS
35	40	36	8.733	17.95
36	44	40	6.513	33.85
40	49	41	9.894	48.43
49	30	39	0.578	14.37
183	37	36	1.952	24.67
185	30	40	2.187	18.65
186	37	39	6.786	18.68
187	50	41	3.717	13.12
188	46	40	3.266	22.89
189	30	42	3.339	14.29
190	48	40	1.404	18.86
191	25	38	5.567	9.727
200	50	40	5.048	18.64

XIAP	Latency		Amplitude	
4 wpi	OD	OS	OD	OS
183	42	37	4.874	34.75
35	32	38	4.546	7.644
36	42	39	3.165	16.39
40	44	43	7.716	25.79
49	37	35	3.123	16.83
185	41	42	4.252	10.52
186	39	35	9.469	13.12
187	50	37	6.192	26.79
188	44	44	3.962	11.21
189	50	37	4.879	28.25
190	30	39	0.757	20.33
191	31	39	3.666	22.89
200	40	37	5.822	11.04

Flicker ERG Data - cont'd

GFP	latency		Amplitude	
Baseline	OD	OS	OD	OS
52	39	39	29.34	37.92
54	40	37	28.36	32.3
59	40	41	39.41	44.36
61	34	35	37.52	45.53
162	39	37	20.17	20.53
164	38	36	15.29	22.61
165	35	35	24.04	26.9
167	36	39	14.14	24.73
168	35	36	19.7	34.15
169	40	36	26.5	24.44
170	45	41	13.59	28.83
172	38	39	22.37	37.99
173	37	37	31.75	29.79
174	37	34	22.33	47.76
175	43	39	13.88	11.98
176	35	35	4.59	4.44
177	39	40	13.66	7.47
178	35	39	32.02	16.47

GFP	Latency		Amplitude	
24 hpi	OD	OS	OD	OS
52	47	37	0.887	11.35
54	47	37	2.241	27.61
59	41	39	3.888	17.47
61	47	35	8.776	14.15
162	46	36	4.453	22.52
164	47	38	3.092	19.22
165	27	38	3.057	17.83
166	45	40	3.749	32.77
167	26	40	1.024	25.01
168	40	40	0.351	27.1
169	50	43	10.11	19.98
170	50	41	3.191	17.15
172	32	39	6.832	27.79
173	37	39	0.829	15.86
175	28	39	0.663	22.85
176	50	37	1.136	19.67
177	29	38	2.262	18.91
178	50	43	3.266	11.76

Flicker ERG Data – cont'd

GFP	Latency		Amplitude	
2 wpi	OD	OS	OD	OS
52	27	43	3.243	12.64
54	40	36	9.141	27.92
59	39	38	5.972	32.85
61	43	41	2.651	19.11
162	32	37	4.199	25.96
164	27	37	0.048	28.6
165	47	36	2.58	22.91
166	49	41	4.125	22.19
167	45	37	8.591	3.42
168	41	38	4.259	22.95
169	26	37	0.884	20.88
170	47	39	3.393	14.59
172	38	38	2.764	26.14

GFP	Latency		Amplitude	
4 wpi	OD	OS	OD	OS
52	45	38	5.263	18.06
54	25	39	0.304	7.304
59	50	39	2.813	17.33
61	48	32	4.368	5.756
162	42	37	6.01	18.59
164	46	38	10.87	22.16
165	50	37	7.203	13.97
166	46	40	5.518	24.59
167	25	38	0.039	5.39
168	40	40	1.024	25.01
169	42	41	23.46	19.96
170	25	38	0	14.99
172	50	37	4.815	30.9

Flicker ERG Latency and amplitude Ratios (OD:OS)

	XIAP base		XIAP 24h	
	Latency	Amplitude	Latency	Amplitude
35	1.054054	0.9538389	0.771429	0.0228212
36	1.114286	0.6868201	1.388889	0.3024721
40	1.027027	1.2017576	0.756757	0.0837633
49	0.972973	0.5171359	1.153846	0.0782659
183	1.055556	0.5313464	1.2	0.328594
184	0.947368	1.0453202	1.282051	0.2735146
185	1.027778	0.7521127	0.657895	0.0080453
186	0.971429	1.2213333	0.675676	0.041597
187	1.027027	0.8561565	0.657895	0
188	1.078947	0.3936535	0.625	0
189	1	0.6419518	0.641026	0
190	1.026316	0.7198516	0.738095	0.0425627
191	1.025	0.4573928	1.111111	0.7936577
194	0.975	0.6430732	0.666667	0.1242013
195	1	0.9088752	0.852941	0.2962246
197	1.179487	0.9432555	1.2	0.2082436
199	1.04878	0.7289581	1.195122	0.1509985
200	1	1.0974627	0.794872	0.3087273
201	0.975	0.7766497	1.351351	0.1916063
AVG	**1.026633**	**0.7935235**	**0.90998**	**0.1845315**
N	**19**	**19**	**15**	**15**
SQRT N	**4.358899**	**4.3588989**	**3.872983**	**3.8729833**
STDEV	**0.055546**	**0.242373**	**0.275684**	**0.2082018**
STERR	**0.012743**	**0.0556042**	**0.071181**	**0.0537575**

	XIAP 2w		XIAP 4w	
	Latency	Amplitude	Latency	Amplitude
35	1.111111	0.4865181	1.135135	0.140259
36	1.1	0.1924077	0.842105	0.5947148
40	1.195122	0.2042949	1.076923	0.1931056
49	0.769231	0.0402227	1.023256	0.2991857
183	1.027778	0.0791244	1.057143	0.1855615
185	0.75	0.1172654	0.97619	0.4041825
186	0.948718	0.3632762	1.114286	0.7217226
187	1.219512	0.2833079	1.351351	0.231131
188	1.15	0.1426824	1	0.3534344
189	0.714286	0.2336599	1.351351	0.172708
190	1.2	0.0744433	0.769231	0.0372356
191	0.657895	0.5723245	0.794872	0.1601573
200	1.25	0.2708155	1.081081	0.5273551
AVG	**1.007204**	**0.235411**	**1.044071**	**0.3092887**
N	**13**	**13**	**13**	**13**
SQRT N	**3.605551**	**3.6055513**	**3.605551**	**3.6055513**
STDEV	**0.214234**	**0.1607987**	**0.1803**	**0.201778**
STERR	**0.059418**	**0.0445975**	**0.050006**	**0.0559632**

Flicker ERG latency and amplitude ratios (OD:OS) - end

	GFP base		GFP 24h	
	Latency	Amplitude	Latency	Amplitude
52	1	0.7737342	1.27027	0.0781498
54	1.081081	0.8780186	1.27027	0.0811662
59	0.97561	0.888413	1.051282	0.2225529
61	0.971429	0.824072	1.342857	0.620212
162	1.054054	0.9824647	1.277778	0.1977353
164	1.055556	0.6762494	1.236842	0.1608741
165	1	0.8936803	0.710526	0.1714526
167	0.923077	0.5717752	1.125	0.1144034
168	0.972222	0.5768668	0.65	0.0409436
169	1.111111	1.0842881	1	0.012952
170	1.097561	0.471384	1.162791	0.506006
172	0.974359	0.5888392	1.219512	0.1860641
173	1	1.0657939	0.820513	0.2458438
174	1.088235	0.4675461	0.948718	0.0522699
175	1.102564	1.1585977	0.717949	0.0290153
176	1	1.0337838	1.351351	0.0577529
177	0.975	1.8286479	0.763158	0.1196192
178	0.897436	1.9441409	1.162791	0.2777211
AVG	**1.015516**	**0.9282386**	**1.010495**	**0.1551895**
N	**18**	**18**	**14**	**14**
SQRT N	**4.242641**	**4.2426407**	**3.741657**	**3.7416574**
STDEV	**0.063394**	**0.4089736**	**0.239994**	**0.130556**
STERR	**0.014942**	**0.096396**	**0.064141**	**0.0348926**

	GFP 2w		GFP 4w	
	Latency	Amplitude	Latency	Amplitude
52	0.627907	0.2565665	1.184211	0.2914175
54	1.111111	0.3273997	0.641026	0.041621
59	1.026316	0.181796	1.282051	0.1623197
61	1.04878	0.1387232	1.5	0.7588603
162	0.864865	0.1617488	1.135135	0.3232921
164	0.72973	0.0016783	1.210526	0.4905235
165	1.305556	0.1126146	1.351351	0.5156049
166	1.195122	0.1858945	1.15	0.2244002
167	1.216216	2.5119883	0.657895	0.0072356
168	1.078947	0.1855773	1	0.0409436
169	0.702703	0.0423372	1.02439	1.1753507
170	1.205128	0.2325565	0.657895	0
172	1	0.1057383	1.351351	0.1558252
AVG	**1.008645**	**0.3418938**	**1.088141**	**0.3221073**
N	**13**	**13**	**13**	**13**
SQRT N	**3.605551**	**3.6055513**	**3.605551**	**3.6055513**
STDEV	**0.215849**	**0.6576921**	**0.282548**	**0.3426462**
STERR	**0.059866**	**0.182411**	**0.078365**	**0.095033**

T-tests of Flicker ERG ratios

T-TESTS	XIAP vs. GFP				
	Baseline	**24 hpi**	**2 wpi**	**4 wpi**	**4 wpi***
Latency	0.287539	0.070601	0.349923	0.3202444	0.296209
Amplitude	0.118214	0.4657967	0.290057	0.4543318	0.495535

*w/o 183 (a XIAP rat with a cataract at 4 wpi)

XIAP 24 h vs. 4w			**GFP 24 vs. 4w**	
Latency	**Amplitude**		**Latency**	**Amplitude**
0.089467	0.032091		0.38658	0.087031
XIAP 24h vs. 2w			**GFP 24 h vs. 2w**	
Latency	**Amplitude**		**Latency**	**Amplitude**
0.199446	0.157733		0.001014	0.19526

Appendix 3: Rmax and K: values, ratios, means and T-tests

XIAP Rmax and K values

XIAP	Baseline	Baseline	24h	24h	2w	2w	4w	4w
	OD	OD	OD	OD	OD	OD	OD	OD
	K	Rmax	K	Rmax	K	Rmax	K	Rmax
35	0.0662	604.7512	0	249.8056	0.0054	192.1533	0.0032	151.5756
36	0.0047	814.4489	0.0033	68.503	0.0003	175.6122	0.0009	168.9043
40	0.0187	855.6791	0.0017	232.1733	0.0014	407.4264	0.0007	252.4007
49	0.0041	722.3507	0.0014	91.5501	0.0019	111.9654	0.0005	147.698
185	0.0015	670.1754	0.004	149.5759	0.0021	267.2612	0.0012	311.3091
186	0.0088	585.0493	0.0013	131.618	0.0008	271.4734	0.003	392.7419
187	0.0028	757.2218	0.0013	55.2399	0.0009	167.1035	0.0009	252.4621
188	0.0009	699.6028	0.0029	162.1715	0.0007	330.7018	0.0013	324.5878
189	0.0014	475.0567	0.0008	172.0989	0.0008	210.5775	0	232.8806
190	0.005	913.0668	0.0018	50.9635	0.0004	159.0087	0.0002	233.0562
191	0.0011	534.5749	0.0008	31.4255	0.0008	103.557	0.0005	156.6611
200	0.0056	574.9365	0.0018	255.6594	0.0006	460.1298	0.0011	480.9113
183	0.001	744.591	0.0014	380.5528	0.0012	318.7841	0.0006	150.5193
184	0.0023	684.8134	0.0008	113.6966				
194	0.0013	682.7684	0.0016	305.7505				
195	0.0038	759.3365	0.0008	229.2043				
197	0.0023	517.1322	0.0008	210.551				
199	0.0019	784.0528	0.0008	105.8026				
201	0.0052	657.0021	0.0009	330.4806				
AVG	**0.007295**	**686.1374**	**0.001484**	**175.0959**	**0.001331**	**244.2888**	**0.001085**	**250.4391**
w/o 183							**0.001125**	**258.7657**

XIAP Rmax and K Values – cont'd

XIAP	Baseline	Baseline	24h	24h	2w	2w	4w	4w
	OS	OS	OS	OS	OS	OS	OS	OS
	K	Rmax	K	Rmax	K	Rmax	K	Rmax
35	0.1	525.4032	0.0065	229.8362	0.0108	403.9064	0.0046	162.493
36	0.0089	867.1456	0.0016	232.4544	0.0068	818.365	0.0017	413.3744
40	0.0026	628.9391	0.0025	315.6146	0.0052	913.2747	0.0016	637.6198
49	0.0936	946.6293	0.0018	295.2079	0.003	555.7657	0.0057	365.5774
185	0.0057	713.2758	0.0052	483.7583	0.0023	690.9361	0.0009	536.2957
186	0.0015	553.9695	0.0054	456.5381	0.0507	718.6055	0.0004	445.9832
187	0.0058	889.1763	0.0084	523.6884	0.001	706.4358	0.0031	708.759
188	0.0068	1009.869	0.004	420.3842	0.0046	775.7249	0.0014	680.2987
189	0.0056	569.9366	0.0177	538.5019	0.0021	511.1956	0.0024	650.9649
190	0.0111	997.6017	0.0046	713.8486	0.0059	915.7656	0.0038	934.1684
191	0.0035	573.5364	0.0008	276.4655	0.0025	477.3174	0.0015	664.8644
200	0.005	574.4231	0.0011	575.287	0.0032	1003.967	0.0027	555.689
183	0.0028	862.9867	0.0175	628.2962	0.0041	630.738	0.0015	847.2695
184	0.0014	797.9204	0.0054	596.2068				
194	0.0024	778.1204	0.0012	601.9303				
195	0.0046	779.8377	0.0009	261.2451				
197	0.0018	503.9007	0.0237	720.0832				
199	0.0057	843.6488	0.0067	383.1016				
201	0.0042	610.0928	0.003	396.2545				
AVG	**0.014368**	**738.2323**	**0.006211**	**455.1949**	**0.007862**	**701.6922**	**0.002408**	**584.8736**
w/o 183							**0.002483**	**563.0073**

XIAP Rmax and K Ratios

XIAP	Baseline	Baseline	24h	24h	2w	2w	4w	4w
	OD:OS	OD:OS	OD:OS	OD:OS	OD:OS	OD:OS	OD:OS	OD:OS
	K	Rmax	K	Rmax	K	Rmax	K	Rmax
35	0.662	1.151023	0	1.086885	0.5	0.475737	0.695652	0.932813
36	0.52809	0.93923	2.0625	0.294694	0.044118	0.214589	0.529412	0.408599
40	7.192308	1.360512	0.68	0.735623	0.269231	0.446116	0.4375	0.395848
49	0.043803	0.763077	0.777778	0.310121	0.633333	0.201462	0.087719	0.404013
185	0.263158	0.939574	0.769231	0.309196	0.913043	0.38681	1.333333	0.58048
186	5.866667	1.056104	0.240741	0.288296	0.015779	0.377778	7.5	0.88062
187	0.482759	0.851599	0.154762	0.105482	0.9	0.236544	0.290323	0.356203
188	0.132353	0.692766	0.725	0.38577	0.152174	0.426313	0.928571	0.477125
189	0.25	0.833526	0.045198	0.319588	0.380952	0.411931	0	0.357747
190	0.45045	0.915262	0.391304	0.071393	0.067797	0.173635	0.052632	0.24948
191	0.314286	0.932068	1	0.113669	0.32	0.216956	0.333333	0.235629
200	1.12	1.000894	1.636364	0.444403	0.1875	0.458312	0.407407	0.865432
183	0.357143	0.862807	0.08	0.60569	0.292683	0.505414	0.4	0.177652
184	1.642857	0.858248	0.148148	0.1907				
194	0.541667	0.877459	1.333333	0.50795				
195	0.826087	0.973711	0.888889	0.877353				
197	1.277778	1.026258	0.033755	0.292398				
199	0.333333	0.929359	0.119403	0.276174				
201	1.238095	1.076889	0.3	0.834011				

GFP Rmax and K Values

GFP	Baseline	Baseline	24h	24h	2w	2w	4w	4w
	OD	OD	OD	OD	OD	OD	OD	OD
	K	Rmax	K	Rmax	K	Rmax	K	Rmax
52	0.1	714.0846	0.0027	100.3968	0	37.6676	0.0017	83.0531
54	0.0421	520.702	0.0033	77.6704	0.1	95.356	0.0015	104.511
59	0.0439	959.2578	0.0043	70.7375	0.1	104.6504	0.0027	42.8127
61	0.0181	762.8522	0.0027	104.7802	0.1	72.4055	0.0422	56.4246
162	0.0024	499.971	0	25.1616	0	102.0139	0	88.6319
164	0.0031	492.3483	0.001	240.9607	0.0006	295.9496	0.0005	180.5009
165	0.0014	704.054	0.0009	171.8485	0.0011	280.8125	0.0008	167.771
166	0.0087	813.7437	0.0012	234.3955	0	662.5297	0.0023	635.4299
167	0.0013	492.9216	0.002	134.4675	0.0012	284.1911	0.0022	292.2146
168	0.0014	502.429	0.0017	148.2954	0.001	300.8462	0.0008	400.843
169	0.0034	872.0863	0.0007	280.7649	0.0006	360.0343	0.0008	596.6722
170	0.0016	652.8076	0.0009	49.3101	0.1	138.1157	0	141.8864
172	0.002	1171.864	0.0003	165.0647	0.001	314.4626	0.0008	324.1672
173	0.0027	1007.964	0.0006	208.8723				
175	0.0005	346.9362	0.0006	84.7302				
176	0.0009	239.2649	0.0009	64.9488				
177	0.0291	625.2387	0.0008	79.7691				
178	0.0241	741.7525	0.0018	32.54				
179	0.009	634.7012	0.0008	19.7214				
AVG	**0.015563**	**671.3147**	**0.001432**	**120.7598**	**0.031192**	**234.5412**	**0.004331**	**239.6091**

GFP K and Rmax values (cont'd)

GFP	Baseline	Baseline	24h	24h	2w	2w	4w	4w
	OS	OS	OS	OS	OS	OS	OS	OS
	K	Rmax	K	Rmax	K	Rmax	K	Rmax
52	0.0742	741.9369	0.0043	339.1075	0.0049	391.3056	0.007	362.5275
54	0.1	590.7778	0.0061	480.7381	0.0054	417.996	0.0202	284.3791
59	0.0322	983.1758	0.01	298.1545	0.0069	689.8472	0.0385	409.6748
61	0.0324	792.3412	0.0129	257.9656	0.0174	718.0534	0.0024	286.9254
162	0.0039	383.7453	0.0106	468.7084	0.0055	615.6562	0.0012	286.2455
164	0.0267	595.6353	0.0179	500.6477	0.0051	728.3182	0.0111	413.4876
165	0.0036	770.0252	0.0158	645.3711	0.007	712.6611	0.0052	765.842
166	0.0037	799.2988	0.0113	868.4334	0.0069	703.8072	0.0138	841.6776
167	0.0028	735.9817	0.0209	848.6482	0.0072	604.0018	0.0037	742.3287
168	0.0026	715.8124	0.0147	755.047	0.0016	720.65	0.0025	879.7336
169	0.002	796.7907	0.0068	588.1922	0.0035	699.326	0.0019	630.16
170	0.0041	854.9072	0.0075	636.0536	0.0021	596.7502	0.0023	584.1487
172	0.0062	1135.351	0.006	769.8973	0.0015	849.7754	0.0022	1028.626
173	0.0028	922.2834	0.0332	478.3643				
175	0.0005	389.2614	0.0074	629.3495				
176	0.0006	224.49	0.0025	463.6923				
177	0.001	747.1354	0.0407	856.6013				
178	0.0013	611.8295	0.0171	388.3212				
179	0.0008	744.9383	0.0023	609.4762				
AVG	**0.015863**	**712.4062**	**0.013053**	**572.7773**	**0.005769**	**649.8576**	**0.008615**	**578.1351**

GFP Rmax and K ratios

GFP	Baseline	Baseline	24h	24h	2w	2w	4w	4w
	OD:OS	OD:OS	OD:OS	OD:OS	OD:OS	OD:OS	OD:OS	OD:OS
	K	Rmax	K	Rmax	K	Rmax	K	Rmax
52	1.347709	0.96246	0.627907	0.296062	0	0.096261	0.242857	0.229095
54	0.421	0.881384	0.540984	0.161565	18.51852	0.228127	0.074257	0.367506
59	1.363354	0.975673	0.43	0.237251	14.49275	0.151701	0.07013	0.104504
61	0.558642	0.962782	0.209302	0.406179	5.747126	0.100836	17.58333	0.196653
162	0.615385	1.302872	0	0.053683	0	0.165699	0	0.309636
164	0.116105	0.826594	0.055866	0.481298	0.117647	0.406347	0.045045	0.436533
165	0.388889	0.914326	0.056962	0.266279	0.157143	0.394034	0.153846	0.219067
166	2.351351	1.018072	0.106195	0.269906	0	0.941351	0.166667	0.754956
167	0.464286	0.669747	0.095694	0.158449	0.166667	0.470514	0.594595	0.393646
168	0.538462	0.7019	0.115646	0.196406	0.625	0.417465	0.32	0.455641
169	1.7	1.094499	0.102941	0.477335	0.171429	0.51483	0.421053	0.946858
170	0.390244	0.763601	0.12	0.077525	47.61905	0.231446	0	0.242894
172	0.322581	1.03216	0.05	0.214398	0.666667	0.370054	0.363636	0.315146
173	0.964286	1.0929	0.018072	0.436639				
175	1	0.891268	0.081081	0.134631				
176	1.5	1.065815	0.36	0.140069				
177	29.1	0.836848	0.019656	0.093123				
178	18.53846	1.212352	0.105263	0.083797				
179	11.25	0.852018	0.347826	0.032358				

Rmax and K Mean Ratios

K	GFP	XIAP	GFP	XIAP	GFP	XIAP	GFP	XIAP
OD:OS	**Baseline**	**Baseline**	**24h**	**24h**	**2w**	**2w**	**4w**	**4w**
AVG	3.838461	1.238044	0.181231	0.599285	6.790923	0.359739	1.541186	0.999683
N	19	19	19	19	13	13	13	13
SQRT N	4.358899	4.358899	4.358899	4.358899	3.605551	3.605551	3.605551	3.605551
STDEV	7.656419	1.925866	0.186817	0.588373	13.70825	0.300441	4.823412	1.987161
STERR	1.756503	0.441824	0.042859	0.134982	3.801984	0.083327	1.337774	0.551139

Rmax	GFP	XIAP	GFP	XIAP	GFP	XIAP	GFP	XIAP
OD:OS	**Baseline**	**Baseline**	**24h**	**24h**	**2w**	**2w**	**4w**	**4w**
AVG	0.950383	0.949493	0.221945	0.423652	0.345282	0.348584	0.382472	0.48628
N	19	19	19	19	13	13	13	13
SQRT N	4.358899	4.358899	4.358899	4.358899	3.605551	3.605551	3.605551	3.605551
STDEV	0.163694	0.147775	0.1426	0.28284	0.229098	0.120682	0.23403	0.254326
STERR	0.037554	0.033902	0.032715	0.064888	0.06354	0.033471	0.064908	0.070537

Rmax and K T-Tests

T-Tests	Baseline	24 hpi	2 wpi	4 wpi	4 wpi*
K	0.083167	0.003733	0.058286	0.356568	0.370712
Rmax	0.493033	0.004978	0.481911	0.144833	0.096424

*without 183 (cataract in right eye)

Appendix 4: H+E-stained Retinal Cross-sections: Cell Counts, Ratios and T-tests

OD=right eye (R); OS=left eye (L); observers: 1,2,3

a = parapapillary region, b = mid-periphery

XIAP	Slide #	INL a1	INL a2	INL a3	INL b1	INL b2	INL b3
4 wpi	35L	150	161	119	167	173	150
	36L	220	227	172	252	290	192
	183L26	284		270	220		221
	185L	323		249	313		291
	186L	281		170	287		211
	187L20.5	337		283	224		180
	188L	304		233	297		192
	190L11	363		253	407		225
	191L27.4	220	266	233	238		175
	200L	290	313	222	262	322	182
	35R	175	179	133	207	220	126
	36R	251	264	175	206	201	137
	183R	256		243	244		266
	185R3.4	275		199	212		154
	187R2.6	228		203	226		174
	188R	170		157	230		188
	189R9.4	226		208	266		232
	190R	199		147	176		140
	191R	166	163	120	198		126
	200R18.5	250	256	164	236	207	145
24 hpi	194L23.6	282		213	224		184
	195L11.5	251	231	190	204	202	156
	197L19.7	256	213	193	258	247	225
	199L30.5	259	280	230	257	322	194
	201L30.3	293	344	182	272	271	202
	194R6.5	249		206	278		224
	195R17.1	224	244	204	242	216	215
	197R8.6	354	327	264	251	331	183
	199R16.5	253	261	213	238	336	171
	201R8.2	291	411	246	236	304	204
O hpi	192L18.6	252	247	252	259	278	224
	196L11.7	319	288	232	260	214	206
	203L30.4	284	439	242	251	412	215
	192R13.5	262	224	218	339	240	210
	203R17.5	281	352	222	210	321	181

Cell Counts – XIAP (end)

	Slide #	GCLa1	GCL a2	GCL a3	GCL b1	GCL b2	GCL b3
4 wpi	35L	23	21	22	15	17	18
	36L	26	23	37	22	18	23
	183L26	30		16	32		26
	185L	43		68	34		44
	186L	30		31	29		38
	187L20.5	39		51	33		40
	188L	40		50	29		25
	190L11	36		34	40		37
	191L27.4	26	36	35	26		24
	200L	24	29	31	21	6	35
	35R		2	19	18	10	22
	36R	14	12	15	11	10	12
	183R	23		32	43		36
	185R3.4	26		32	28		24
	187R2.6	30		31	19		19
	188R	12		13	22		22
	189R9.4	39		49	33		35
	190R	8		6	11		9
	191R	11		14	17		16
	200R18.5	17	16	23	11	10	15
24 hpi	194L23.6	23		26	13		20
	195L11.5	22	21	24	35	37	43
	197L19.7	26	26	30	21	29	31
	199L30.5	32	21	49	13	10	19
	201L30.3	27	23	31	23	9	29
	194R6.5	32		43	12		22
	195R17.1	23	20	26	19	9	31
	197R8.6	18	18	31	39	23	38
	199R16.5	21	22	27	33	35	44
	201R8.2	30	48	40	24	21	29
0 hpi	192L18.6	29	23	37	31	24	40
	196L11.7	29	36	32	30	15	30
	203L30.4	35	29	49	45	34	60
	192R13.5	27	25	30	28	25	40
	203R17.5	23	16	36	11	8	17

GFP	Slide #	INL a1	INL a2	INL a3	INL b1	INL b2	INL b3
4 wpi	52L	226	220	154	272	268	190
	61L	296	317	317	288	331	187
	162L	263	258	215	228	211	155
	164L35.2	290	272	219	229	197	173
	166L	278	261	159	274	179	188
	167L18.4	347	316	219	230	281	169
	168L	253	252	178	283	243	222
	169L24.3	240	280	186	245	342	171
	170L	267	209	216	356	374	258
	172L31.4	288	291	225	393	334	241
	52R	157	182	126	160	160	124
	61R	179	184	193	150	162	120
	162R8.2	235	189	159	n/a		n/a
	164R26.2	222		171	203	136	153
	165R2.7	228	211	155	259	242	206
	166R20.3	206	186	152	227	139	139
	168R3.5	235	231	170	197	294	176
	169R	264	293	187	185	192	153
	170R	154	124	127	174	179	126
24 hpi	173L20.5	245	227	207	226	229	169
	175L23.4	347	269	264	391	421	279
	176L14.3	280	215	208	200	174	182
	177L26.6	264	272	201	251	269	212
	179L11.5	226	316	202	214	276	206
	173R22.3	176	207	176	216	254	191
	175R17.5	258	247	208	237	281	190
	176R	224	186	205	201	188	192
	177R	253	228	248	163	124	145
	178R	211	383	222	181	198	170
	179R14.7	219	223	247	148	108	155
0 hpi	51L	256	186	164	201	200	132
	53L	229	236	139	194	189	19
	180L11.2	223	209	186	232	173	189
	182L23.6	281		213	245	290	177
	53R	280	289	165	164	187	125
	180R12.5	230		189	197	220	161

Cell Counts - GFP (end)

	Slide #	GCLa1	GCL a2	GCL a3	GCL b1	GCL b2	GCL b3
4 wpi	52L	24	20	28	14	15	15
	61L	28	24	67	21	23	35
	162L	28	22	37	24	18	31
	164L35.2	27	30	41	15	15	28
	166L	16	9	16	14	5	24
	167L18.4	36	7	49	14	9	21
	168L	23	19	28	24	21	30
	169L24.3	20	17	24	21	15	24
	170L	21	17	37	33	35	48
	172L31.4	37	21	44	34	16	38
	52R	9	7	19	14	10	17
	61R	16	14	15	14	11	14
	162R8.2	19	24	22	n/a		n/a
	164R26.2	20		23	8	6	11
	165R2.7	15	17	17	24	19	23
	166R20.3	24	11	31	19	10	21
	168R3.5	12	5	15	10	2	12
	169R	26	24	43	30	30	32
	170R	13	12	27	10	11	9
24 hpi	173L20.5	34	24	41	29	34	34
	175L23.4	30	8	41	29	12	32
	176L14.3	26	17	30	8	5	14
	177L26.6	25	19	37	24	8	28
	179L11.5	39	27	49	28	23	38
	173R22.3	28	23	29	28	18	45
	175R17.5	38	19	44	21	9	32
	176R	33	27	37	11	4	10
	177R	26	11	26	19	13	21
	178R	29		40	17	12	19
	179R14.7	23	21	35	16	14	24
0 hpi	51L	22	18	31	29	24	36
	53L	17	14	149	24	26	29
	180L11.2	19	12	29	28	18	30
	182L23.6	36	28	45	24	18	34
	53R	26	22	24	24	23	23
	180R12.5	13	9	26	22	16	31

Average ratios

XIAP 4 wpi	INL avg a	INL avg b
35 R/L	1.1320383	1.2197818
36 R/L	1.1071155	0.7413685
183 R/L	0.9007042	1.1563554
185 R/L	0.825295	0.6792453
187 R/L	0.6969362	0.9877976
188 R/L	0.6165151	0.7725437
190 R/L	0.5646185	0.4461157
191 R/L	0.6274496	0.7759664
200 R/L	0.806233	0.857651
MEAN	**0.808545**	**0.848536**
STDEV	**0.207424**	**0.241138**
N	**9**	**9**
SQRT N	**3**	**3**
STDERR	**0.069141**	**0.080379**

XIAP 4wpi	GCL avg a	GCL avg b
35 R/L	0.4794372	1.0034858
36 R/L	0.4885354	0.5257649
183 R/L	1.3833333	1.3641827
185 R/L	0.5376197	0.684492
187 R/L	0.688537	0.5253788
188 R/L	0.28	0.8193103
190 R/L	0.1993464	0.2591216
191 R/L	0.4115385	0.6602564
200 R/L	0.667331	0.5806452
MEAN	**0.570631**	**0.713626**
STDEV	**0.34415**	**0.319589**
N	**9**	**9**
SQRT N	**3**	**3**
STERR	**0.114717**	**0.10653**

GFP 4 wpi	INL avg a	INLavg b
52R/L	0.780048	0.612627
162R/L	0.736047	
164R/L	0.77317	0.885428
166R/L	0.726825	0.781455
168R/L	0.933526	0.731095
169R/L	1.050602	0.73785
170R/L	0.586014	
MEAN	**0.798033**	**0.749691**
STDEV	**0.151082**	**0.098369**
N	**7**	**5**
SQRT N	**2.645751**	**2.236068**
STERR	**0.057104**	**0.043992**

GFP 4 wpi	GCL avg a	GCL avg b
52 R/L	0.4678571	0.9333333
164 R/L	0.4339055	0.4420635
166 R/L	1.5532407	1.4107143
168 R/L	0.4402038	0.3039683
169 R/L	1.5011438	1.5873016
170 R/L	0.6848866	0.268272
162 R/L	0.788025	
MEAN	**0.8384661**	**0.8242755**
STDEV	**0.4891845**	**0.576881**
N	**7**	**6**
Root N	**2.6457513**	**2.4494897**
STERR	**0.1848944**	**0.2355107**

XIAP 24 hpi	INL avg a	INL avg b
194R/L	0.925057	1.229231
195R/L	1.007464	1.154891
197R/L	1.428633	0.964547
199R/L	0.962878	0.950331
201R/L	1.097983	0.981537
MEAN	**1.084403**	**1.056107**
N	**5**	**5**
SQRT N	**2.236068**	**2.236068**
STDDEV	**0.202952**	**0.127341**
STERR	**0.09076**	**0.05694**

XIAP 24hpi	GCL avg a	GCL avg b
194	1.5225753	1.0115385
195	1.0270563	0.5023435
197	0.8059829	1.2920176
199	0.7516298	2.7847503
201	1.4961301	1.4589372
MEAN	**1.1206749**	**1.4099174**
N	**5**	**5**
SQRT N	**2.236068**	**2.236068**
STDEV	**0.3696215**	**0.8498331**
STERR	**0.1652998**	**0.3800569**

Average ratios (end)

GFP 24 hpi	INL avg a	INL avg b
52R/L	0.826834	1.068451
164R/L	0.768168	0.654835
166R/L	0.883212	1.046802
168R/L	0.913322	0.65234
169R/L	0.969129	0.715756
mean	**0.872133**	**0.827637**
N	**5**	**5**
SQRT N	**2.236068**	**2.236068**
STDDEV	**0.059705**	**0.183992**
STERR	**0.0267**	**0.08228**

GFP 24hpi	GCL avg a	GCL avg b
173	0.8297266	0.9394861
175	1.5716125	0.8247126
176	1.3635998	0.9630952
177	0.7738834	1.0555556
179	0.6939357	0.6039011
AVG	**1.0465516**	**0.8773501**
N	**5**	**5**
SQRT N	**2.236068**	**2.236068**
STDEV	**0.3943056**	**0.1735766**
STERR	**0.1763388**	**0.0776258**

Ratios were calculated for each observer's counts (right eye:left eye).
The ratios were then averaged for each rat and plotted.

T-Test for Cell counts

T-Test*	INL a	INL b	GCL a	GCL b
XIAP vs. GFP 24 hpi	0.03956	0.04003	0.38348	0.11827
XIAP vs. GFP 4 wpi	0.45418	0.26158	0.12279	0.34067

***Student's T-test, one-tailed distribution, two-sample unequal variance.**
Significance at P<0.05

Appendix 5: TUNEL-positive Cell counts, averages and T-Tests

TUNEL positive cell counts

		440*	440	880*	880	1320*	1320	
	Slide	INL	GCL	INL	GCL	INL	GCL	notes
GFP	173	11	0	0	0	3	0	1170, not 1320
	175	5	0	2	0	4	1	
	176	1	0	1	0	2	0	
	177	9	1	13	1	39	3	
	178	0	0	3	8	0	19	
	179	17	4	13	0	11	1	
XIAP	194	0	0	0	0	0	0	1050, not 880
	195	0	4	0	2	0	0	
	197	3	7			2	3	
	199	0	0	15.5	0	0	0	340, not 440
	201	0	0	0	9	0	0	

Total Cell counts

	Slide	440 INL	440 GCL	880 INL	880 GCL	1320 INL	1320 GCL
GFP	173	304	33	276	15	260	26
	175	289	24	245	5	250	16
	176	209	9	300	13	197	12
	177	238	4	186	19	311	36
	178	391	12	276	22	191	31
	179	290	19	274	30	287	15
XIAP	194	171	5	257	31	207	7
	195	272	22	263	26	223	19
	197	275	31			278	56
	199	156	11	264	14	245	12
	201	246	19	181	21	229	19

*440, 880, and 1320 are the approximate distances (μm) from the optic nerve head. Alternate distances indicated in "Notes" column.

% TUNEL Positive

	Slide	440 INL	440 GCL	880 INL	880 GCL	1320 INL	1320 GCL
GFP	173R	3.618421	0	0	0	1.15385	0
	175R	1.730104	0	0.816327	0	1.6	6.25
	176R	0.478469	0	0.333333	0	1.01523	0
	177R	3.781513	25	6.989247	5.263158	12.5402	8.33333
	178R	0	0	1.086957	36.36364	0	61.2903
	179R	5.862069	21.05263	4.744526	0	3.83275	6.66667
	AVG	**2.578429**	**7.675439**	**2.328398**	**6.937799**	**3.357**	**13.7567**
XIAP	194R	0	0	0	0	0	0
	195R	0	18.18182	0	7.692308	0	0
	197R	1.090909	22.58065			0.71942	5.35714
	199R	0.	0	5.871212	0	0	0
	201R	0	0	0	42.85714	0	0
	AVG	**0.218182**	**8.152493**	**1.467803**	**12.63736**	**0.14389**	**1.07143**

T-TEST, GFP vs. XIAP

440 INL	440 GCL	880 INL	880 GCL	1320 INL	1320 GCL
0.02448	0.473655	0.33063	0.325209	0.076669	0.122755

Appendix 6: Semi-quantitative Analysis of Optic Nerve Cross-sections: ratings means and T-tests

Ratings

OS	Rating	Avg Damage	Notes	OD	Rating	Avg Damage	Notes
162	0	0		162	3	0.3	
164	0	0		164	2	0.2	
165	0	0		165	1	0.1	
166	0	0		166	2.5	0.25	pinkish-purple objects
167	0	0		167			
168				168	2.5	0.25	
169	0	0	only one dying axon	169	1	0.1	
170	0	0	several pinkish-purple objects	170	1	0.1	
172	0	0		172	1	0.1	
AVG GFP OS		**0**		**AVG GFP OD**		**0.175**	
183	0	0	10% pinkish-purple objects	183			
185	0	0	a few thick axons	185	0	0	a few "dark" degenerating axons
186	0	0	pinkish-purple objects	186	0	0	
187	0	0		187	2	0.2	excellent e.g. of "1" rating
188	0	0		188	1	0.1	
189	0	0		189	1	0.1	
191	0	0		191	3	0.3	
200	0	0	pinkish-purple objects	200	0	0	
AVG XIAP OS		**0**		**AVG XIAP OD**		**0.1**	

Average Damage

OD GFP	Rating	Avg Damage	T-TEST GFP vs. XIAP OD 0.09208463
162	3	0.3	
164	2	0.2	
165	1	0.1	
166	2.5	0.25	
168	2.5	0.25	
169	1	0.1	
170	1	0.1	
172	1	0.1	
Avg		**0.175**	
N=8	**Root N=**	**2.8284271**	
STDEV		**0.0845154**	
SE		**0.0298807**	
OD XIAP	**Rating**	**Avg Damage**	
185	0	0	
186	0	0	
187	2	0.2	
188	1	0.1	
189	1	0.1	
191	3	0.3	
200	0	0	
Avg		**0.1**	
N=7	**Root N=**	**2.6457513**	
STDEV		**0.1154701**	
SE		**0.0436436**	

Appendix 7: Optic Nerve Cross-sectional Area: Calculations, means and T-Tests

π=3.14

Calculation of Area of optic nerve cross-sections:

	diameter1	diameter2	radius1	radius2	Area (μm^2)
XIAP	10x mag	10x mag	10x mag	10x mag	π*r1*r2
4 wpi	OS	OS	OS	OS	OS
183	n/a				
185	630	560	315	280	276948
186	490	710	245	355	273101.5
187	530	640	265	320	266272
188	640	510	320	255	256224
189	640	570	320	285	286368
191	530	520	265	260	216346
200	550	500	275	250	215875

	diameter1	diameter2	radius1	radius2	Area (μm^2)
XIAP	10x mag	10x mag	10x mag	10x mag	π*r1*r2
4 wpi	OD	OD	OD	OD	OD
183	440	465	220	232.5	160611
185	620	500	310	250	243350
186	380	660	190	330	196878
187	400	405	200	202.5	127170
188	610	510	305	255	244213.5
189	670	530	335	265	278753.5
191	400	600	200	300	188400
200	470	600	235	300	221370

	diameter1	diameter2	radius1	radius2	Area (μm^2)
GFP	10x mag	10x mag	10x mag	10x mag	π*r1*r2
4 wpi	OS	OS	OS	OS	OS
162	600	550	300	275	259050
164	540	492	270	246	208558.8
165	520	575	260	287.5	234715
166	640	550	320	275	276320
167	500	500	250	250	196250
169	580	577.5	290	288.75	262935.75
170	560	475	280	237.5	208810
172	530	580	265	290	241309
~~168~~	~~360~~	~~340~~	~~180~~	~~170~~	~~96084~~

	diameter1	diameter2	radius1	radius2	Area (μm^2)
GFP	10x mag	10x mag	10x mag	10x mag	π*r1*r2
4 wpi	OD	OD	OD	OD	OD
162	510	465	255	232.5	186162.75
164	515	410	257.5	205	165752.75
165	620	475	310	237.5	231182.5
166	515	500	257.5	250	202137.5
167	280	300	140	150	65940
169	547.5	442.5	273.75	221.25	190180.969
170	375	460	187.5	230	135412.5
172	617.5	502.5	308.75	251.25	243580.594
168	500	450	250	225	176625

168 L omitted because optic nerve sample was poor

XIAP vs. GFP T-Test (OD) P = 0.121610794882173

Mean Optic Nerve Cross-sectional Areas

XIAP OS	Mean Area
AVG	255876.36
N	7
ROOT N	2.6457513
STDEV	28697.874
SE	10846.777

XIAP OD	Mean area
AVG	214305
N	8
ROOT N	2.82842712
STDEV	49174.7417
SE	17385.8967

GFP OS	Mean area
AVG	235993.5688
N	8
ROOT N	2.828427125
STDEV	29239.782
SE	10337.82407

GFP OD	Mean area
AVG	177441.618
N	9
ROOT N	3
STDEV	52970.5536
SE	17656.8512

Appendix 8. One-way Analysis of Variance (ANOVA) – Rmax Ratios (OD:OS)

Anova: Single Factor
Baseline
SUMMARY

Groups	*Count*	*Sum*	*Average*	*Variance*
GFP Rmax	19	18.05727	0.9503826	0.0267957
XIAP Rmax	19	18.04036	0.9494928	0.02183738

ANOVA

Source of Variation	*SS*	*df*	*MS*	*F*	*P-value*	*F crit*
Between Groups	7.52E-06	1	7.522E-06	0.00030933	0.986065	4.1131614
Within Groups	0.875395	36	0.0243165			
Total	0.875403	37				

Anova: Single Factor
24h
SUMMARY

Groups	*Count*	*Sum*	*Average*	*Variance*
GFP Rmax	19	4.216952	0.221945	0.020335
XIAP Rmax	19	8.049396	0.423652	0.079999

ANOVA

Source of Variation	*SS*	*df*	*MS*	*F*	*P-value*	*F crit*
Between Groups	0.38652	1	0.386517	7.70465	0.008683	4.113161
Within Groups	1.806	36	0.050167			
Total	2.19252	37				

Anova: Single Factor

2w

SUMMARY

Groups	*Count*	*Sum*	*Average*	*Variance*
GFP Rmax	13	4.488665	0.345282	0.052486
XIAP Rmax	13	4.531598	0.348584	0.014564

ANOVA

Source of Variation	*SS*	*df*	*MS*	*F*	*P-value*	*F crit*
Between Groups	7.09E-05	1	7.09E-05	0.002115	0.963702	4.259675
Within Groups	0.804601	24	0.033525			
Total	0.804672	25				

Anova: Single Factor

4w

SUMMARY

Groups	*Count*	*Sum*	*Average*	*Variance*
GFP Rmax	13	4.972135	0.382472	0.05477
XIAP Rmax	13	6.321642	0.48628	0.064682

ANOVA

Source of Variation	*SS*	*df*	*MS*	*F*	*P-value*	*F crit*
Between Groups	0.070045	1	0.070045	1.172771	0.289593	4.259675
Within Groups	1.433425	24	0.059726			
Total	1.50347	25				

Appendix 9: One-way ANOVA of Percentage TUNEL-positive cells

Anova: Single Factor
GFP vs XIAP: INL Para-papillary
SUMMARY

Groups	*Count*	*Sum*	*Average*	*Variance*
GFP INL	6	15.47058	2.578429	5.017814
XIAP INL	5	1.090909	0.218182	0.238017

ANOVA

Source of Variation	*SS*	*df*	*MS*	*F*	*P-value*	*F crit*
Between Groups	15.193	1	15.193	5.250809	0.04766	5.117357
Within Groups	26.04114	9	2.893459			
Total	41.23414	10				

Anova: Single Factor
GFP vs XIAP: INL Mid-periphery
SUMMARY

Groups	*Count*	*Sum*	*Average*	*Variance*
GFP INL	6	20.14202	3.357003	21.85033
XIAP INL	5	0.719424	0.143885	0.103514

ANOVA

Source of Variation	*SS*	*df*	*MS*	*F*	*P-value*	*F crit*
Between Groups	28.15672	1	28.15672	2.310754	0.162803	5.117357
Within Groups	109.6657	9	12.18508			
Total	137.8224	10				

Anova: Single Factor
XIAP vs GFP: GCL Para-papillary
SUMMARY

Groups	*Count*	*Sum*	*Average*	*Variance*
GFP GCL	6	46.05263	7.675439	142.9478
XIAP GCL	5	40.76246	8.152493	127.0371

ANOVA

Source of Variation	*SS*	*df*	*MS*	*F*	*P-value*	*F crit*
Between Groups	0.620674	1	0.620674	0.004568	0.947592	5.117357
Within Groups	1222.888	9	135.8764			
Total	1223.508	10				

Anova: Single Factor
XIAP vs GFP: GCL Mid-periphery
SUMMARY

Groups	*Count*	*Sum*	*Average*	*Variance*
GFP GCL	6	82.54032	13.75672	554.7942
XIAP GCL	5	5.357143	1.071429	5.739796

ANOVA

Source of Variation	*SS*	*df*	*MS*	*F*	*P-value*	*F crit*
Between Groups	438.8635	1	438.8635	1.412181	0.265106	5.117357
Within Groups	2796.93	9	310.77			
Total	3235.794	10				

Appendix 10: One-way ANOVA of Cell Counts in H&E-stained Cross-sections

Anova: Single Factor
Para-papillary and Mid-periphery
SUMMARY

Groups	*Count*	*Sum*	*Average*	*Variance*
XIAP 4w INL	18	14.91373	0.828541	0.048034
GFP 4w INL	12	9.334687	0.777891	0.016589

ANOVA

Source of Variation	*SS*	*df*	*MS*	*F*	*P-value*	*F crit*
Between Groups	0.018471	1	0.018471	0.51768	0.477796	4.195982
Within Groups	0.999054	28	0.035681			
Total	1.017525	29				

Anova: Single Factor
Para-papillary and Mid-periphery
SUMMARY

Groups	*Count*	*Sum*	*Average*	*Variance*
XIAP 4w GCL	18	11.55832	0.642129	0.109213
GFP 4w GCL	13	10.81492	0.831917	0.258368

ANOVA

Source of Variation	*SS*	*df*	*MS*	*F*	*P-value*	*F crit*
Between Groups	0.271889	1	0.271889	1.590621	0.217289	4.182965
Within Groups	4.957041	29	0.170932			
Total	5.22893	30				

Anova: Single Factor
Para-papillary and Mid-periphery
SUMMARY

Groups	*Count*	*Sum*	*Average*	*Variance*
XIAP 24h INL	10	10.70255	1.070255	0.025736
GFP 24h INL	10	8.498849	0.849885	0.02313

ANOVA

Source of Variation	*SS*	*df*	*MS*	*F*	*P-value*	*F crit*
Between Groups	0.242815	1	0.242815	9.938071	0.005508	4.413863
Within Groups	0.439791	18	0.024433			
Total	0.682607	19				

Anova: Single Factor
Para-papillary and Mid-periphery
SUMMARY

Groups	*Count*	*Sum*	*Average*	*Variance*
XIAP 24h GCL	10	12.65296	1.265296	0.404944
GFP 24h GCL	10	9.619509	0.961951	0.090444

ANOVA

Source of Variation	*SS*	*df*	*MS*	*F*	*P-value*	*F crit*
Between Groups	0.460092	1	0.460092	1.8575	0.189722	4.413863
Within Groups	4.458494	18	0.247694			
Total	4.918586	19				